HIGH VOLTAGE BREAKDOWN STUDY

W. R. Bell, et al

Ion Physics Corporation
Burlington, Massachusetts

March 1968

AD

TECHNICAL REPORT ECOM-00394-12

HIGH VOLTAGE BREAKDOWN STUDY

TWELFTH QUARTERLY PROGRESS REPORT

16 August 1967 through 15 November 1967

Prepared by:

ION PHYSICS CORPORATION

BURLINGTON, MASSACHUSETTS

MARCH 1968

ECOM

UNITED STATES ARMY ELECTRONICS COMMAND · FORT MONMOUTH, N.J. 07703

SPONSORED BY: Advanced Research Projects Agency, ARPA Order No. 517
CONTRACT DA-28-043-AMC-00394(E)

ION PHYSICS CORPORATION
Burlington, Massachusetts 01803

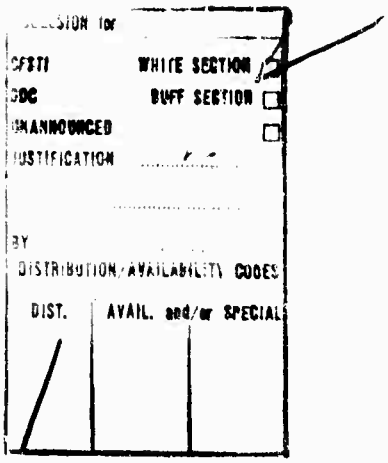

NOTICES

Disclaimers

The findings in this report are not to be construed as an official Department of the Army position, unless so designated by other authorized documents.

The citation of trade names and names of manufacturers in this report is not to be construed as official Government indorsement or approval of commercial products or services referenced herein.

Disposition

Destroy this report when it is no longer needed. Do not return to the originator.

Technical Report ECOM-00394-12

HIGH VOLTAGE BREAKDOWN STUDY

Twelfth Quarterly Progress Report
16 August 1967 through 15 November 1967

Report No. 12

Contract No. DA-28-043-AMC-00394(E)
AMC Task No. 7900.21.243.40.00

March 1968

Prepared for

U.S. ARMY ELECTRONICS COMMAND
FORT MONMOUTH, NEW JERSEY 07703

Sponsored by

ADVANCED RESEARCH PROJECTS AGENCY
ARPA Order No. 517

Prepared by

W. R. Bell, M. J. Mulcahy and A. Watson
ION PHYSICS CORPORATION
BURLINGTON, MASSACHUSETTS

TABLE OF CONTENTS

TABLE OF CONTENTS (Continued)

TABLE OF CONTENTS (Continued)

LIST OF ILLUSTRATIONS

LIST OF ILLUSTRATIONS (Continued)

LIST OF ILLUSTRATIONS (Continued)

LIST OF ILLUSTRATIONS (Continued)

LIST OF TABLES

PURPOSE

The factors influencing breakdown in high voltage vacuum devices will be studied. The information obtained will provide the basis for improvement in the design of microwave and modulator tubes that must operate at voltages greater than 100 kilovolts without breakdown.

ABSTRACT

Statistical and physical analyses of the block of eight experiment were carried out for unconditioned gaps and for conditioned gaps with and without perpendicular magnetic field. The other factors examined were anode and cathode treatment (vacuum or hydrogen firing) and electrode size. Prebreakdown current and breakdown voltage values were examined in the statistical analysis. Second order and higher order interactions were found to be important in addition to main factor effects. The magnetic field significantly affected the breakdown voltage and also interacted with other factors. The theoretical model of the breakdown mechanism developed was consistent with the results and trends of the statistical analysis. The 300 kv apparatus was disassembled for complete overhaul, cleaning and remachining. This included electropolishing of the vacuum chamber and polishing of all gold O-ring surfaces. The box heating oven was replaced with a form fitting as heater blanket unit and the controls for both and the electrode heaters were made completely automatic. The latter have now been removed from the vacuum envelope and the complete system has been reassembled, baked and made vacuum tight.

LECTURES, CONFERENCES AND PUBLICATIONS

Lectures and Conferences

A complete list of Lectures and Conference for this Quarter will be given in the next Quarterly Progress Report.

Publications

Watson, A. and Mulcahy, M. J., "Application of Statistical Design to High Voltage Vacuum Breakdown", Presented at the Conference on High-Voltage Insulation in Vacuum, London, England (September 1967).

Watson, A., Bell, W. and Mulcahy, M. J., "High Voltage Vacuum Breakdown in a Weak Transverse Magnetic Field", Presented at the Conference on High-Voltage Insulation in Vacuum, London, England (September 1967).

Watson, A., "Electrode Size and Pretreatment Effects on Vacuum Breakdown in a Transverse Magnetic Field", Presented at the 20th Annual Gaseous Electronics Conference, San Francisco, California (October 1967).

Watson, A., "Field Enhancement in Vacuum Breakdown", Presented at the 20th Annual Gaseous Electronics Conference, San Francisco, California (October 1967).

SECTION 1

INTRODUCTION

The work reported herein describes the twelfth three months of a study of high voltage breakdown in vacuum with particular application to problems encountered in the development of high power vacuum tubes.

The objectives of this period were to clean and overhaul the 300 kv system including electropolishing of the vacuum chamber, to carry out statistical and physical analyses of the complete block of eight experiment and to finalize the design and selection of factors and levels for the next block experiment.

1.1 300 kv System

The 300 kv system was completely overhauled during the reporting period. The vacuum chamber was electropolished and all flanges and the gold O-ring surfaces polished and machined where necessary. A replacement bakeable column for the feedthrough bushing was installed, baked and vacuum tested. Redesign and test of electrode heater, support and adjusting mechanisms were effected. These remove both heaters and thermocouples from the vacuum envelope. The high voltage power supply was overhauled and the cable and bushing connections were completed for the energy storage system. Evaluation tests have been carried out on the vacuum crowbar for the latter, and a nonlinear current monitor was constructed and installed to measure current buildup.

1.2 The Block of Eight Experiment

Statistical and physical analyses of the results of the block of eight experiment have been carried out. Both prebreakdown current and breakdown voltage values were examined for unconditioned gaps and for conditioned gaps without and with perpendicular magnetic fields. The three other factors were anode and cathode treatment and electrode area. The statistical analysis yielded significant trends for higher order interactions as well as main factor effects. These were observed to be influenced both by conditioning and the presence of the magnetic field. They were also found to be consistent with the model of breakdown developed from the physical analysis.

1.3 Design of Second Block Experiment

The design of the second block experiment has been completed and the factors selected. It will be a 32 treatment 2^5 full factorial experiment

involving 5 inflexible factors. It will be split into two 16 treatment 2^4 full factorial blocks to enable a meaningful analysis to be carried out at the halfway stage and to facilitate the incorporation of three additional flexible factors in parallel experiments. The factors will be as follows:

(1) Inflexible: anode material, cathode material, electrode treatment, anode size and anode shape;

(2) Flexible: magnetic field, gas exposure and stored energy.

The inflexible factors will be examined at two levels and the flexible over a range of values.

SECTION 2

300 KV TEST VEHICLE

2.1 Vacuum Chamber

During the reporting period, overhaul of the vacuum chamber was completed and trial bakeouts carried out. These included the modified electrode heater and support structures which, because of heat transfer problems, needed further modifications. Electrode bake in a 'cold' chamber using the latest version of this electrode-heater structure has yielded temperatures in excess of 400°C at the face of the electrodes. The new bakeable column has been installed in the chamber and has undergone two successful bakeouts to 350°C.

2.1.1 Pumping System

The pumping system described in the Eleventh Quarterly Progress Report has continued to operate satisfactorily. The roughing section consists of one Varian gasp pump and two Varian sorption pumps which are isolated from the main chamber by means of a Varian 1-1/2 inch bakeable valve. The main pumping system consists of one General Electric 500 liters/sec triode ion pump and after trial chamber and electrode bakeouts low 10^{-9} torr pressure has been achieved.

2.1.2 Feedthrough Bushing

A new bakeable column has been installed to replace the unit which was used throughout both the pilot and the block of eight experiment. This has been baked to 350°C in the chamber without developing any vacuum leaks. Subsequently, it withstood 300 kv without difficulty. During this time, it was observed to glow along the alumina rings which were observable through the viewport and not obscured by the electrostatic shield. Upon removal from the chamber all alumina rings were found to be discolored but the electrical characteristics of the bushing were in no way affected. The discoloration was caused by electron bombardment of alumina.

2.1.3 Bakeable Leak Valve

A Varian bakeable leak valve was installed on the vacuum pumping line during the previous reporting period. This can consistently control leaks as small as 1×10^{-10} torr-liters per second and has now undergone two system bakeouts without experiencing problems.

2.2 High Voltage Power Supply

At the conclusion of the 'block of eight' experiment, the grounding solenoid on the Voltronics 300 kv power supply burned out. A complete and modified grounding assembly was supplied by Universal Voltronics. This has been installed and has operated satisfactorily.

To ensure that cable transient times are constant with and without energy storage connected, the next block experiment of 32 treatments will be performed with approximately 25 feet of cable. A schematic diagram is shown in Figure 2-1. The 100 ohm resistor currently in use will need to be replaced by a higher dissipation resistor such as copper sulfate when the energy storage is attached in order to provide the capability of dissipating the maximum energy (viz, 7000 joules).

2.3 Baking System

2.3.1 Chamber

The new heating system described in previous Quarterly Progress Reports has now been successfully operated a number of times and all control and safety devices tested. These included the ion pump pressure relay which cut off the mantle heater power when the ion pump pressure rose to 1×10^{-5} torr and restored it when the pressure dropped back to 3×10^{-6} torr. When system baking temperature (viz, 375°C) at the viewport was achieved, the relay controls maintained this temperature to within 2°C for the duration of the bake. The electrode heater temperature control at the same time was maintained to within 5°C of 450°C. Both electrode temperatures, as well as the chamber temperature, are continuously recorded.

2.3.2 Electrodes

The heater design described in the previous Quarterly Progress Report (Figure 2-2) proved to be inadequate during a trial bake cycle. With the chamber at 370°C and electrode heater temperature controlled at 510°C, the temperature at the electrode surface was only 370°C after four hours. It was later discovered that the high temperature differential was due to poor interface contact which caused the heat transfer coefficient to the electrode to be low. In addition, there were two interfaces, one between the heater and the stainless steel envelope, and the other between the envelope and the electrode. The design was therefore modified to remove one of the interfaces by welding the heater directly into the support shaft, and reducing the tolerance between the heater diameter and the receiving hole in the electrode. The latter produced a push fit heater and resulted in heat transfer through the sides as well as the end of the heater. This is shown in Figure 2-3. It is now fabricated and in a trial bake produced electrode temperatures in excess of 400°C.

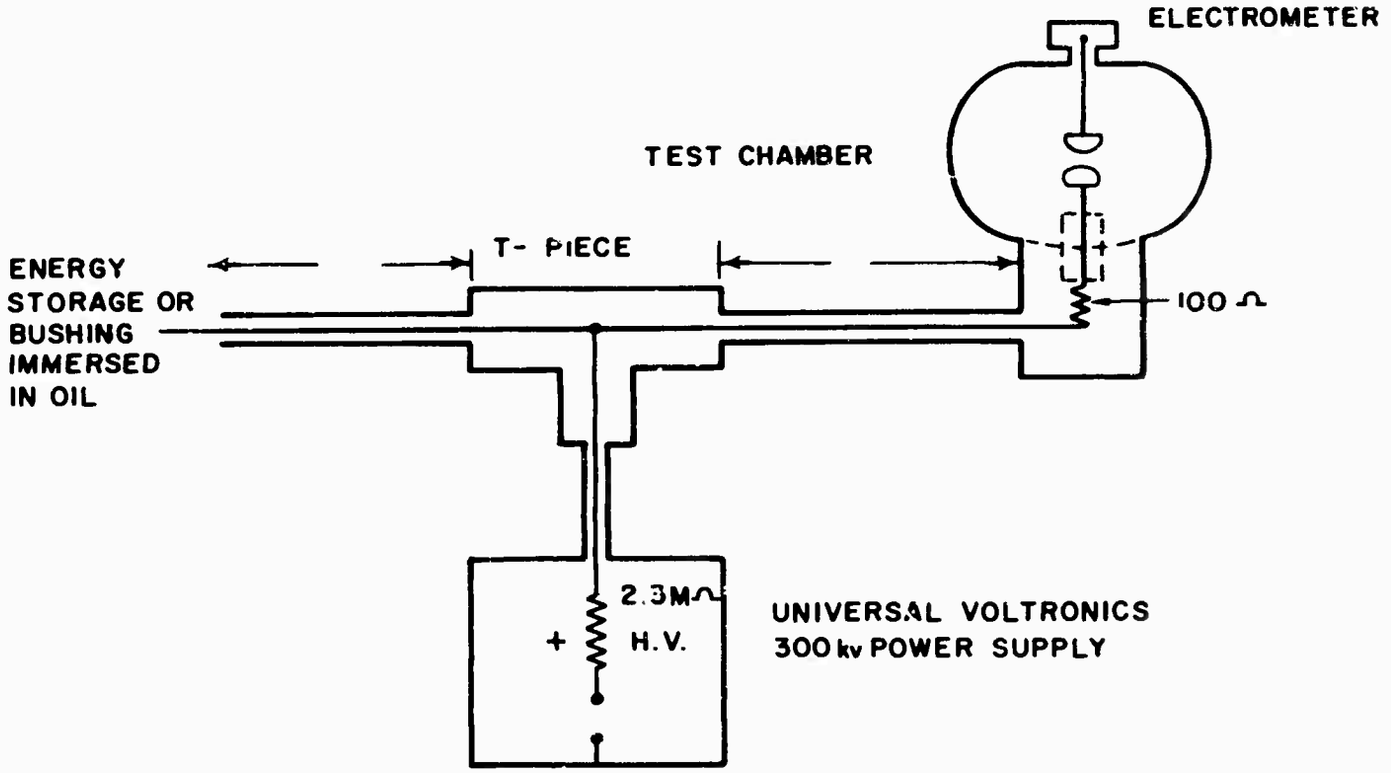

Figure 2-1. Schematic Diagram of High Voltage Circuit

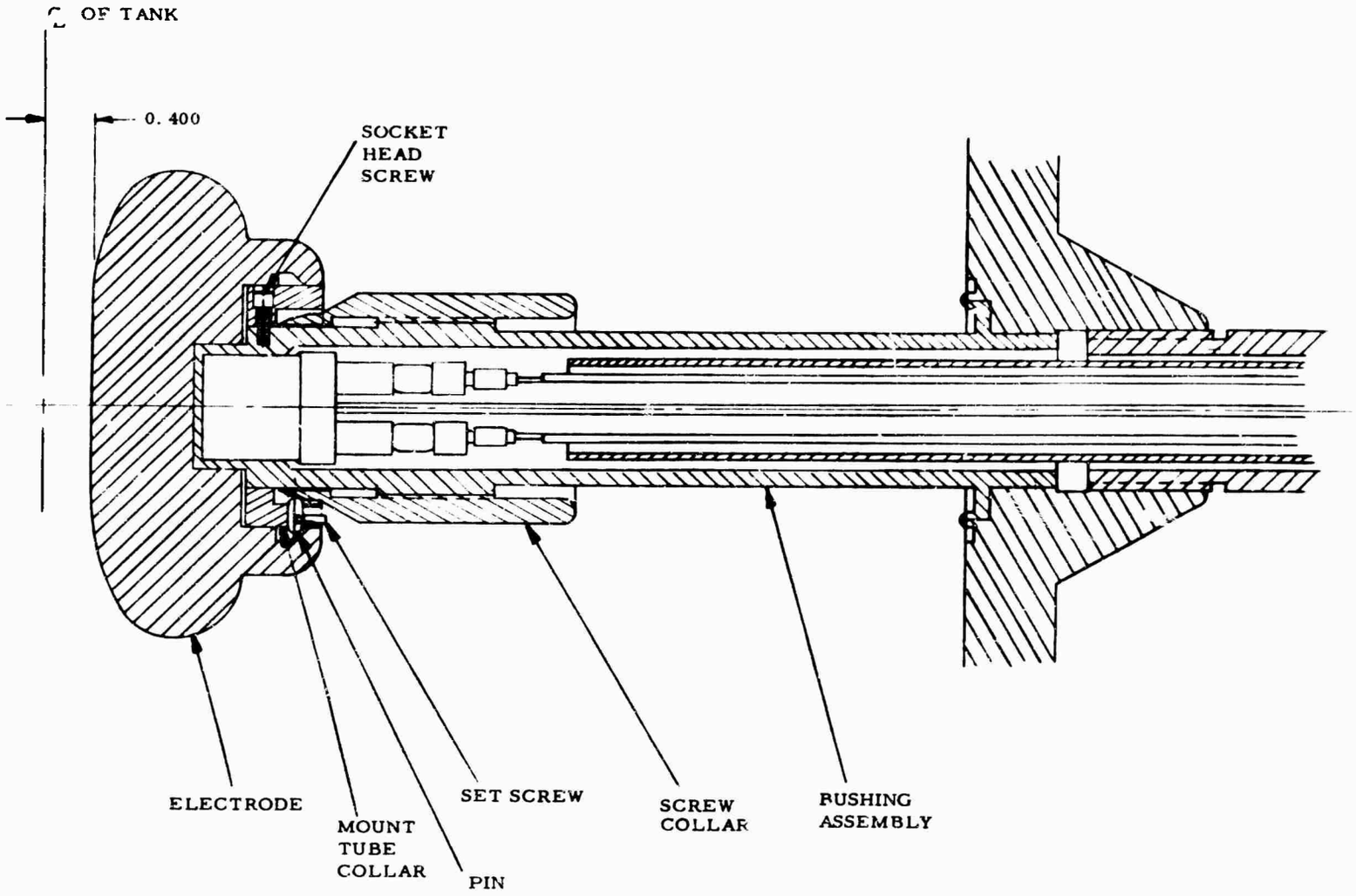

Figure 2-2. Modified Bottom Electrode Support with Quick Disconnect Mechanism

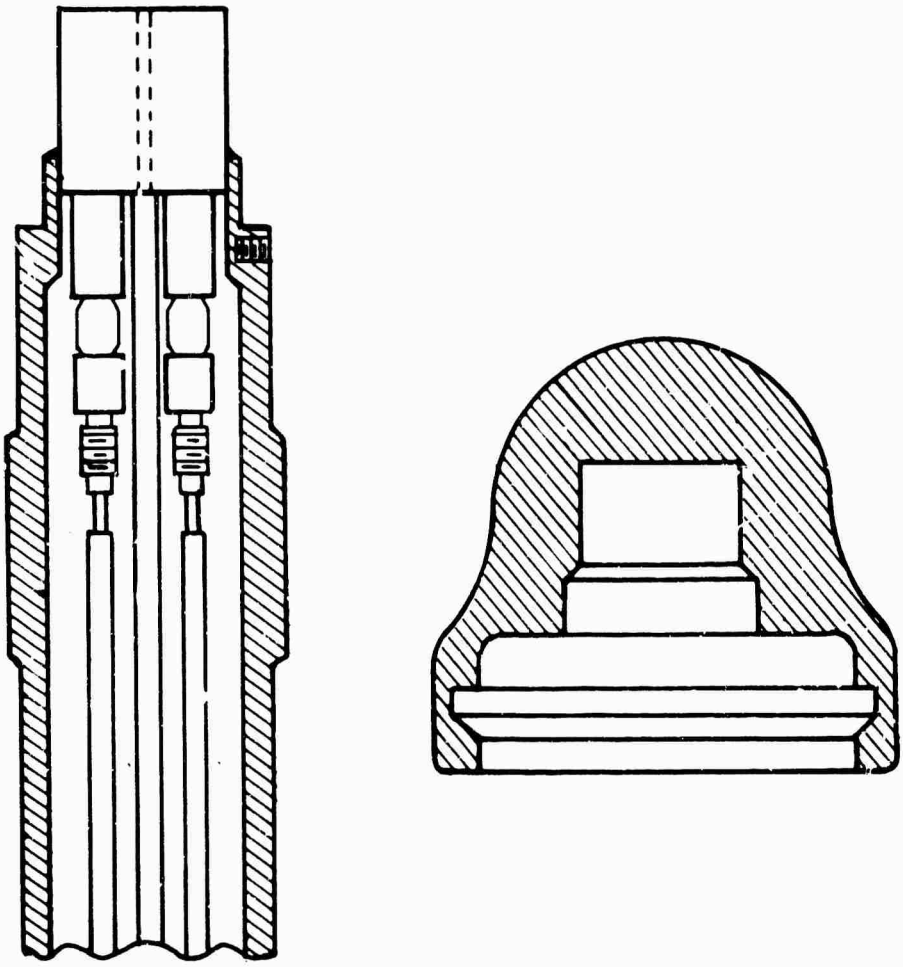

Figure 2-3 Modified New Heater Assembly and
2 Inch Diameter Spherical Cathode

1-2367

2.4 Instrumentation

A non-linear current monitor was constructed from 10 Unitrode diodes (UTR 12) in parallel and may eventually be permanently connected in series with the cathode lead after suitable calibration with a known pulse current source. If it is successful, it will permit observation of current build-up at breakdown from the milliampere to kiloampere range. A trial run on the chamber showed interesting current oscillations in the ampere range which are not easily detectable on the linear Rogowski probe used previously. Typical current and voltage waveforms showing both collapse of voltage and changes in gap current during breakdown are presented and discussed in Section 3.

2.5 Magnetic Field System

The redesign of the pumping system on the chamber has permitted the magnetic field coils to be opened up to 80 deg with a resultant increase in the horizontal field strength to 420 gauss (0.042 inch/m^2) for 300 amperes in each coil. Coil clamps have been fabricated to simplify coil installation and orientation for each treatment.

2.6 Energy Storage System

As indicated in Section 2.2, the cable connecting the energy storage to the power supply and vacuum chamber has been fitted with suitable terminations and installed. Further tests have been carried out on the vacuum crowbar which indicates a 'firing' time of about 5 μsec. Since this may permit excessive discharge of the stored energy across the vacuum gap, back-up designs for a crowbar are currently being studied. The most promising appears to be the IPC pressurized trigger spark gap unit which has a delay time of about 100 nsec down to 50% of the breakdown voltage. Thus, even when added to the trigger circuit delay time of 500 nsec, the total time from initiation of the vacuum gap breakdown to operation of the crowbar would be less than 1.0 μsec.

It is planned to evaluate the vacuum crowbar as soon as possible using a dummy spark gap assembly in conjunction with the energy storage unit.

2.7 Electrode Systems

2.7.1 Electrode Material

Two electrode materials will be used for the next experiment; namely, aluminum and copper. Aluminum was chosen as one of the electrode materials even though it is not a metal used in vacuum tubes because of its wide differences in physical properties from copper, and the initial intention

of this program was to cover as large a range of physical properties of materials as possible.[1]

2.7.2 Electrode Geometry

The cathode size and shape will be held constant throughout the experiment in a 2 inch diameter sphere as shown in Figure 2-3. The anode will be either bruce profile or sphere with diameter of 4 inches or 1.28 inches. The four geometries are shown in Figures 2-4, 2-5, 2-6 and 2-7. For the small diameters the electrode contour is dictated by the heater and gap pumping conductance requirements in addition to the need to produce bruce and spherical profiles in the gap.

2.7.3 Electrode Preparation

Modifications to the procedure for copper described in the previous Quarterly Progress Report will be necessary since the melting point for aluminum is 670°C. Accordingly, the full fabrication, cleaning and firing procedures for both materials are now included.

Copper

(1) Fabrication: The electrodes are machined and ground to a 600 grit silicon carbide finish using green soap and distilled water as a lubricant.

(2) Cleaning:

Wipe with acetone.

Vapor degrease in trichloroethylene until condensation on electrode stops.

Allow electrode to cool to handling temperature (approximately 110°F).

Place in boiling sump of Genesolv-D for 5 minutes.

Place in ultrasonic sump of Genesolv-D for 5 minutes.

Suspend electrode in vapors of Genesolv-D until condensation on electrode stops.

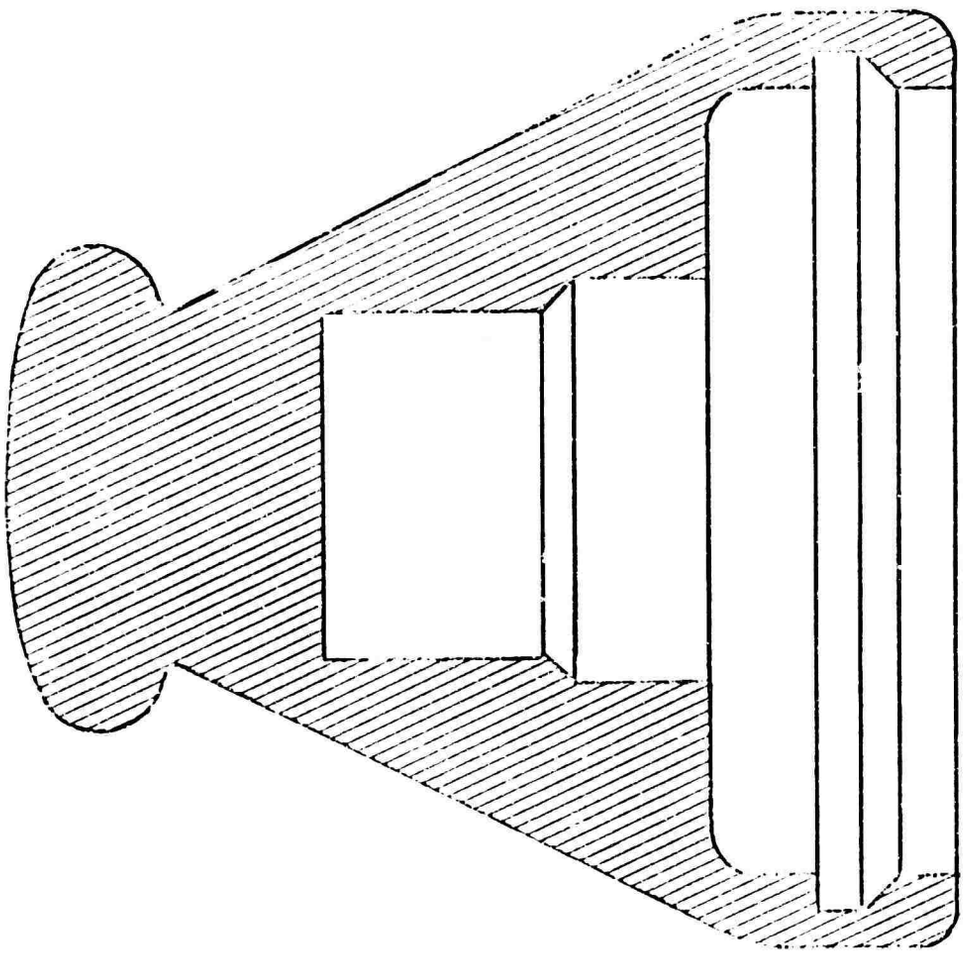

Figure 2-4. Bruce Profile Anode (1.28 Inch Diameter)

1-2368

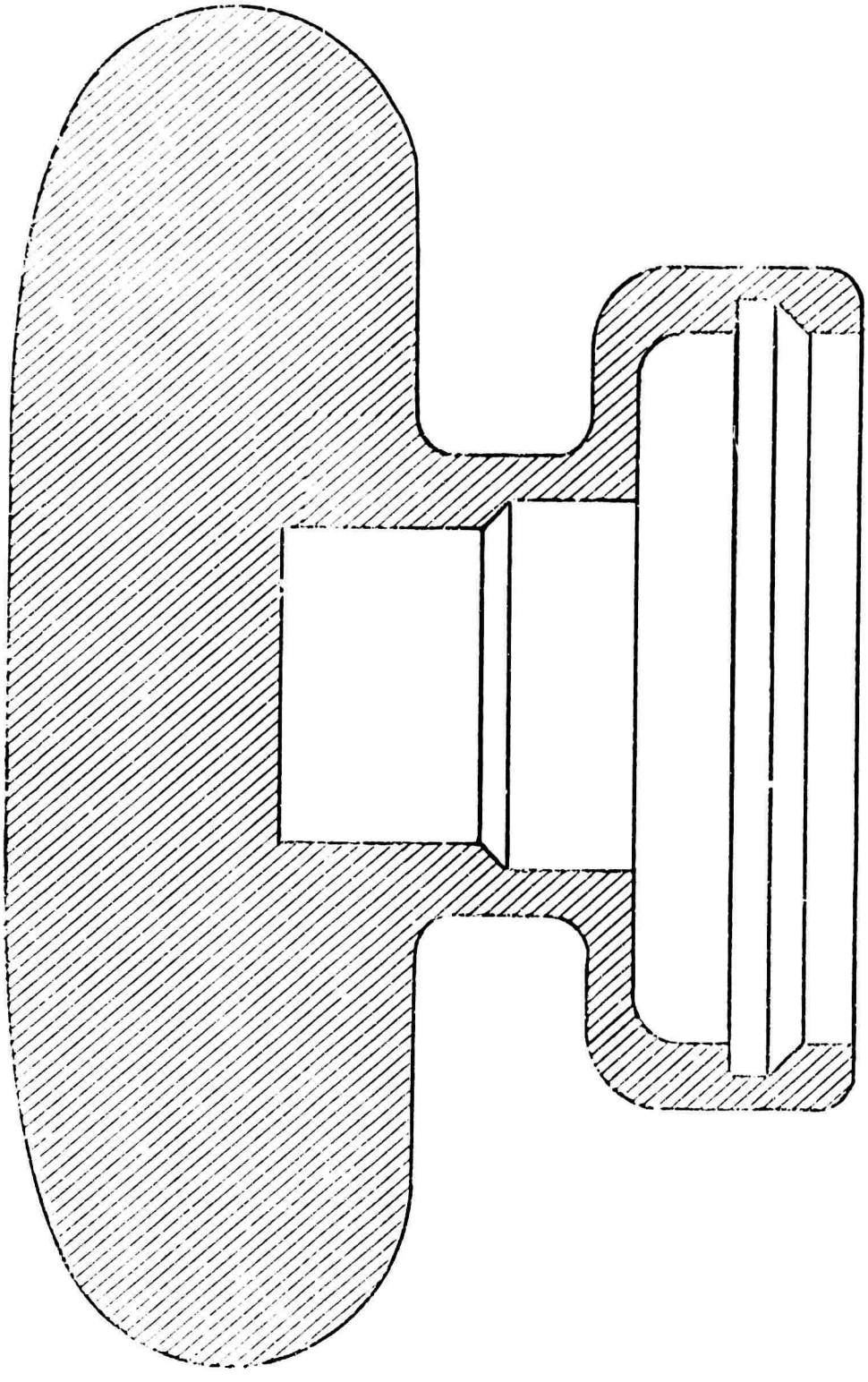

1-2369

Figure 2-5. Bruce Profile Anode (4 Inch Diameter)

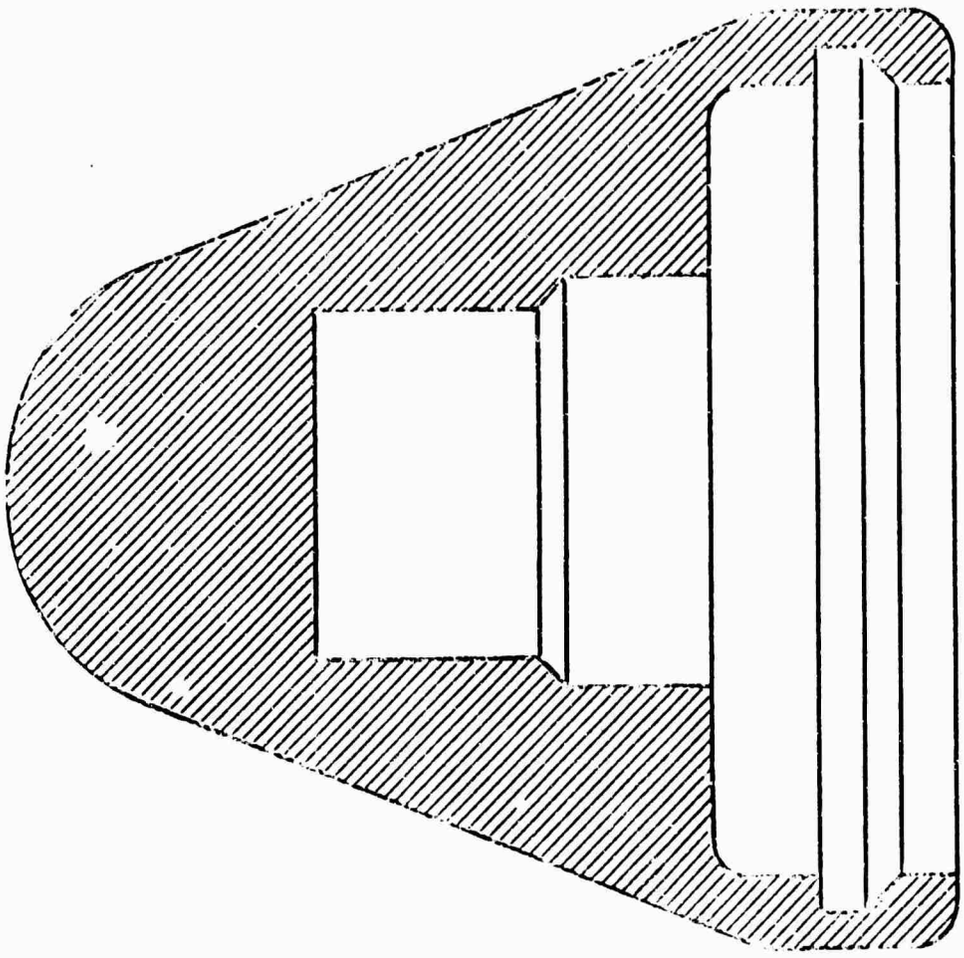

Figure 2-6. Spherical Anode (1.28 Inch Diameter)

1-2370

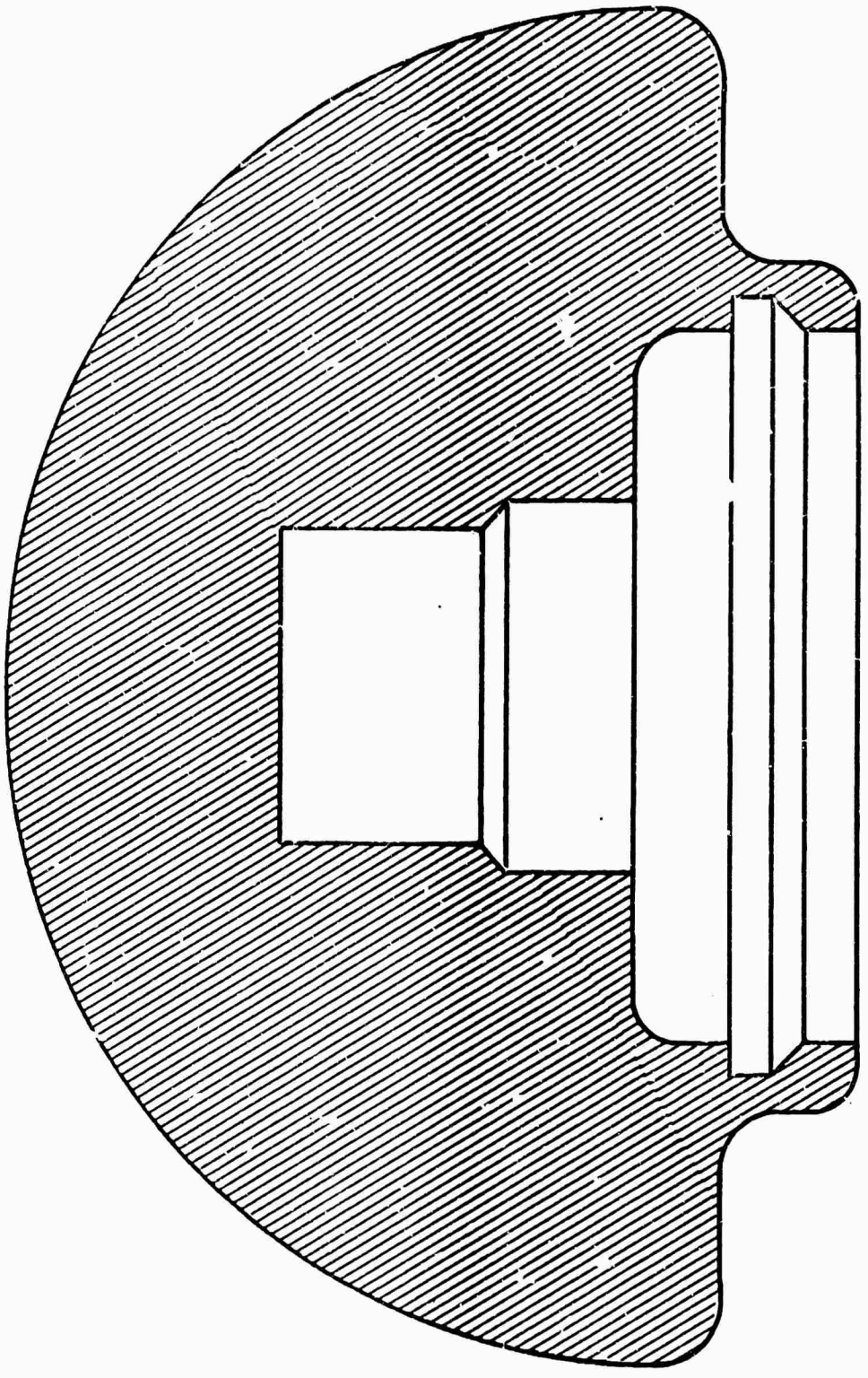

Figure 2-7. Spherical Anode (4 Inch Diameter)

1-2371

Electrodes will be handled only with lint-free cotton gloves after cleaning.

(3) Vacuum Firing: Electrodes are maintained at 900°C in vacuum (< 3×10^{-6} torr) for six hours and then allowed to cool to ambient still under vacuum, at which stage the pressure is about 5×10^{-9} torr. The electrodes are then transported in a dry nitrogen atmosphere to the test chamber.

(4) Hydrogen Firing: Preliminary tests were carried out in which electrodes were fired in vacuum for six hours at 900°C prior to hydrogen firing. This was done because earlier vacuum fired small electrodes had been vacuum etched and it is hoped to produce the same electrode surface structure. Vacuum firing later with large electrodes did not produce this effect and so it was decided to simply fire in hydrogen which is in keeping with high power vacuum tube practice. The firing cycle is as follows: The retort is evacuated and then pure hydrogen introduced at a positive chamber pressure of a few inches of water and the electrodes baked at 900°C for six hours. The hydrogen flow is maintained during cooling to 250°C and is followed by pure nitrogen cooling to 50°C. (Both hydrogen and nitrogen are maintained in a dry state).

Aluminum

(1) Fabrication and Cleaning: Same as for copper.

(2) Vacuum and Hydrogen Firing: Both are carried out at 600°C. Otherwise the procedure is the same as for copper. Currently, samples of aluminum are undergoing trial firing at 600°C in vacuum and in hydrogen. The samples will then be analyzed for hydrogen content. These tests will determine if diffusion of hydrogen into aluminum at high temperature will cause crevices within the metal or surface blisters. Available information indicates that hydrogen is soluble in solid and molten aluminum and apparently forms a hydride with difficulty; a catalyst is needed. Hydrogen from a cylinder did not affect the tensile properties of 2024-Te aluminum alloy which was heated at 920 to 930°F for 20 hours.

2.7.4 Assembly and Installation

The new quick connect/disconnect electrode assembly unit described in the previous Progress Report has operated satisfactorily during the reporting period. The heater and thermocouple feedthrough have been eliminated from the anode support structure and it is anticipated that they will be eliminated from the cathode structure during the current period.

2.7.5 Stress Magnification for the Block Experiment

A scaled up model (2 inch diameter Bruce profile electrodes) was set up in the electrolytic tank and an equipotential plot taken. From the results, a stress magnification plot for a 3 cm gap was obtained and is shown in Figure 2-8. By extrapolating to the electrode surface, it is seen that the field at the electrode is approximately 20% higher than the mean field.

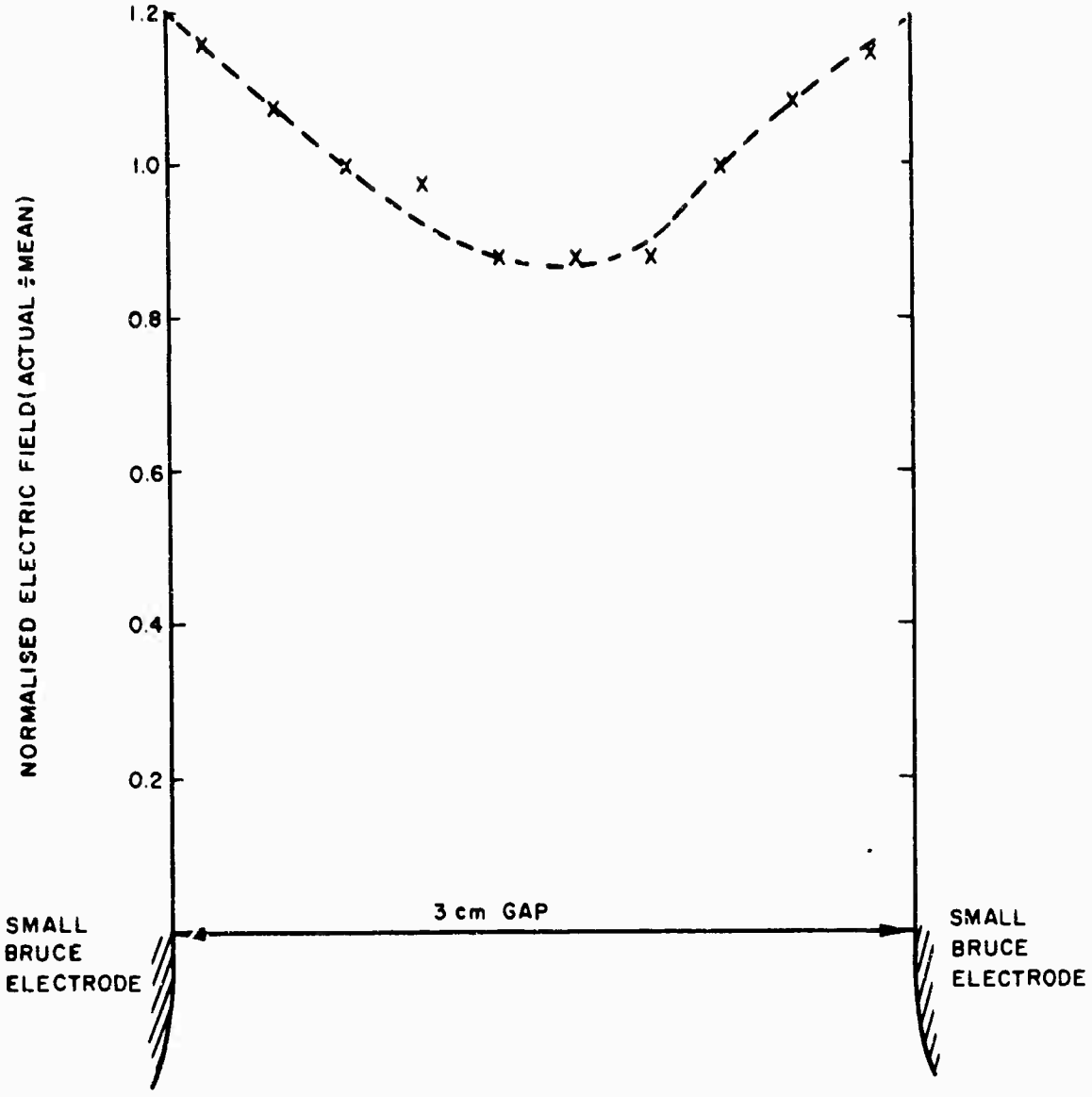

Figure 2-8. Normalized Electric Field for 2 Inch Diameter Bruce Profile Electrodes with 3 cm Gap

1-2372

SECTION 3

STATISTICAL ANALYSIS OF THE RESULTS OF "BLOCK OF EIGHT" EXPERIMENT

3.1 General

The following analyses were carried out to extract as much information as possible from the above experiment. By way of explanation the experiment was run according to Table 3-1 which explains the technique of "stacking". The main part was carried out by investigating the results in the top row. This consisted of measuring the breakdown voltages in 0.25 cm intervals from 0.50 to 3.0 cm in the following gap sequence.

			1.00	1.25	1.50	1.75	2.00	2.25	2.50	2.75	3.00
0.25	0.50	0.75	1.00	1.25	1.50	1.75	2.00	2.25	2.50	2.75	3.00
0.25	0.50	0.75	1.00								

It is readily seen that 25 breakdowns occurred and there were 12 breakdowns between successive tests at any one gap separation. The first and second result for any size gap were therefore referred to arbitrarily as, "unconditioned" and "conditioned" respectively.

The effects of the various factors and interactions have been derived by applying the Yates Algorithm to both sets of data and the results are presented in Tables 3-2 and 3-3 and Figures 3-1 through 3-23. The second row consists of the experiment described in the previous Quarterly Progress Report in which the various factors and interactions were studied with and without the magnetic field applied.

Finally another experiment was performed on an informal basis in the sense that investigations were made into the breakdown voltage as a function of transverse magnetic field for various magnetic field strengths up to 250 gauss. Measurements were made arbitrarily at 2.0 and 3.0 cm gap separations so the results are arbitrarily confounded somewhat with gap separation. With this in mind however, the percentage change in breakdown voltage was calculated and the effect on breakdown voltage was derived by application of the Yates Algorithm. These results are presented in Figures 3-24 through 3-31.

Further to this the average value of the logarithm of the ultimate prebreakdown current was analysed in the same way for the second row experiment and the results appear in Table 3-4 and Figures 3-32 through 3-46.

This pattern of investigation has thus been demonstrated to be highly efficient in terms of output per experiment because each row or "stack" is an independent experiment repeated with magnetic field strength as a flexible factor.

Table 3-1. Technique for Stacking for Block Experiment

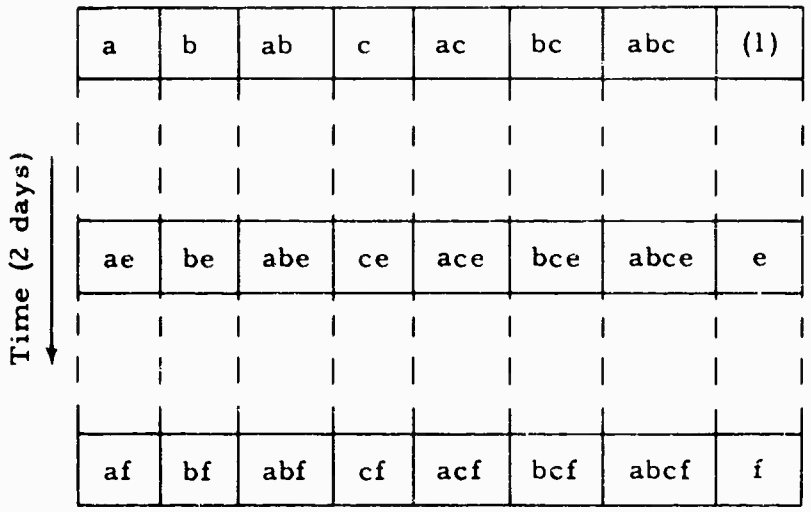

Table 3-2. Yates Algorithm for Unconditioned Gaps without Magnetic Field

	Gap (cm.)							
			1.0					
	0.5	0.75	Upper	Lower	1.5	2.0	2.5	3.0
μ	76	84	61	79	103	119	138	155
A	-17	-39	-10	-17	- 18	- 26	- 20	- 29
B	- 2	-22	-27	-17	- 8	- 23	- 20	- 11
AB	14	- 8	- 9	- 3	- 3	- 20	- 25	- 19
C	-13	-30	-28	-13	- 22	- 41	- 40	- 29
AC	8	- 1	4	13	24	23	35	39
BC	16	- 9	3	23	12	16	15	1
ABC	22	- 1	-15	- 3	9	12	20	19

Table 3-3. Yates Algorithm for Conditioned Gaps without Magnetic Field

	Gap (cm)						
	0.5	0.75	1.0	1.5	2.0	2.5	3.0
μ	93	106	128	142	151	169	171
A	-15	- 15	- 6	2	- 8	- 13	- 14
B	4	- 2	- 8	- 22	18	- 23	- 32
AB	- 4	- 9	- 2	- 10	2	- 13	4
C	-23	- 19	- 36	- 39	- 43	- 58	- 67
AC	12	18	16	34	37	43	29
BC	4	5	18	0	17	13	17
ABC	17	23	22	18	27	13	2

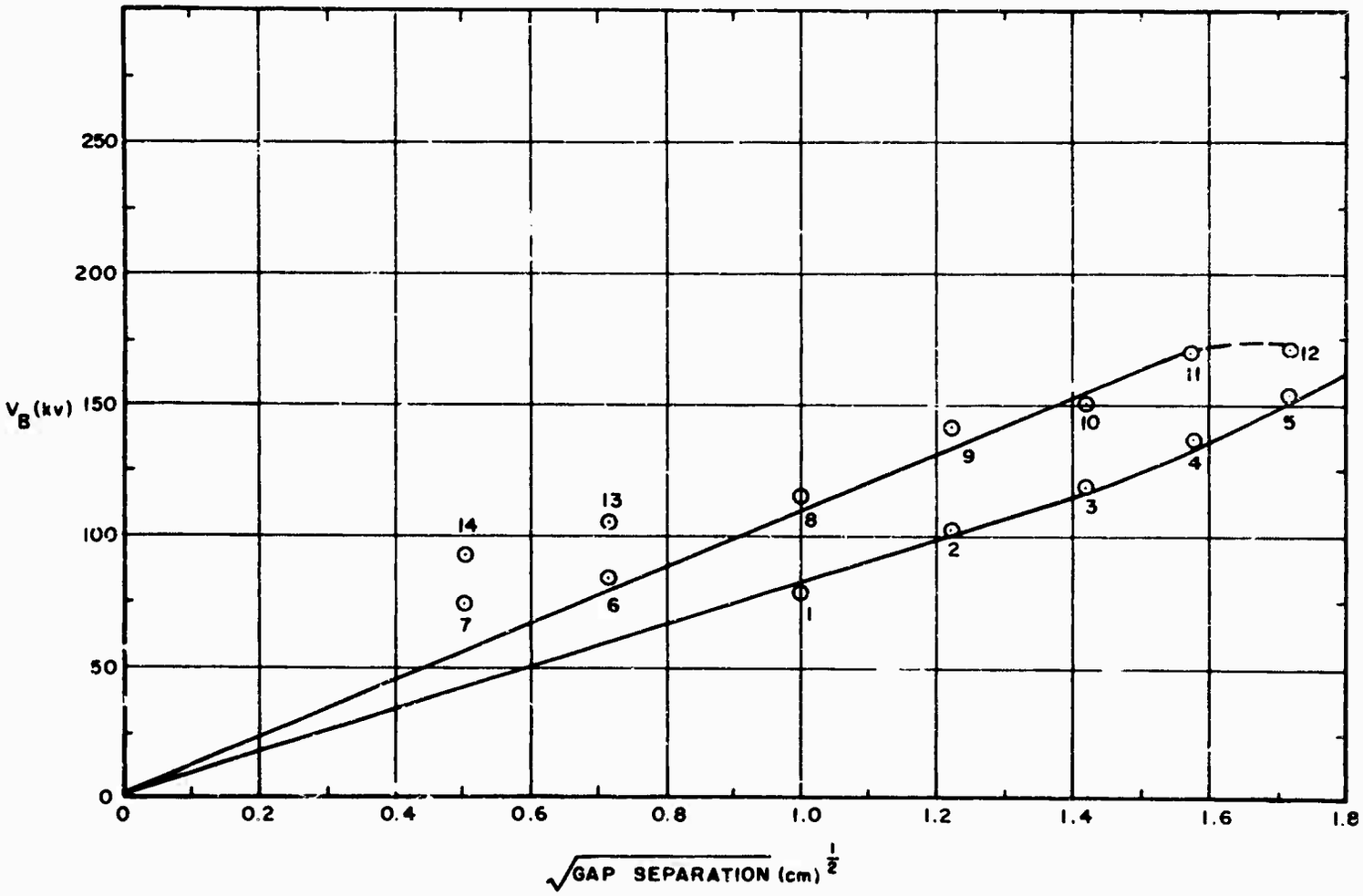

Figure 3-1. The Mean Breakdowr Voltages and Test Sequence

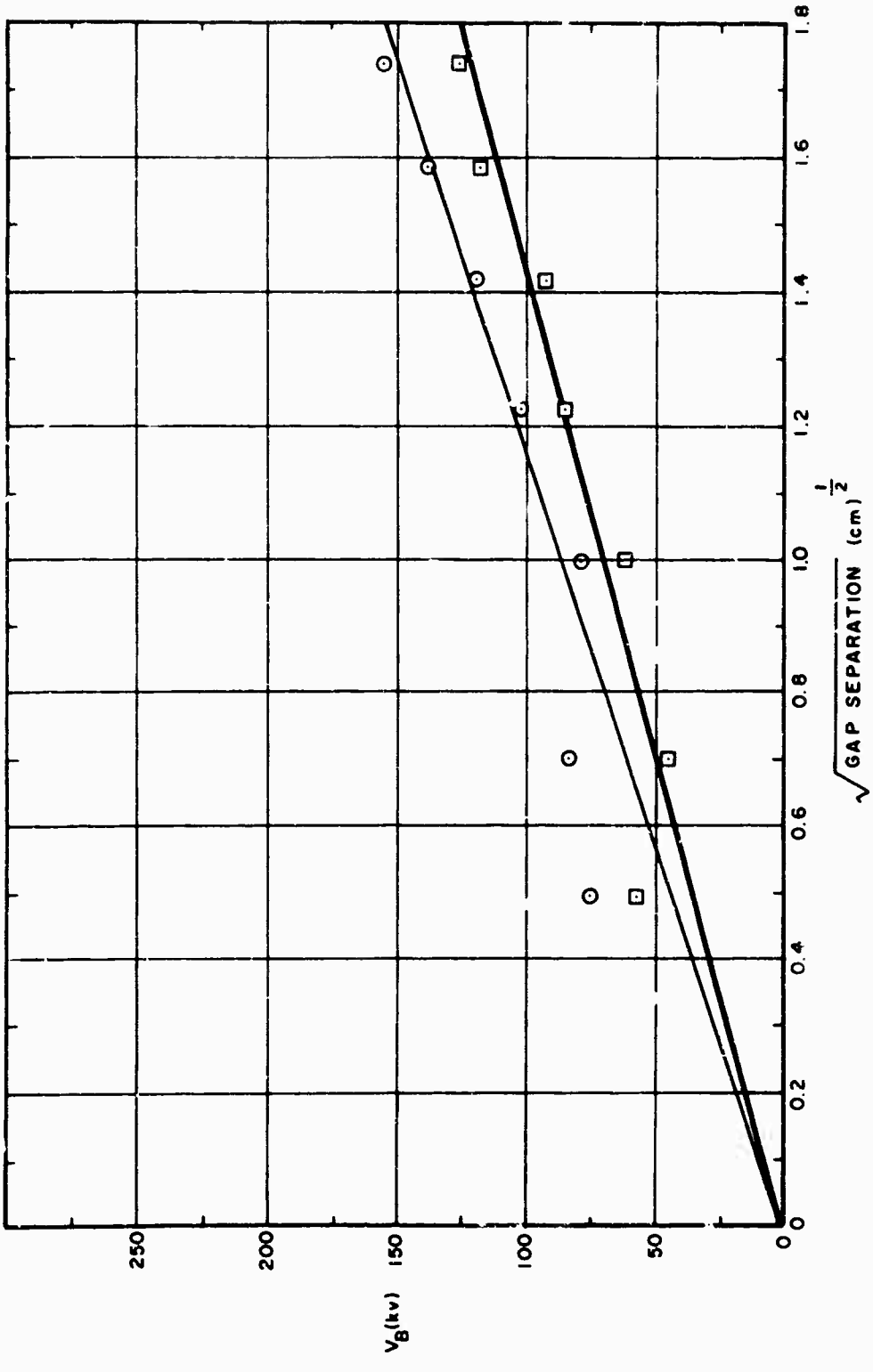

Figure 3-2. A Effect (Unconditioned)

1-2385

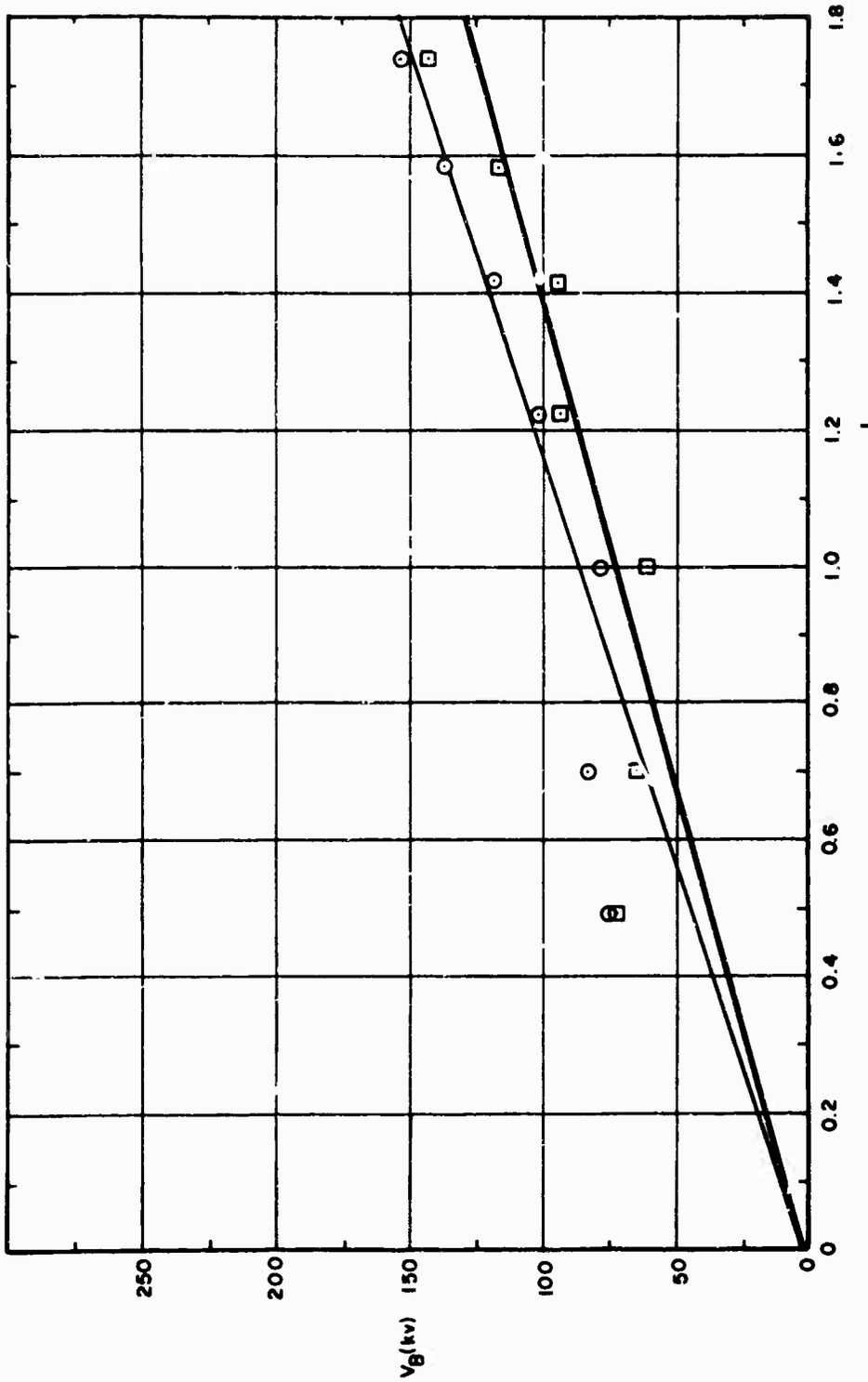

Figure 3-3. B Effect (Unconditioned)

1-2386

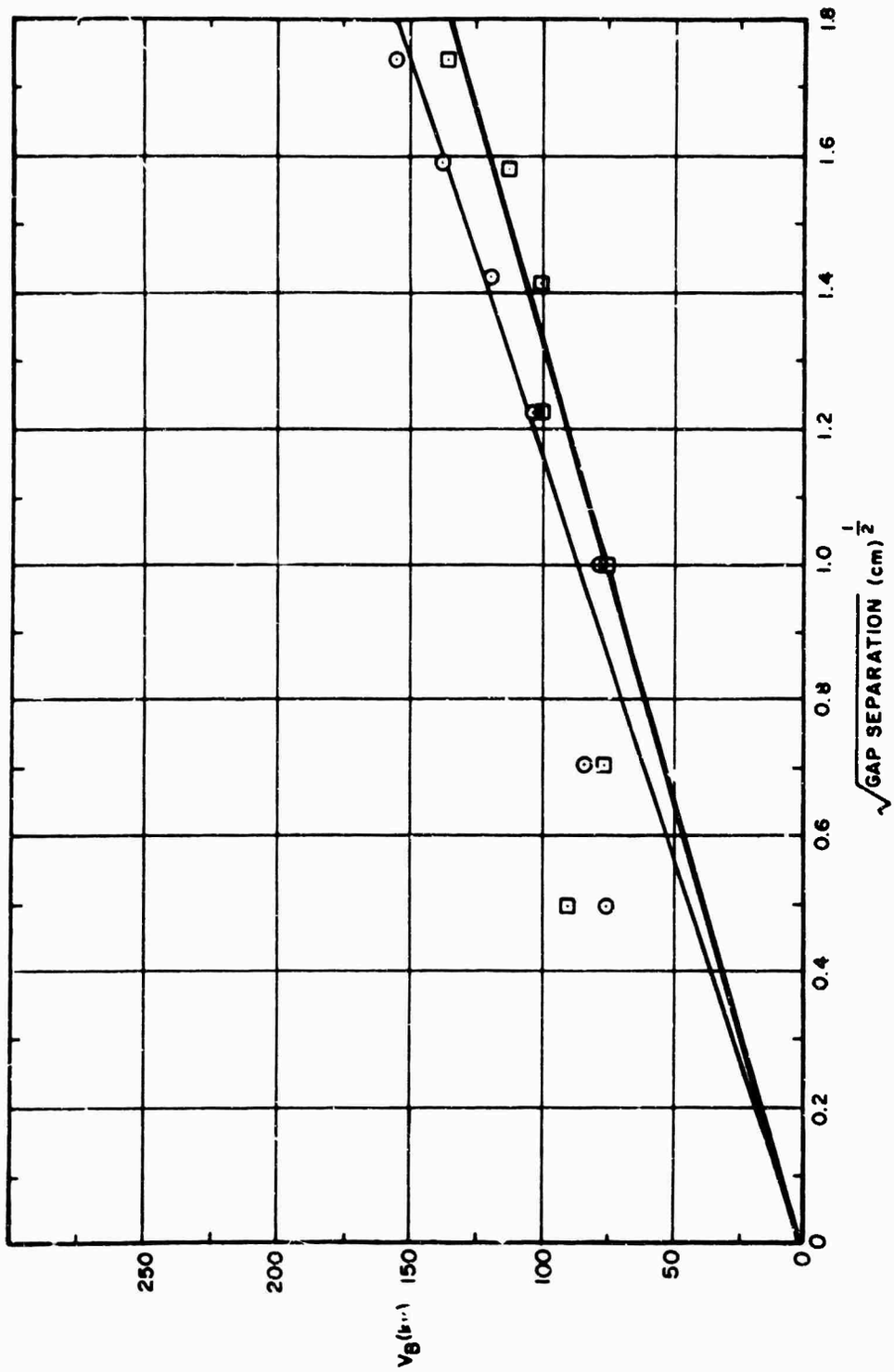

1-2387

Figure 3-4. AB Effect (Unconditioned)

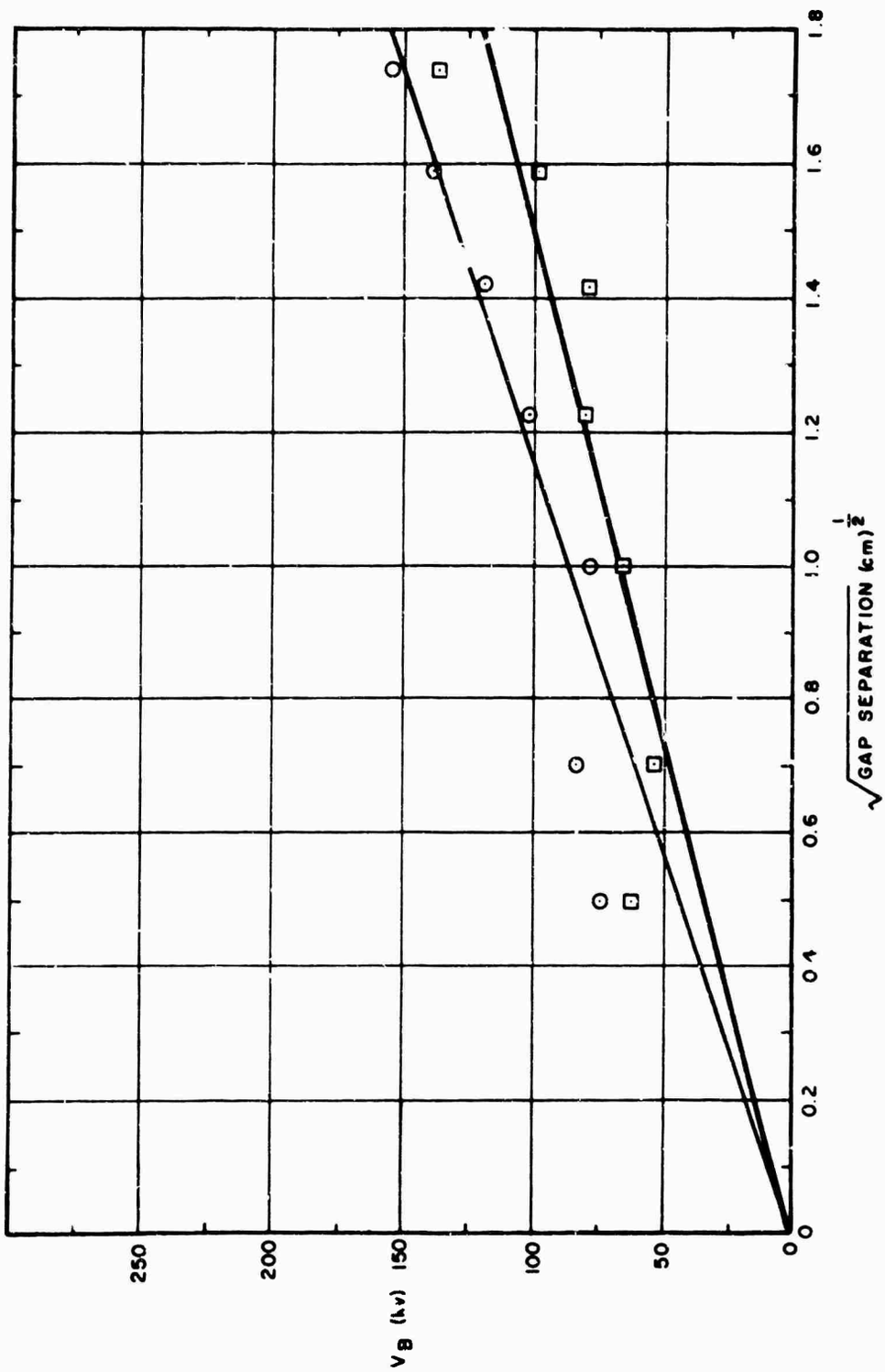

Figure 3-5. The C Effect (Unconditioned)

1-2388

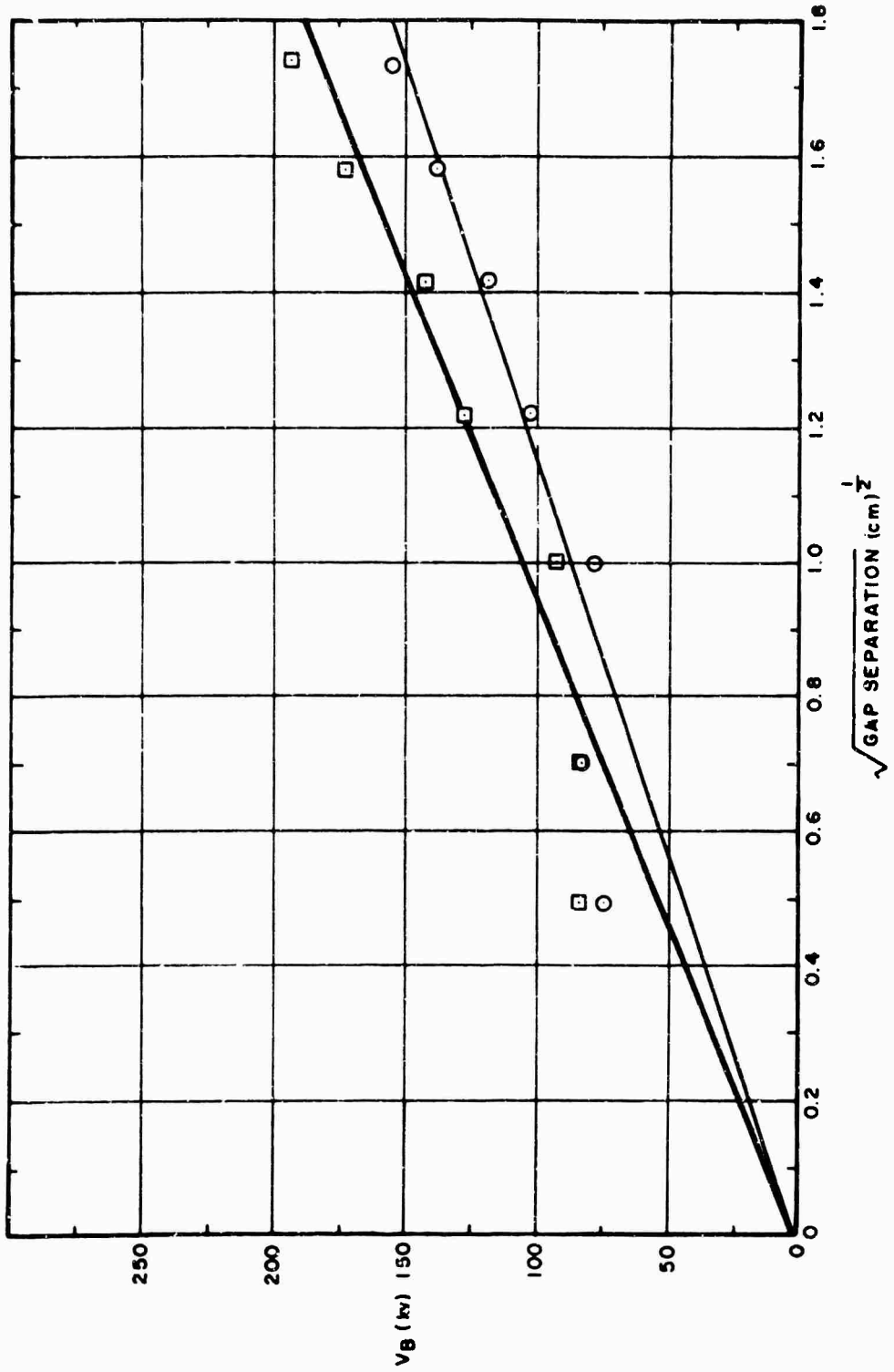

Figure 3-6. AC Effect (Unconditioned)

1-2389

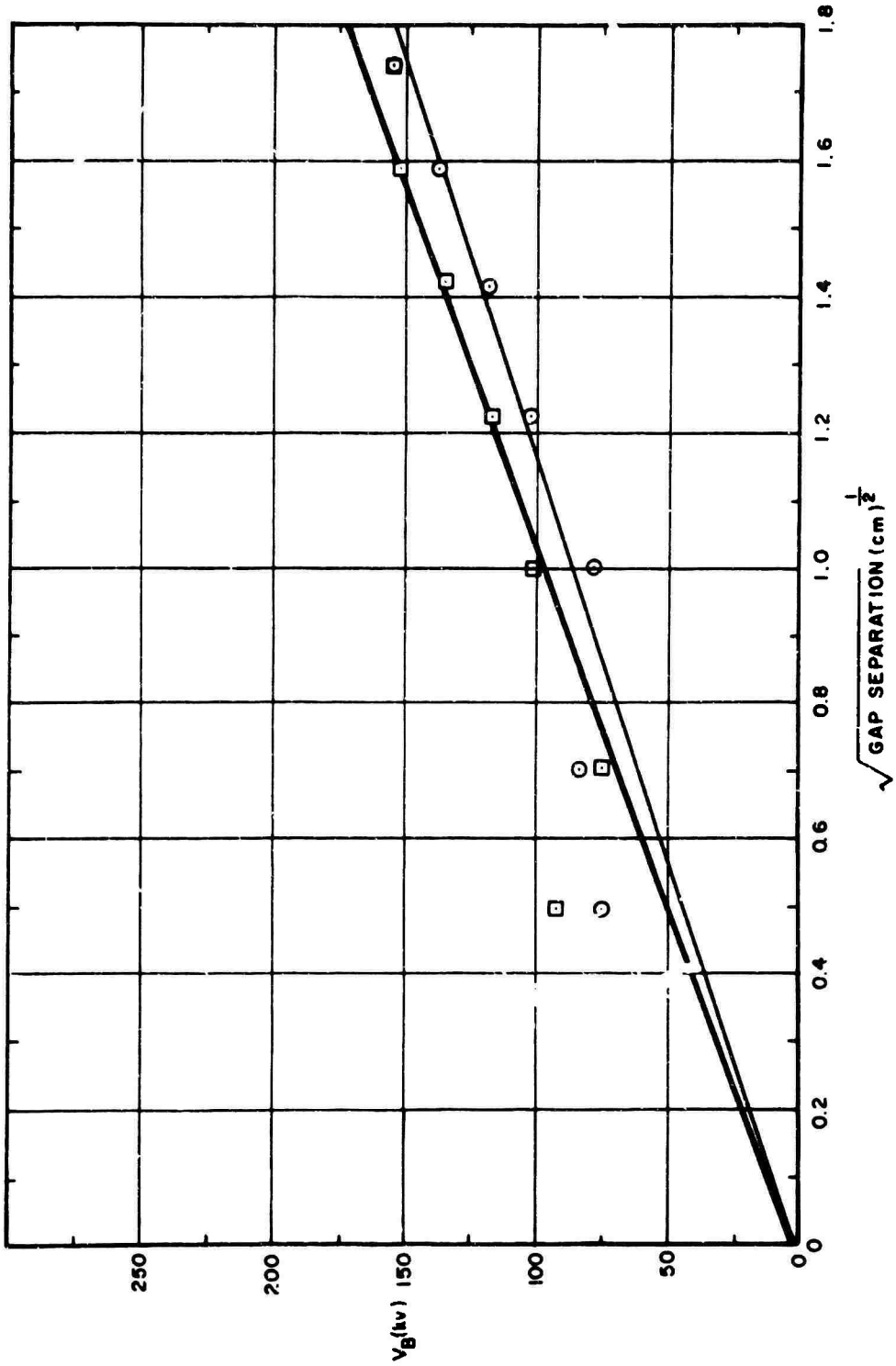

Figure 3-7. BC Effect (Unconditioned)

1-2390

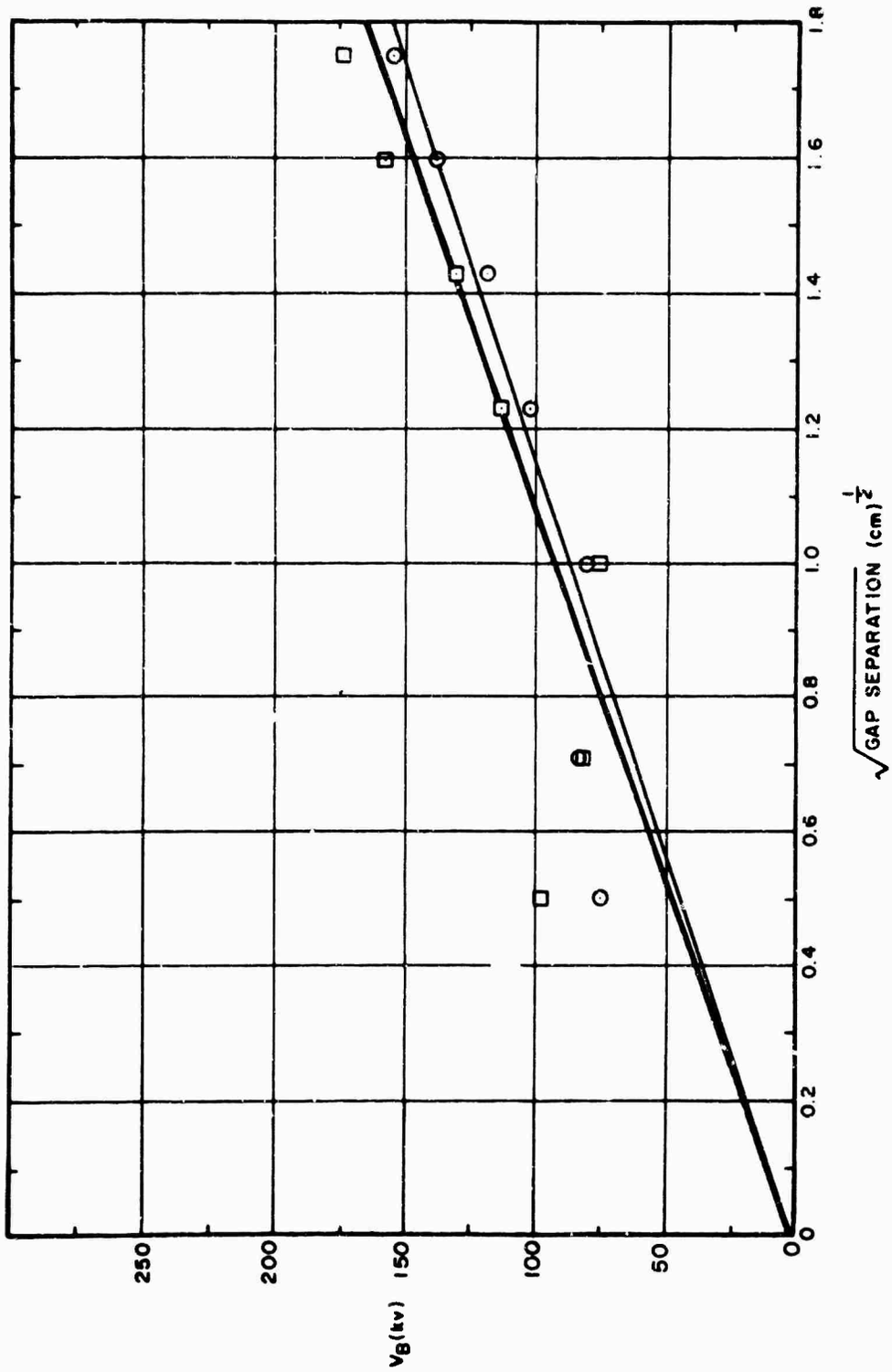

Figure 3-8. ABC Effect (Unconditioned)

1-2391

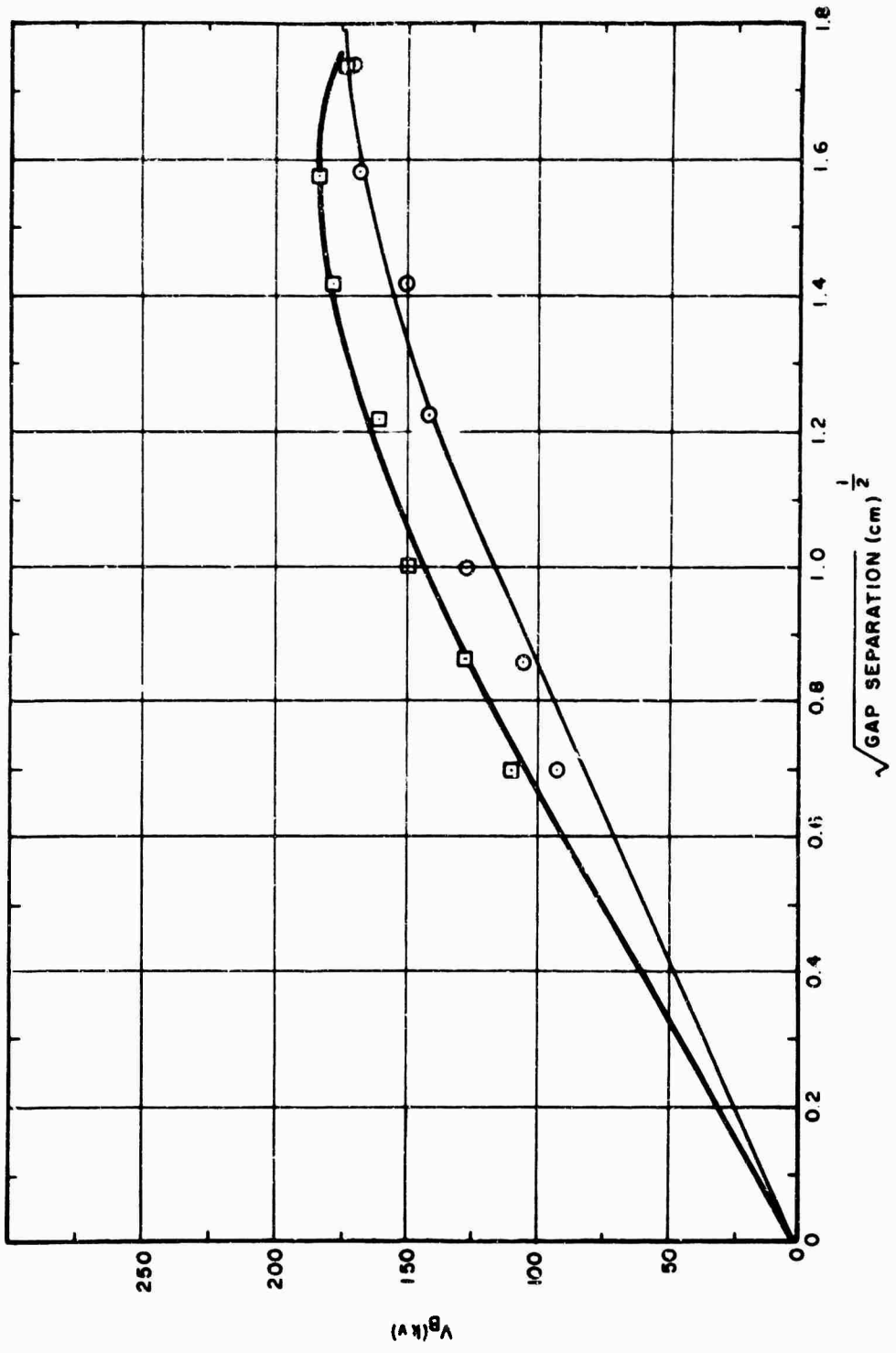

Figure 3-9. ABC Effect (Conditioned)

1-2392

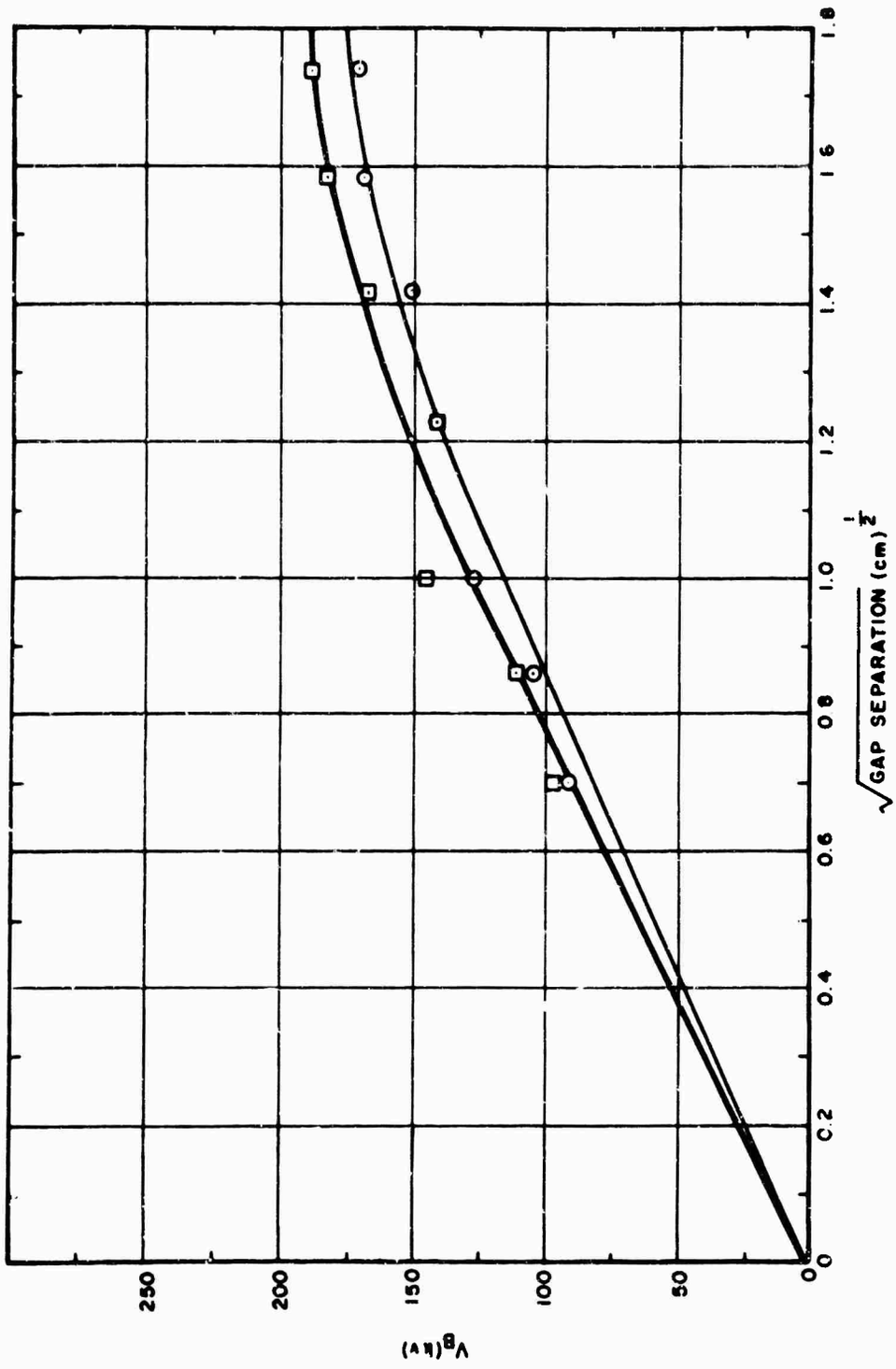

1-2393

Figure 3-10. BC Effect (Conditioned)

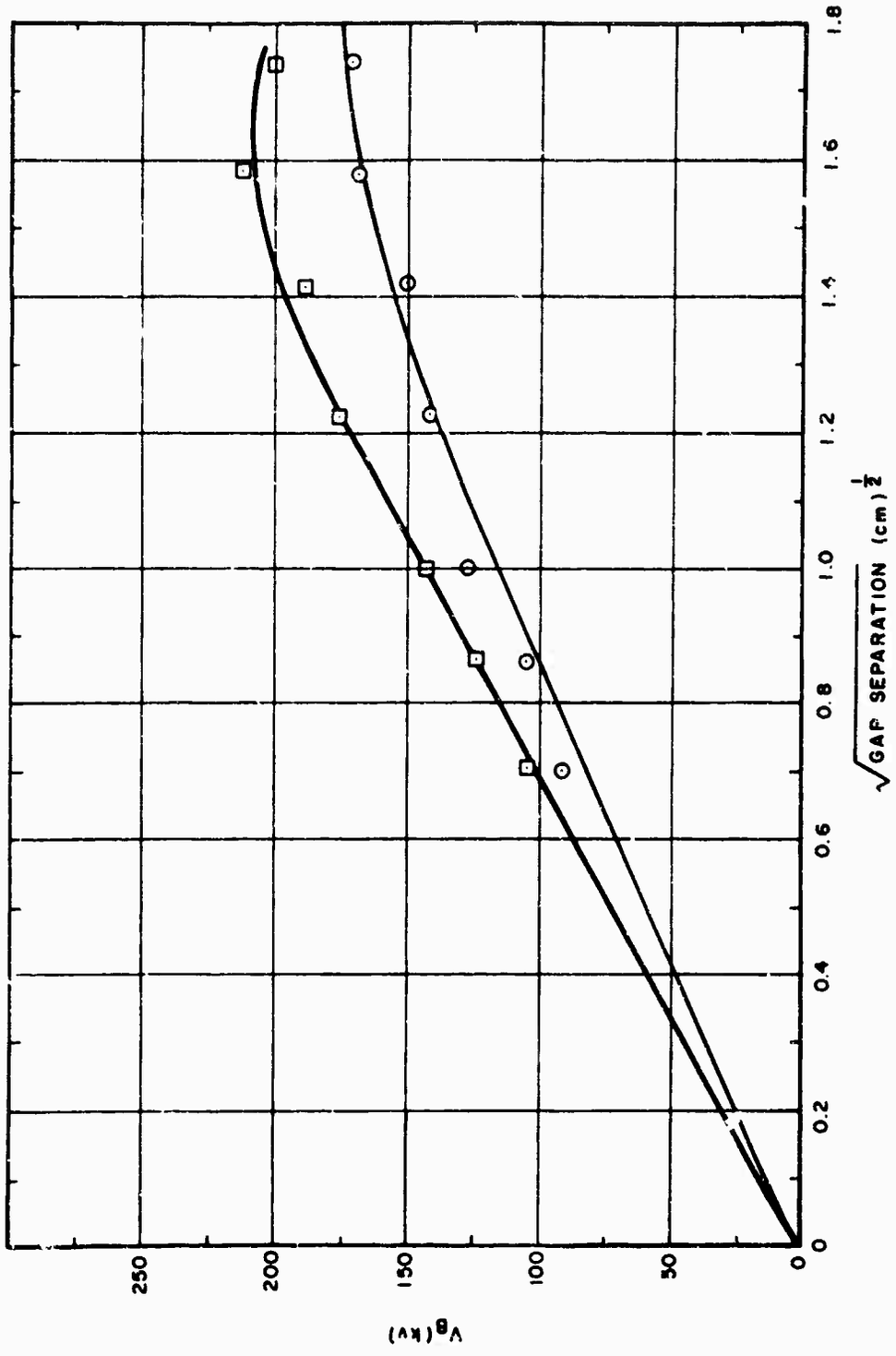

Figure 3-11. AC Effect (Conditioned)

1-2394

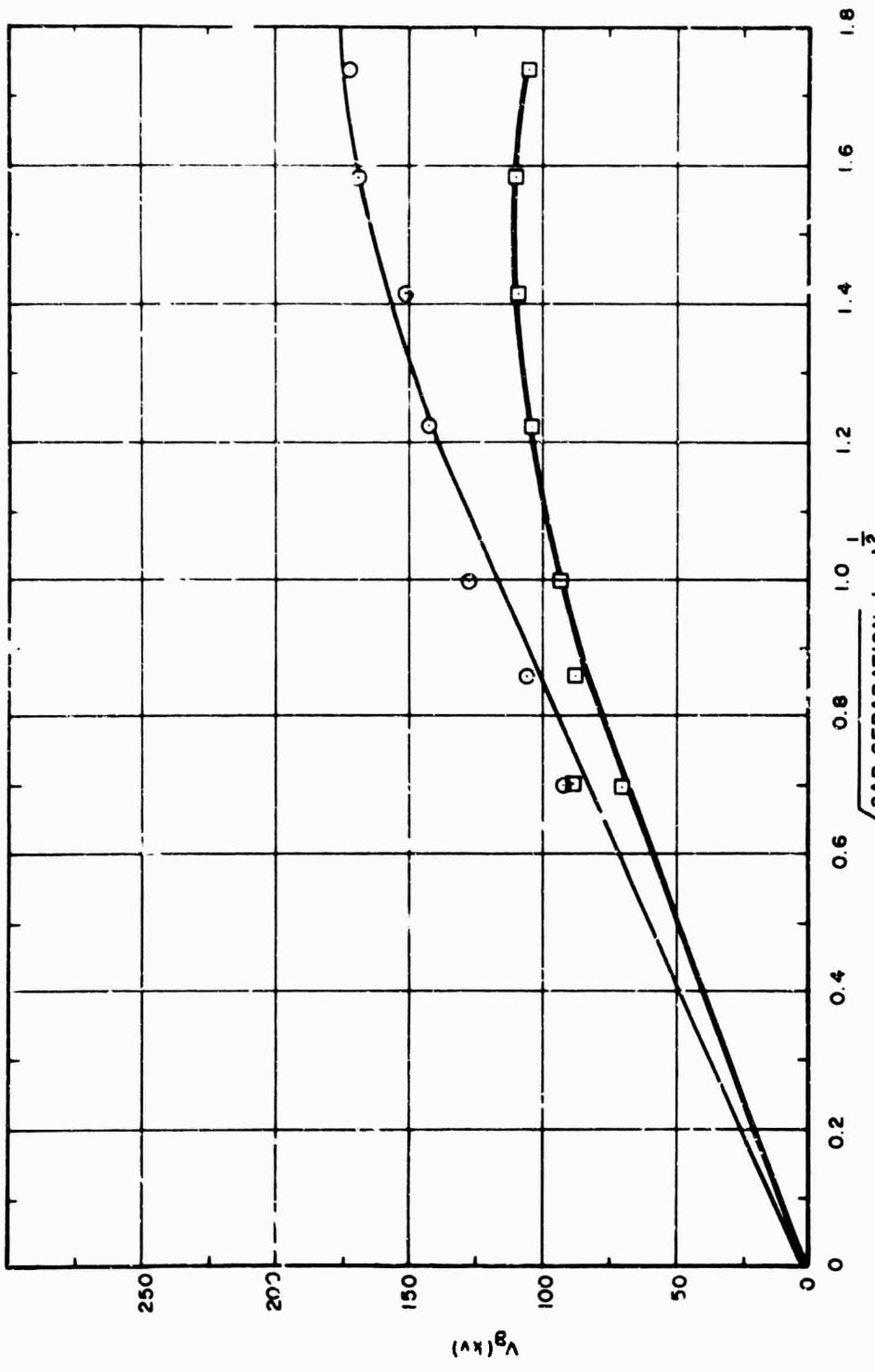

Figure 3-12. C Effect (Conditioned)

1-2395

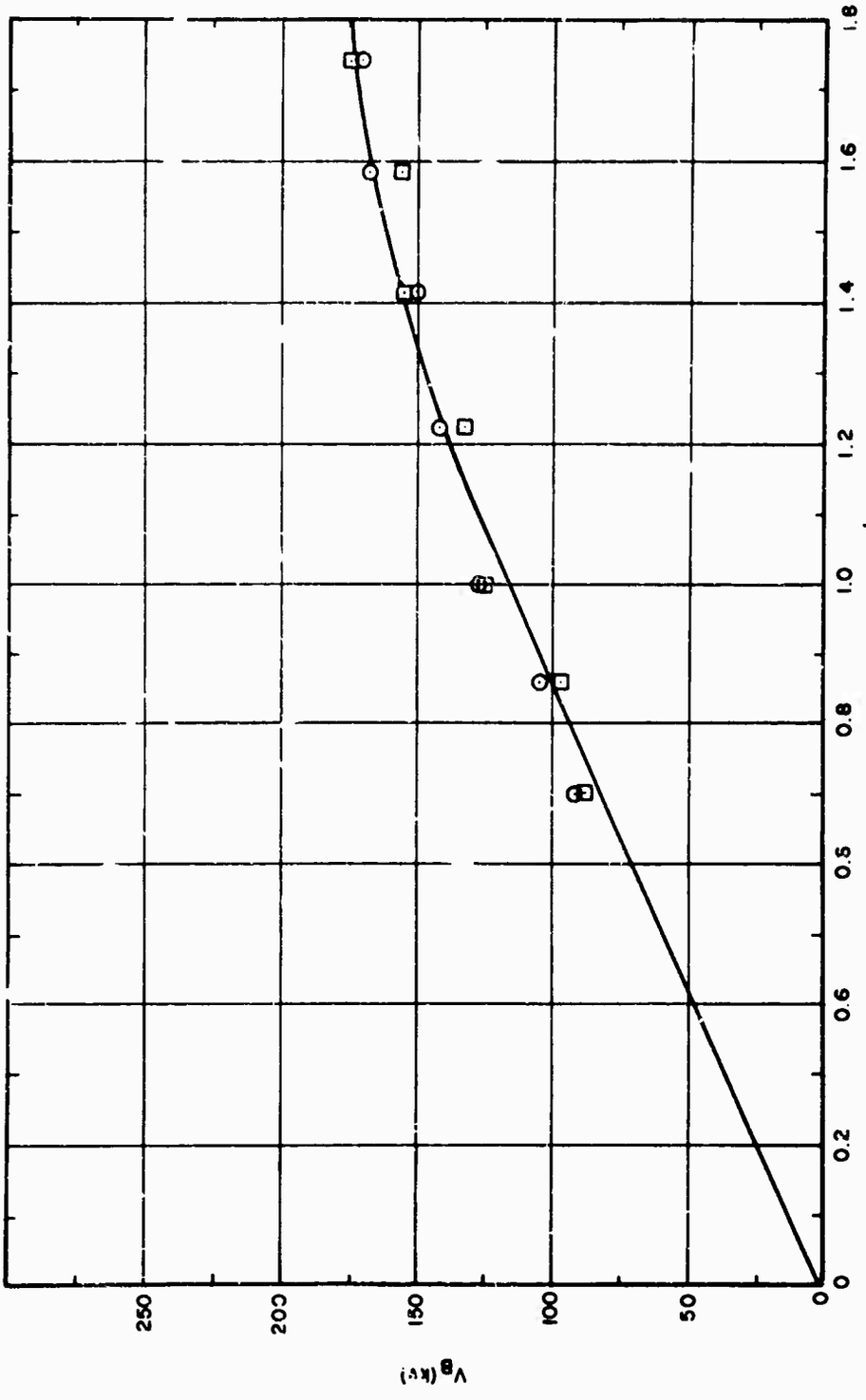

Figure 3-13. AB Effect (Conditioned)

1-2396

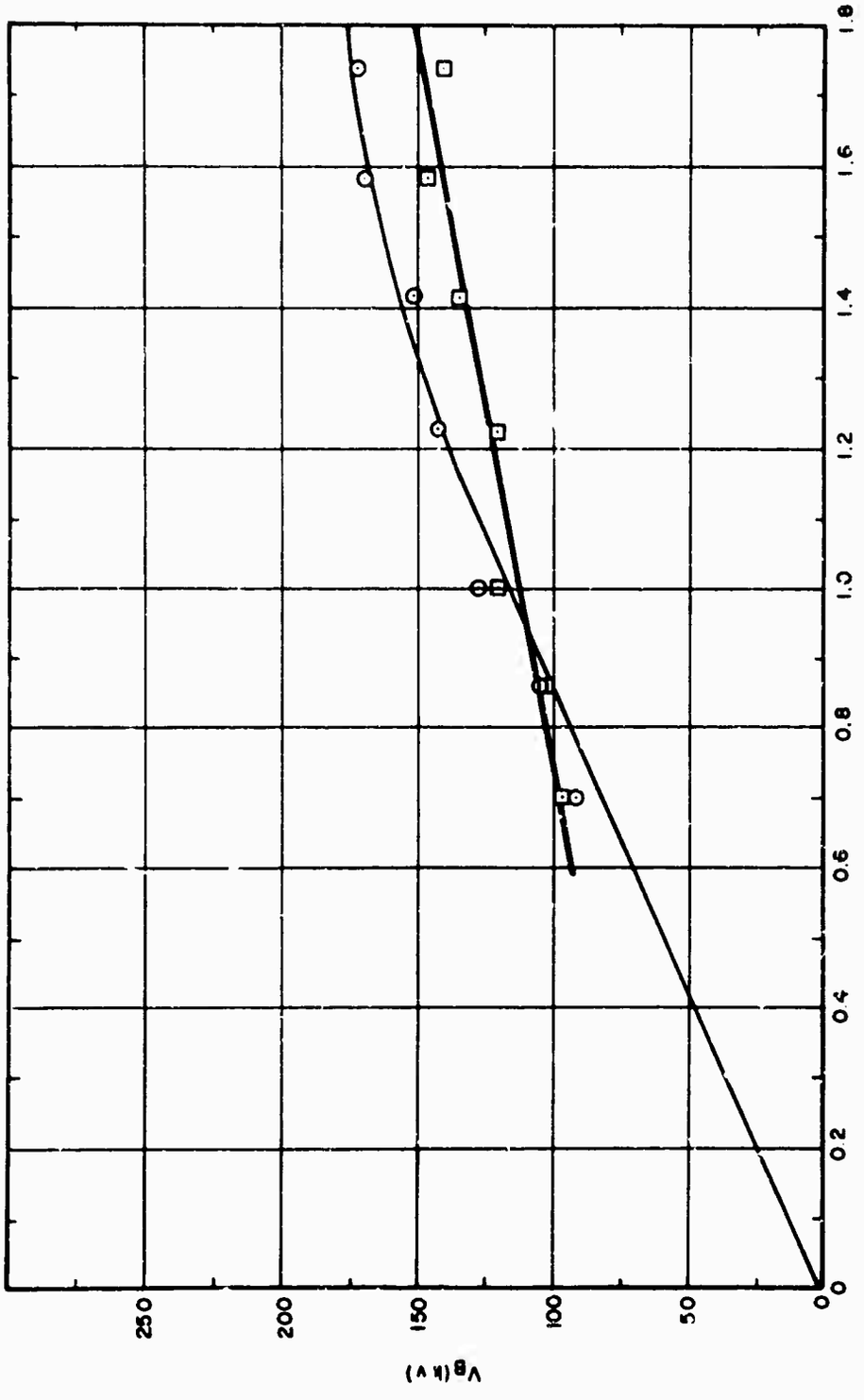

Figure 3-14. B Effect (Conditioned)

1-2397

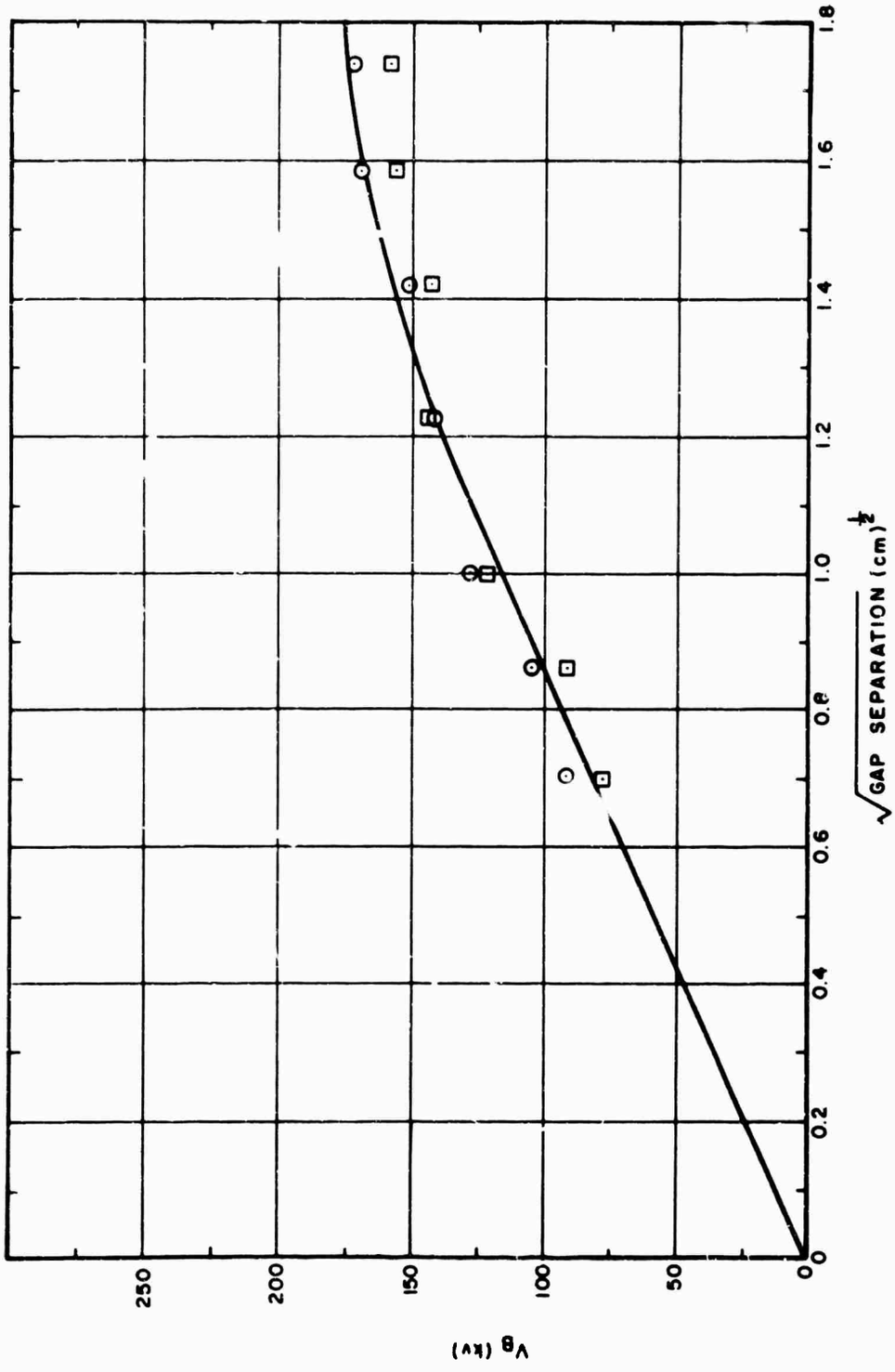

Figure 3-15. A Effect (Conditioned)

1-2398

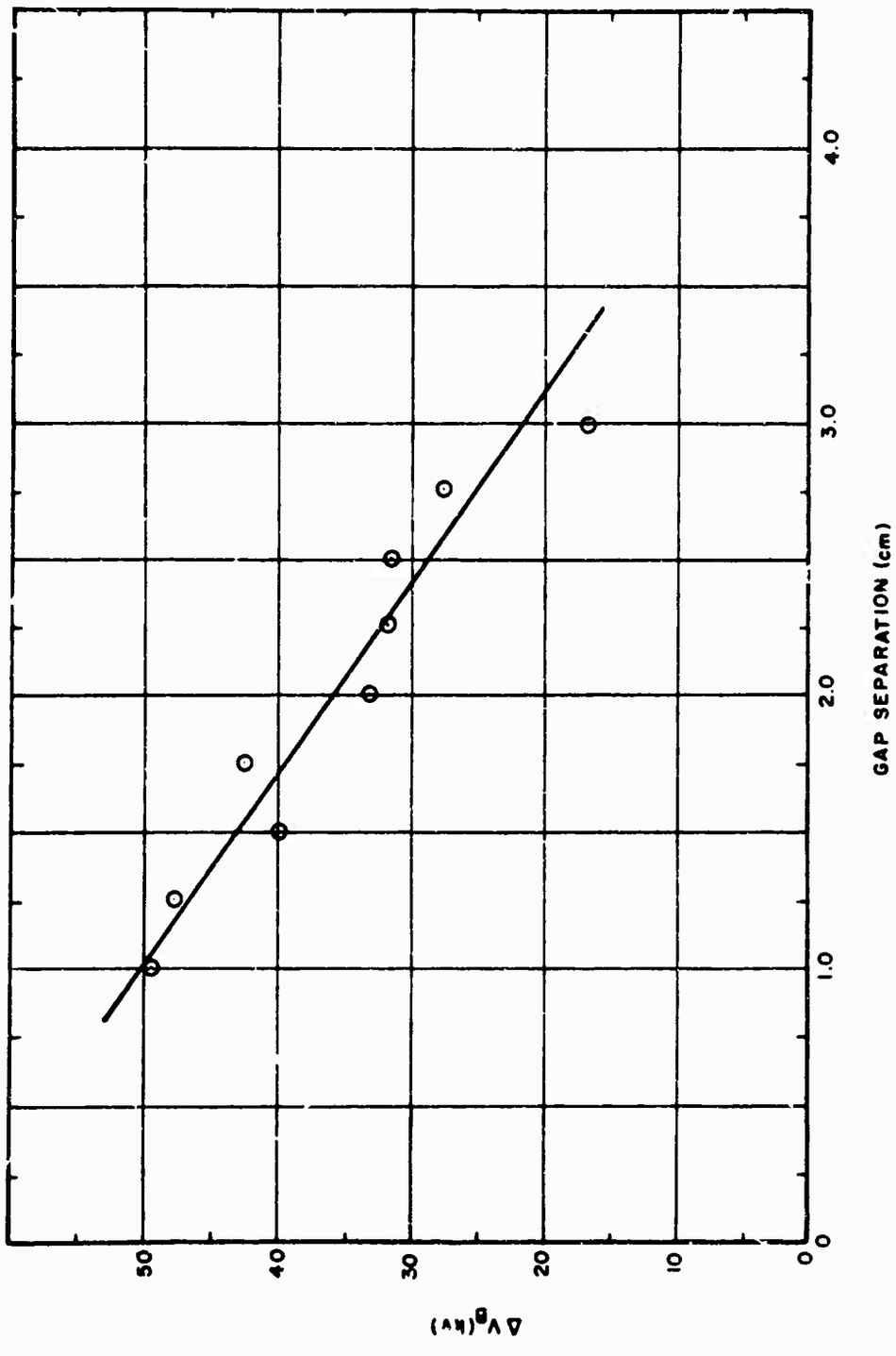

Figure 3-16. The μ Effect

1-2399

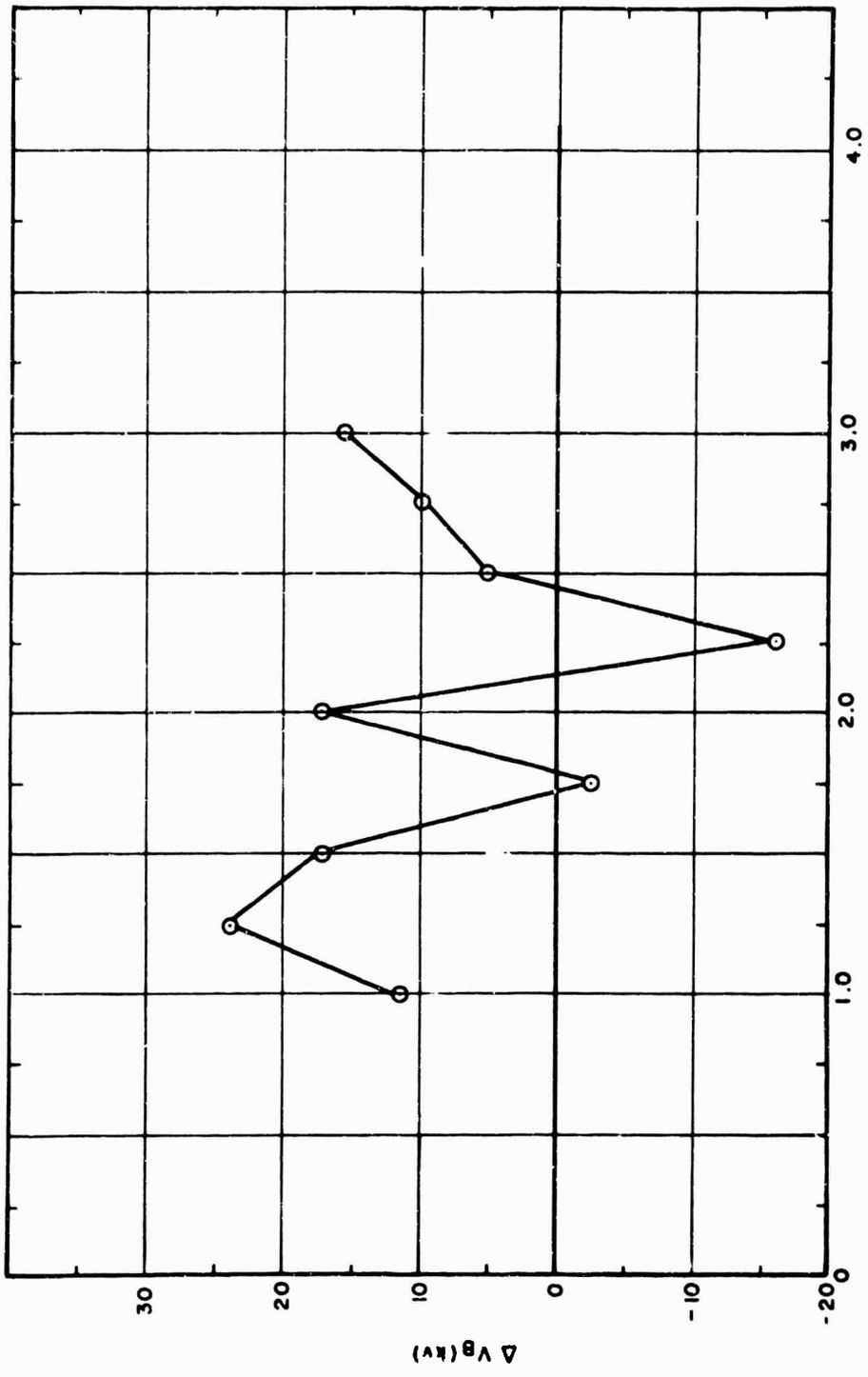

Figure 3-17. The A Effect

1-2400

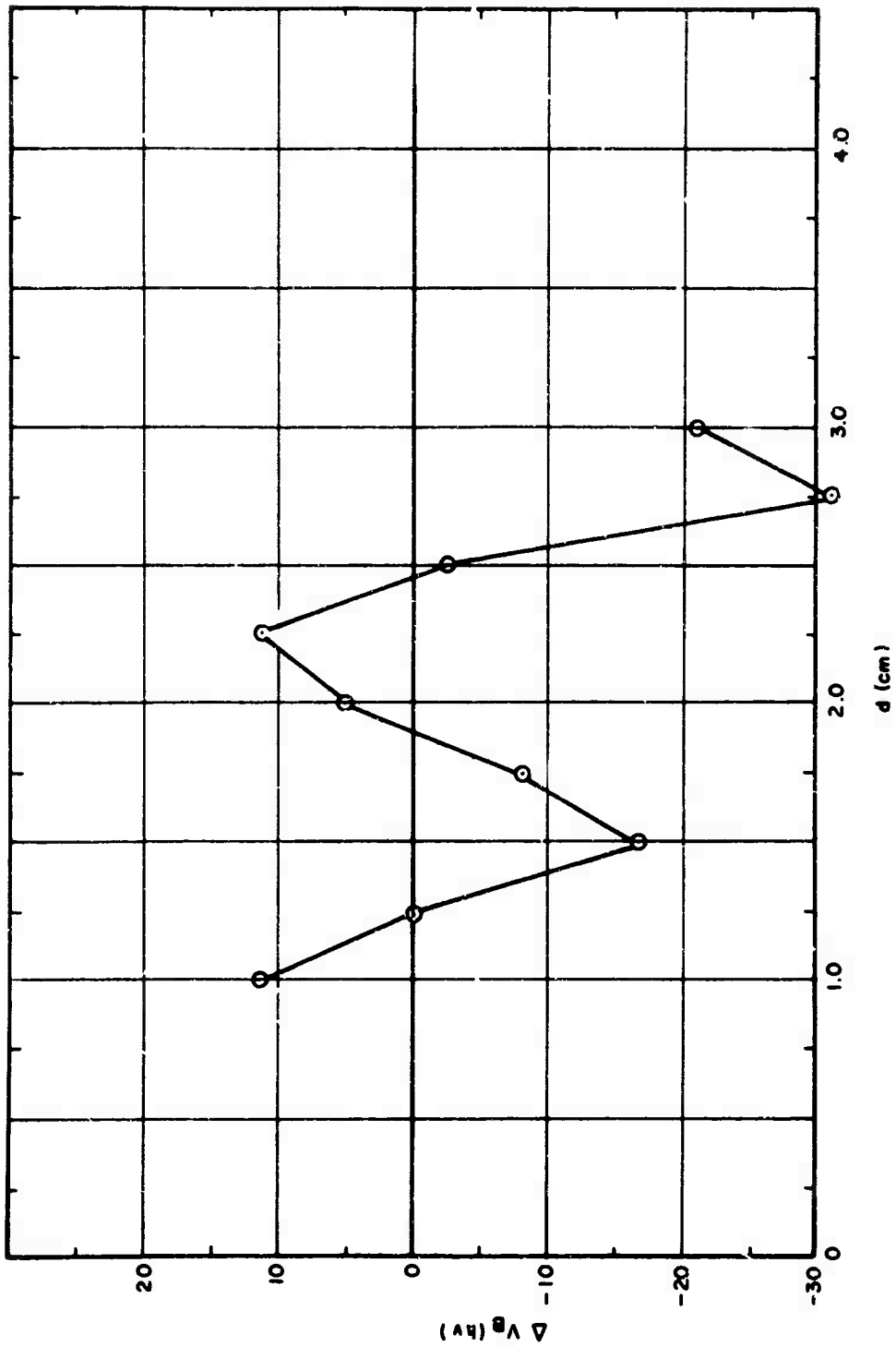

Figure 3-18. The B Effect

1-2401

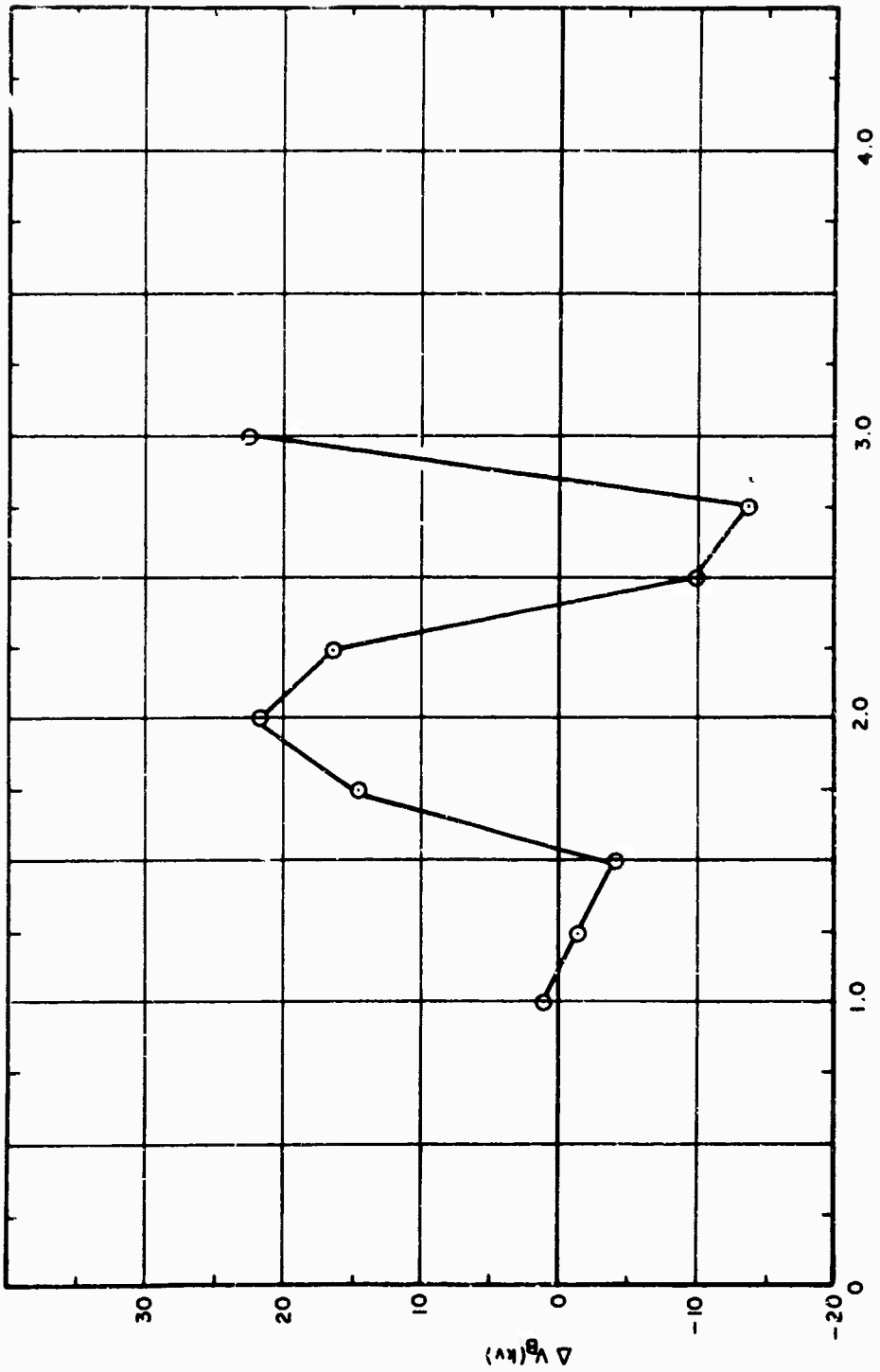

Figure 3-19. The AB Effect

1-2402

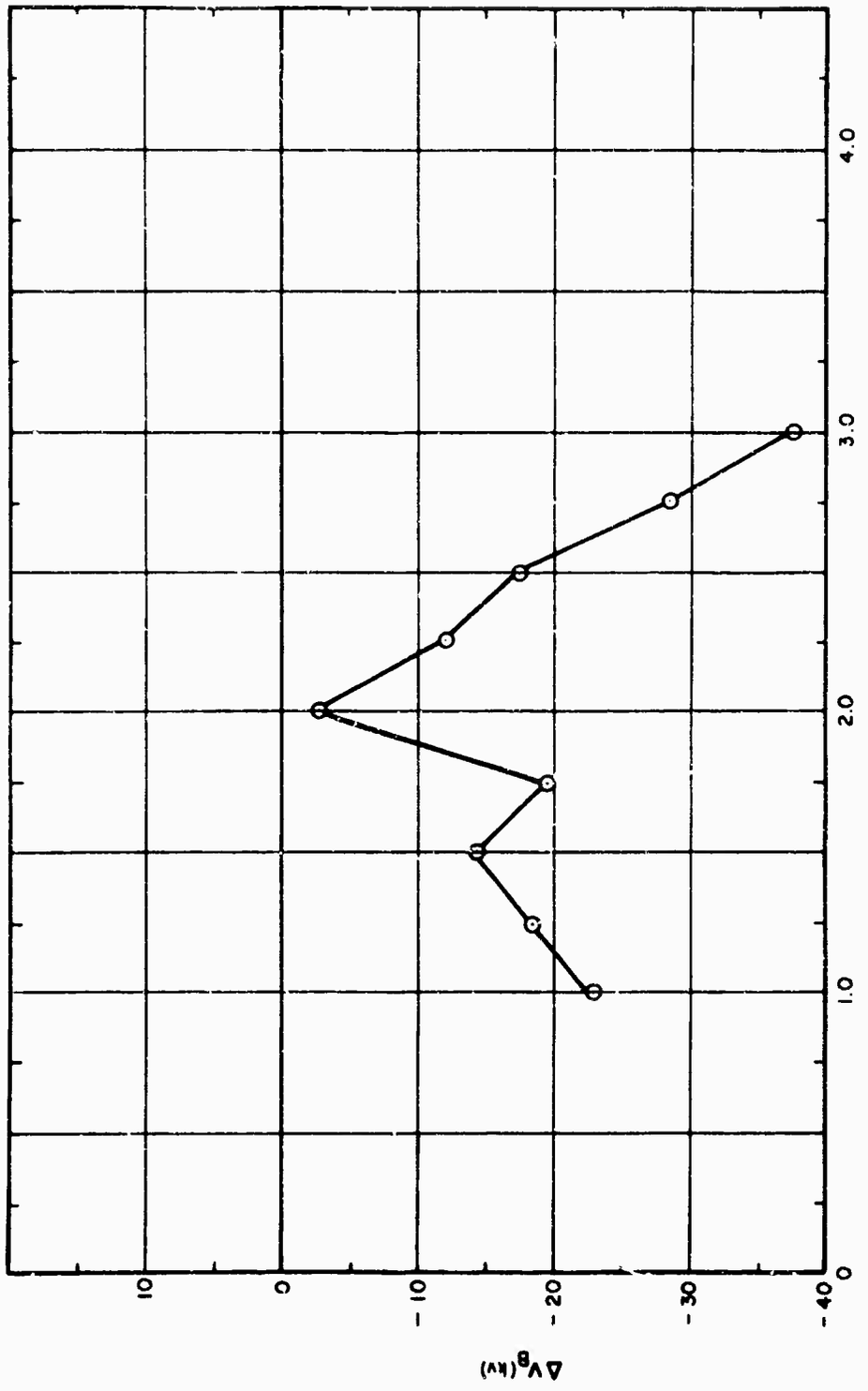

Figure 3-20. The C Effect

1-2403

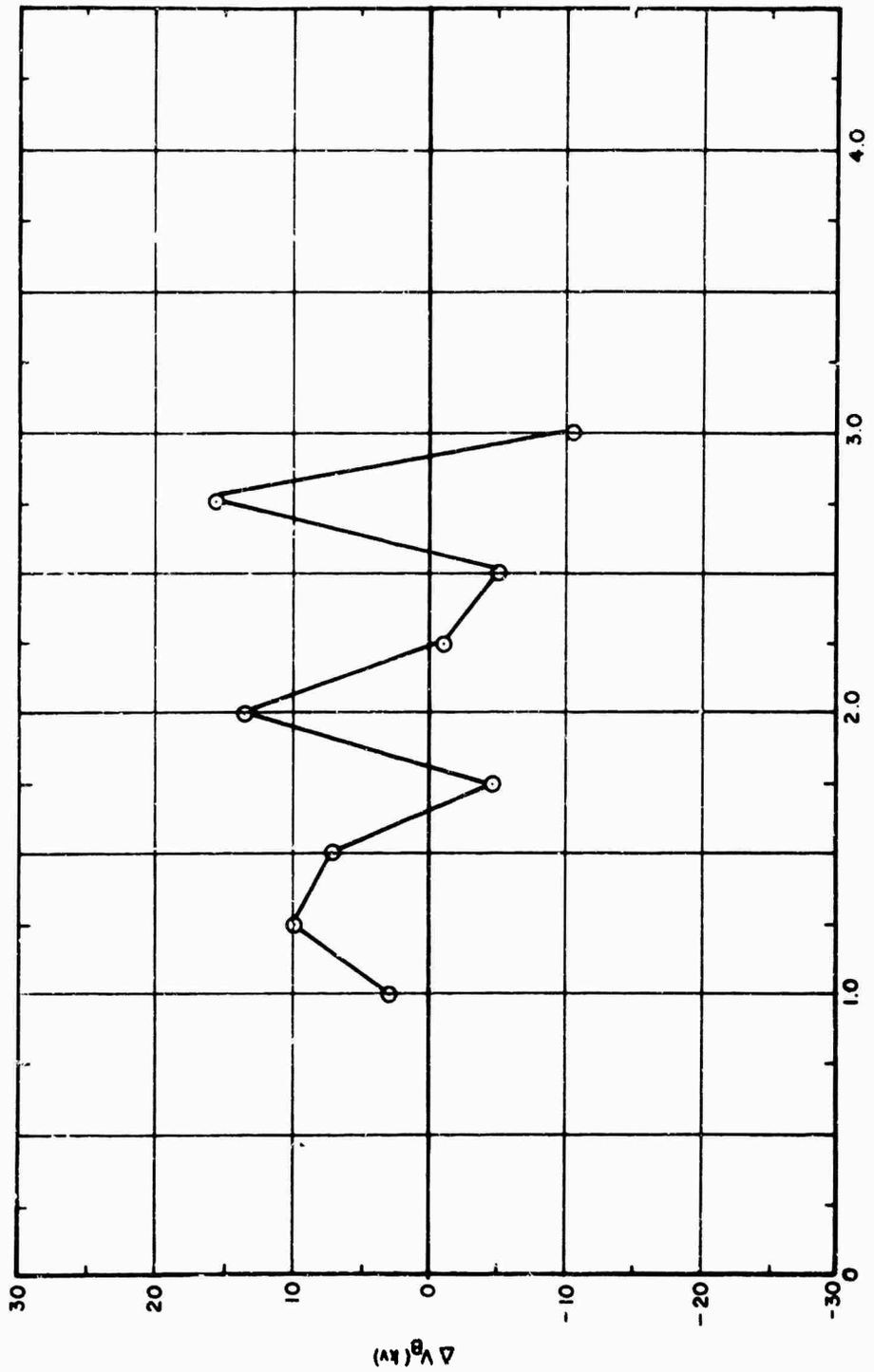

Figure 3-21. The AC Effect

1-2404

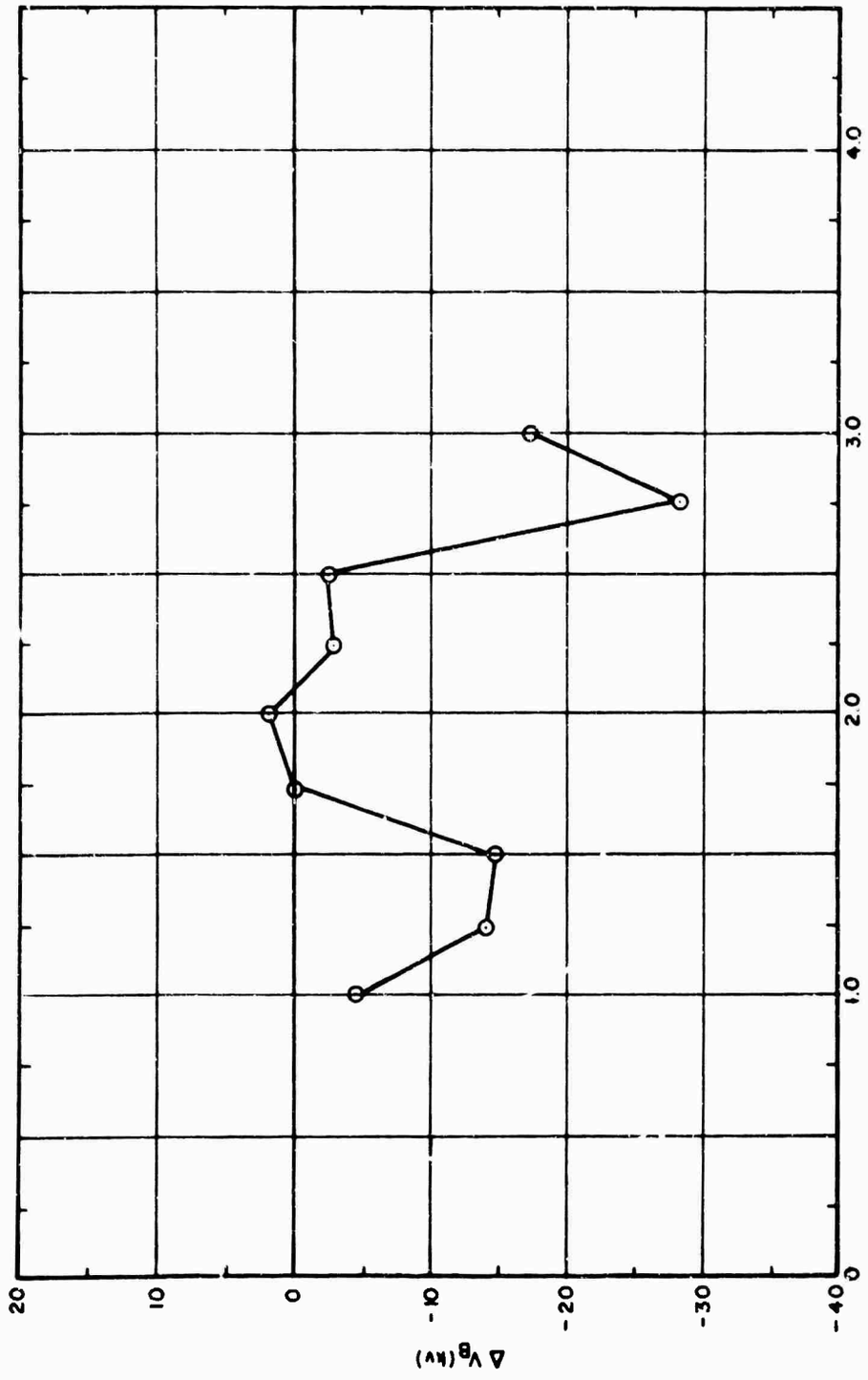

Figure 3-22. The BC Effect

1-2405

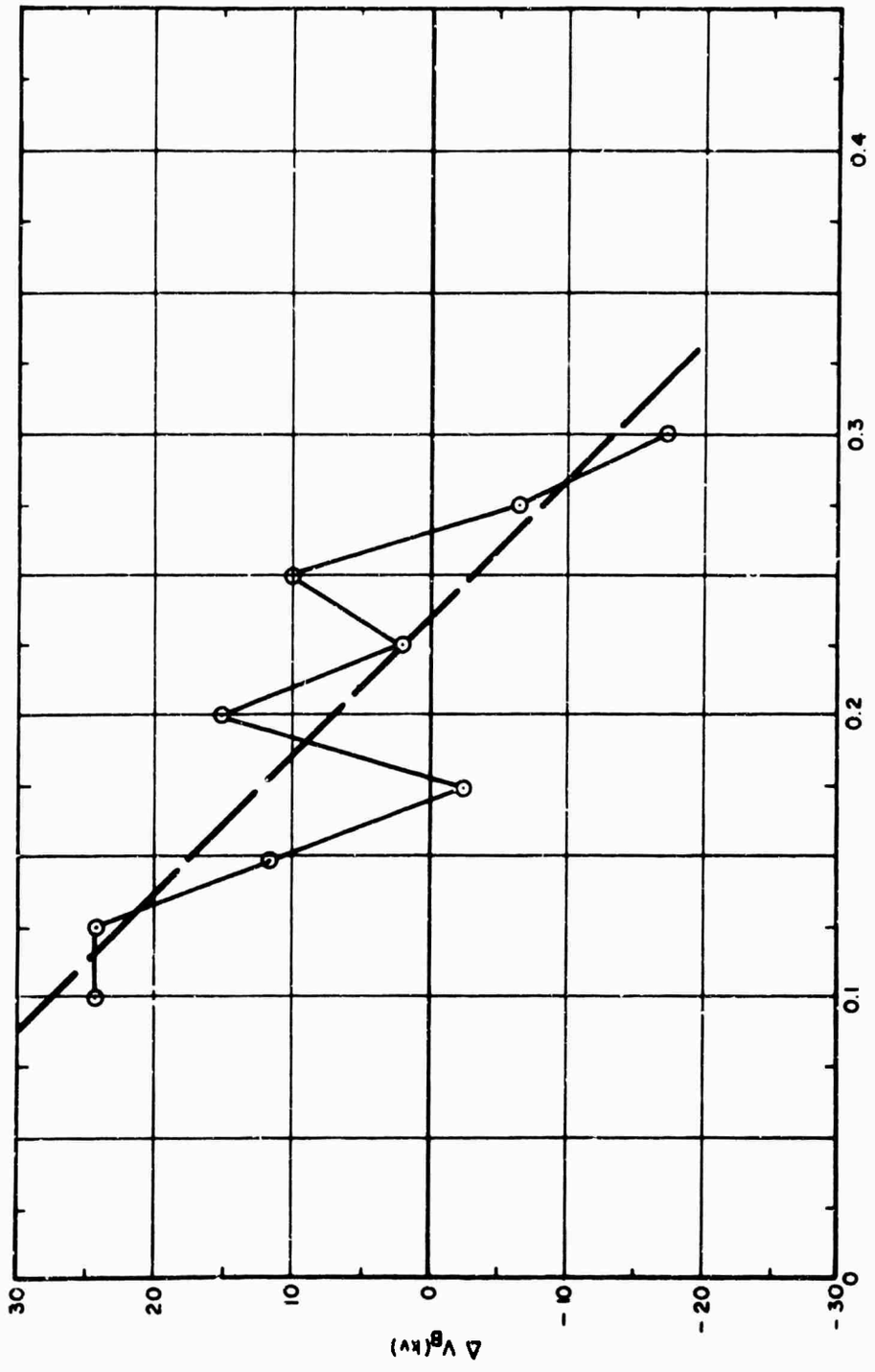

Figure 3-23. The ABC Effect

1-2406

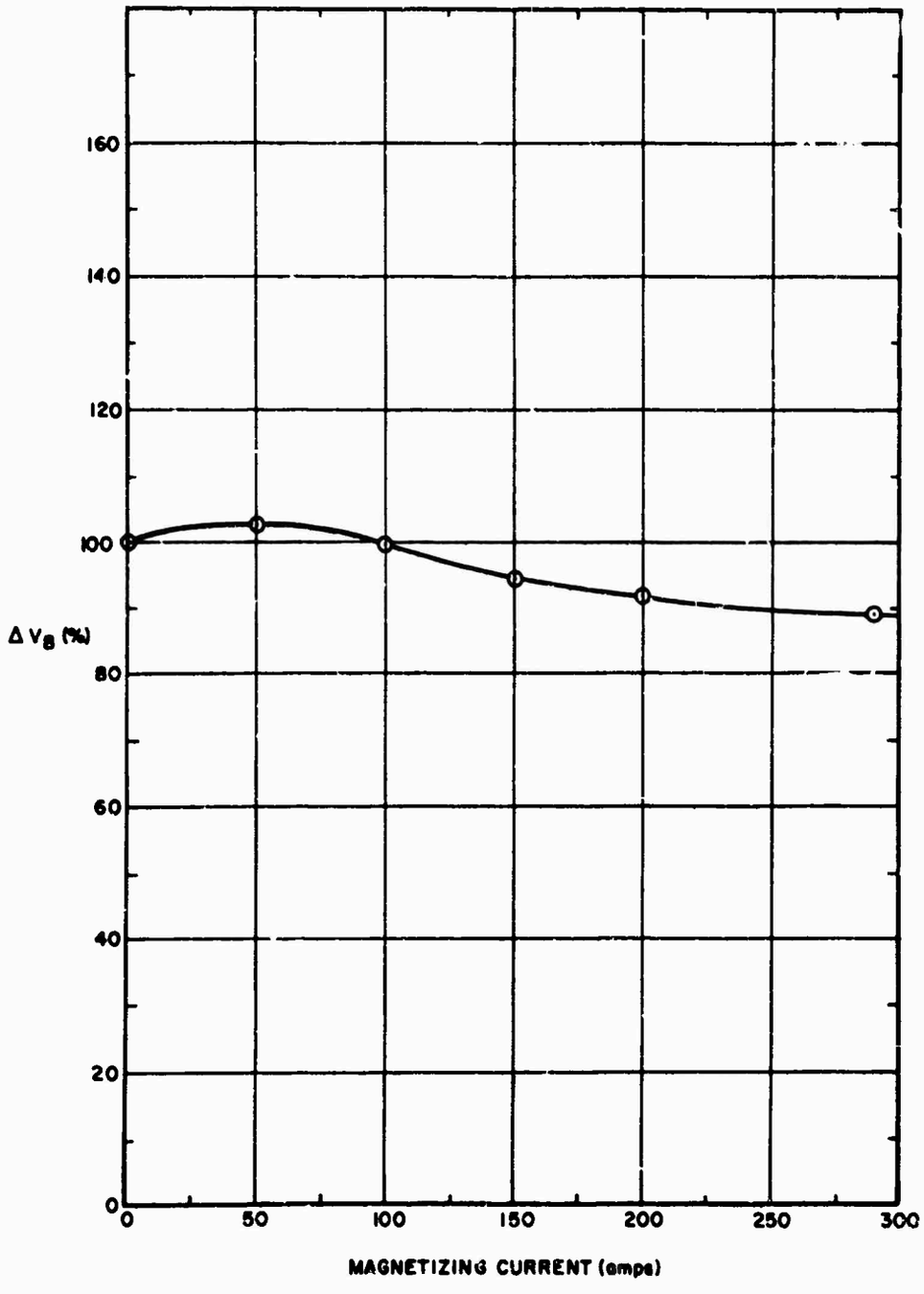

Figure 3-24. The E Effect

1-2407

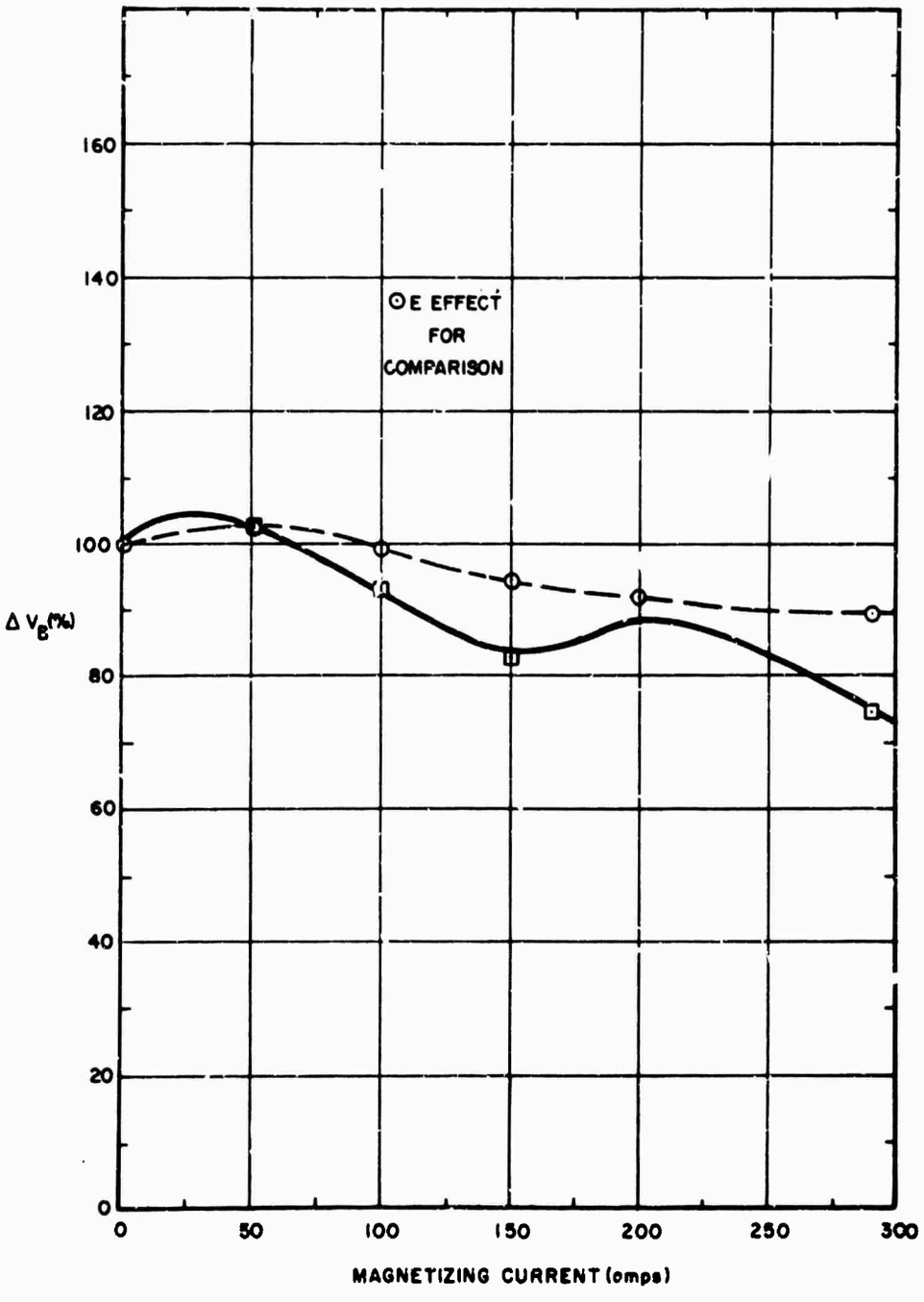

Figure 3-25. The AE Effect

1-2408

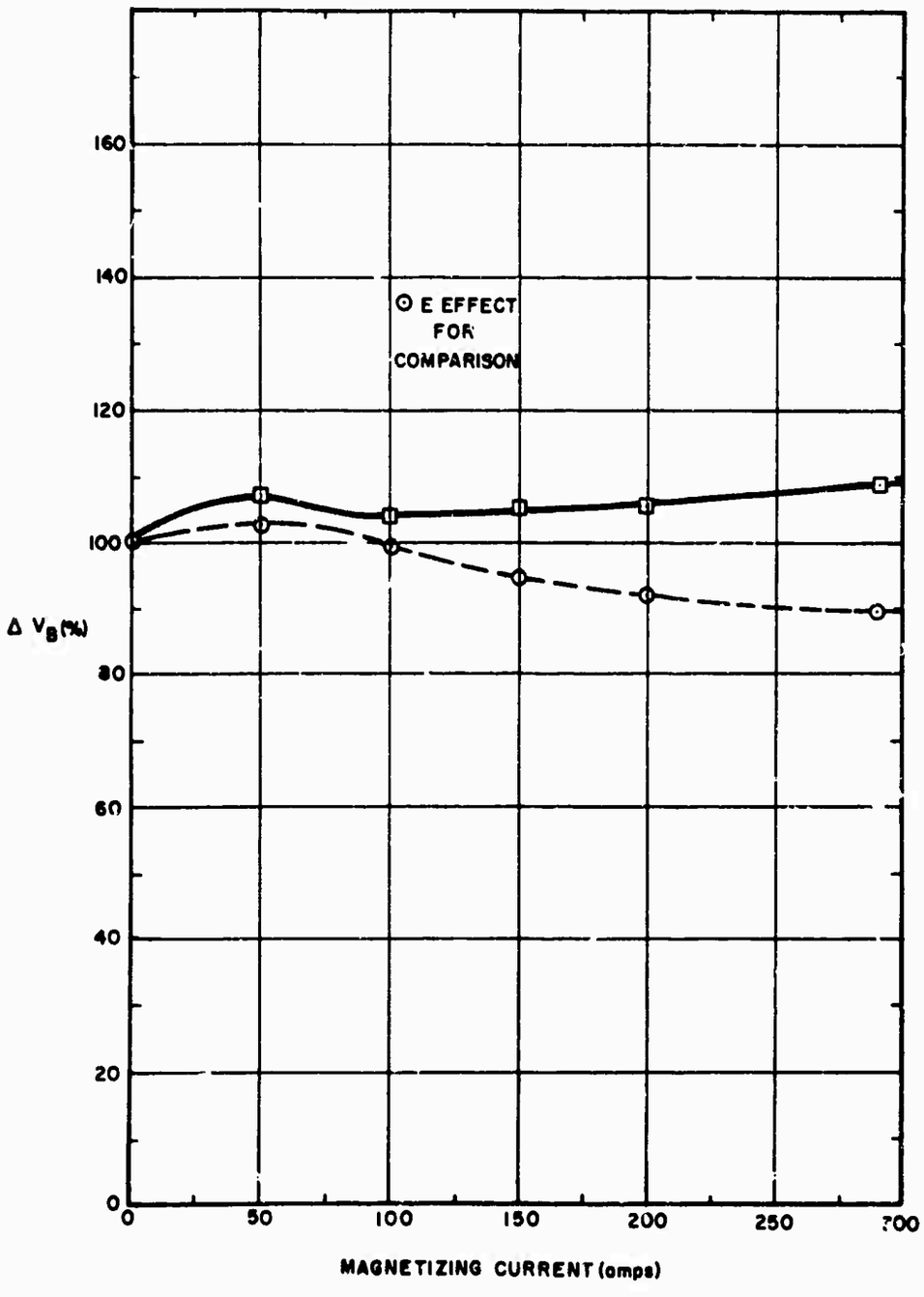

Figure 3-26. The BE Effect

1-2409

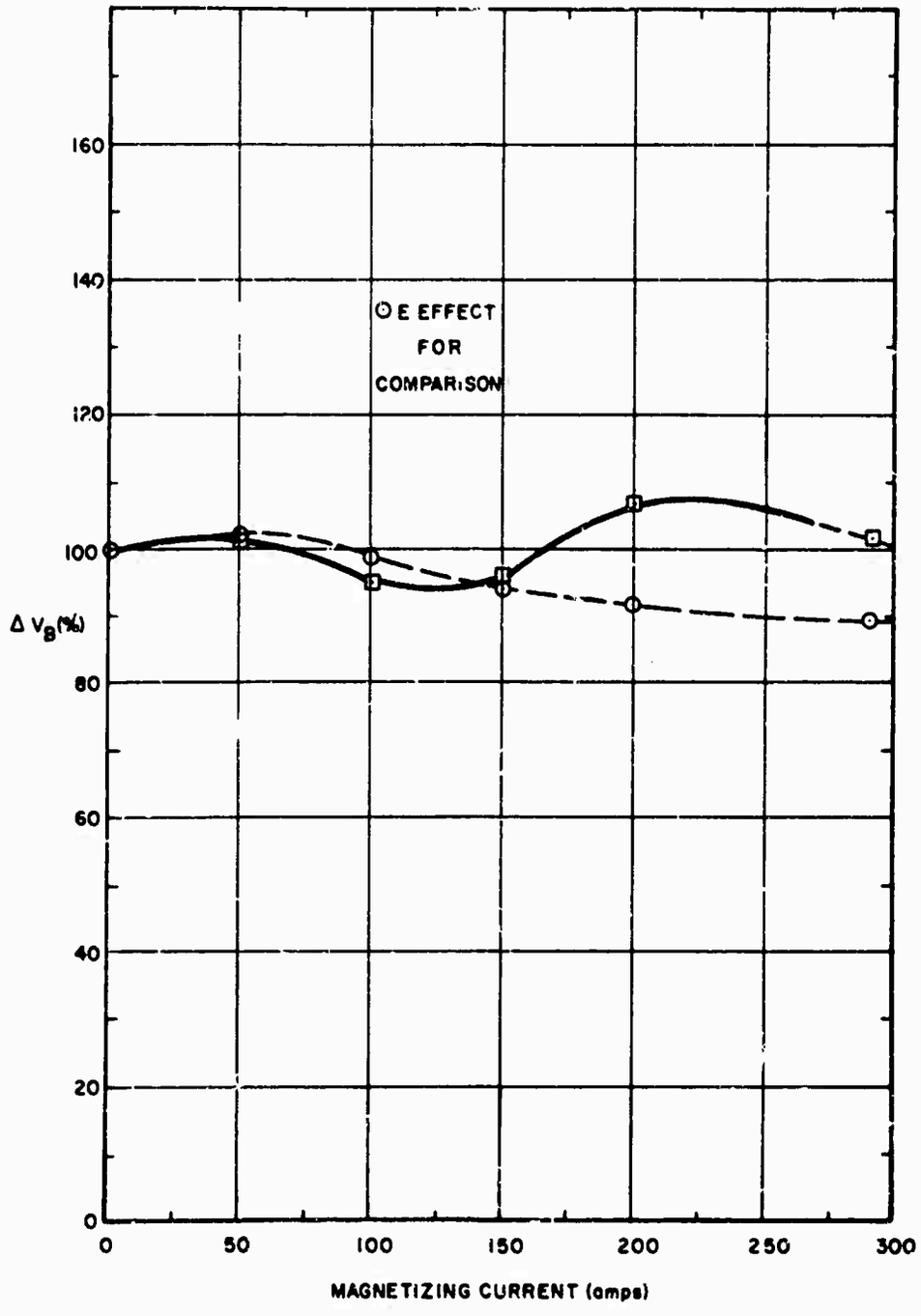

Figure 3-27. The ABE Effect

1-2410

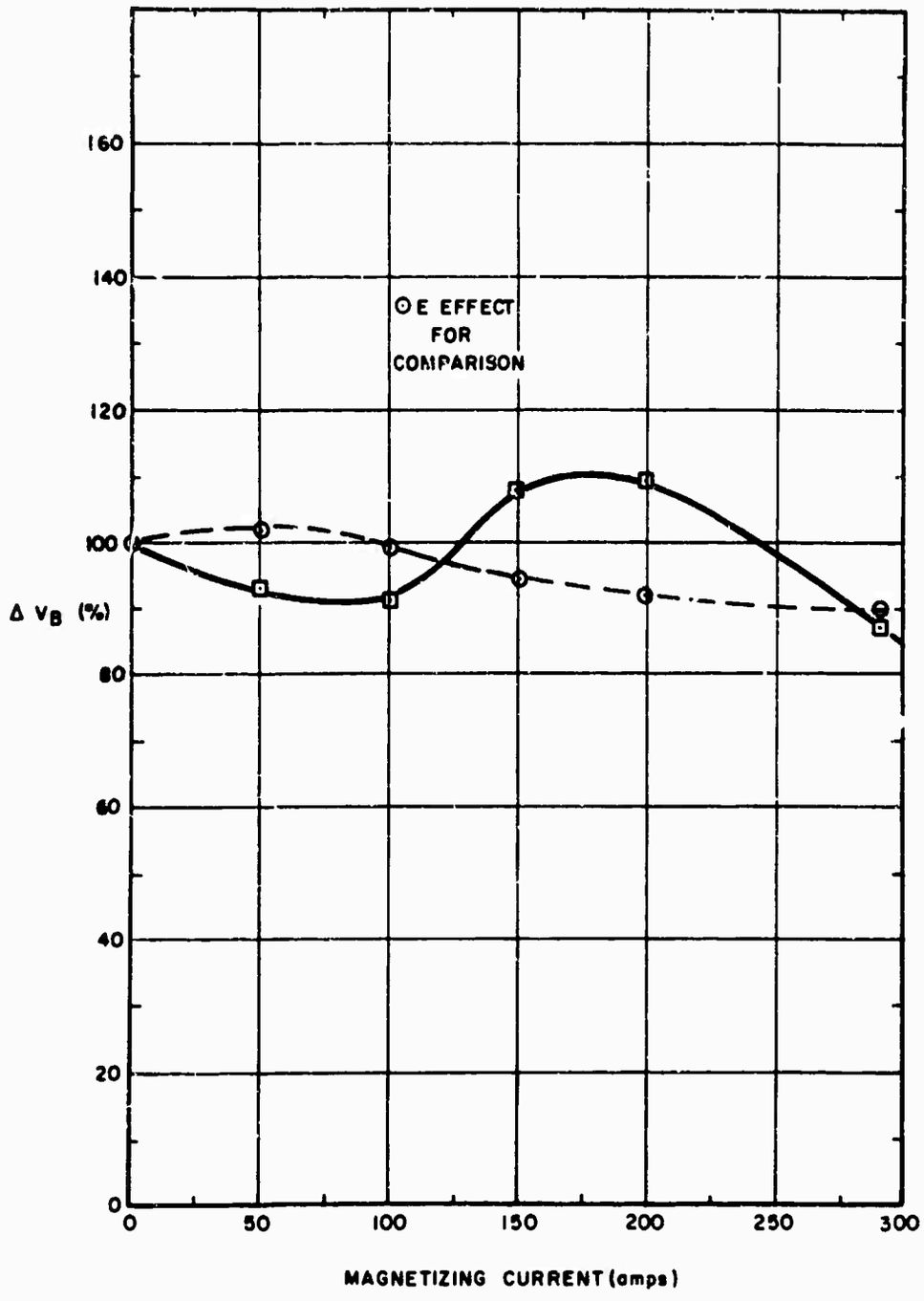

Figure 3-28. The CE Effect

1-2411

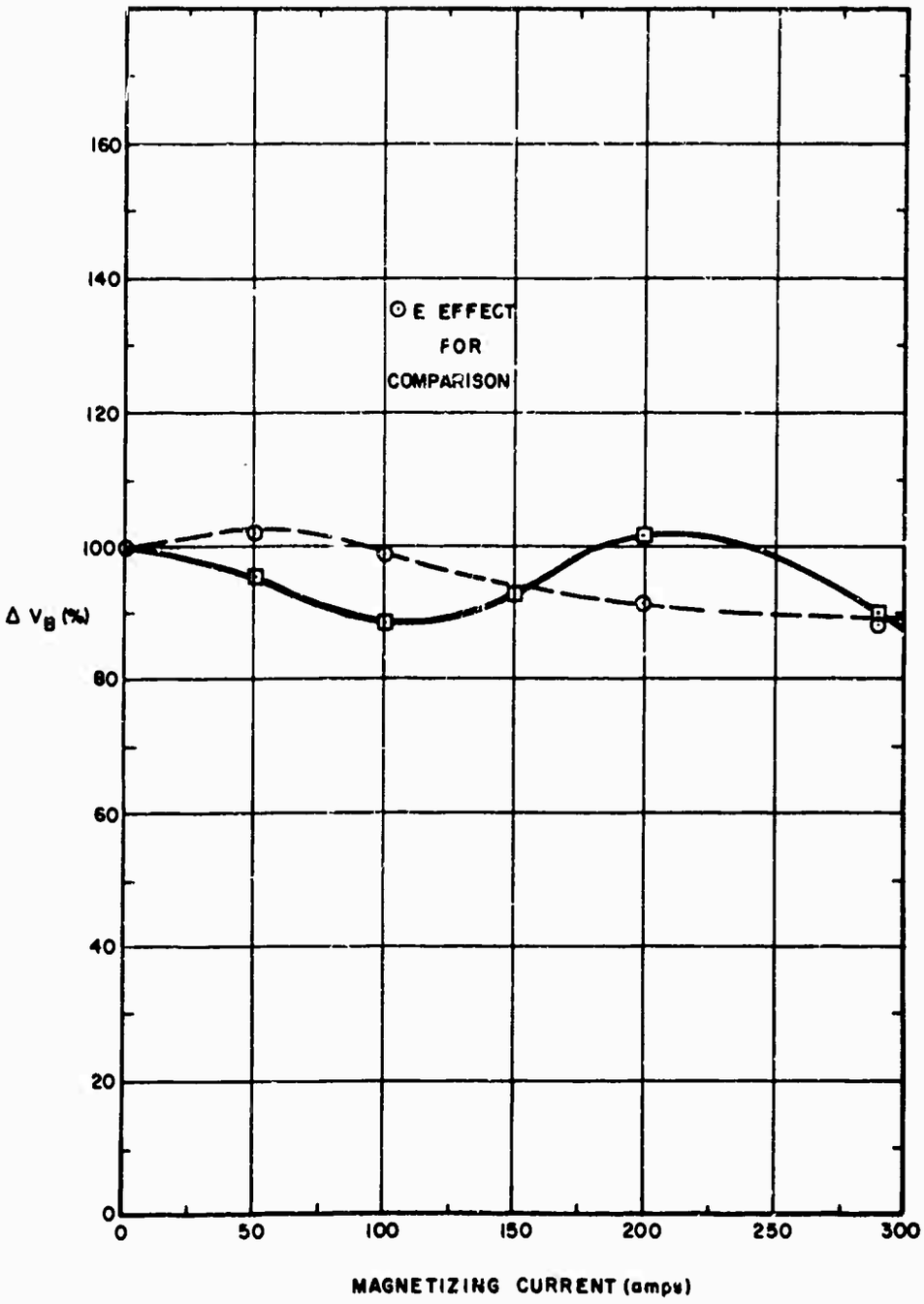

Figure 3-29. The ACE Effect

1-2412

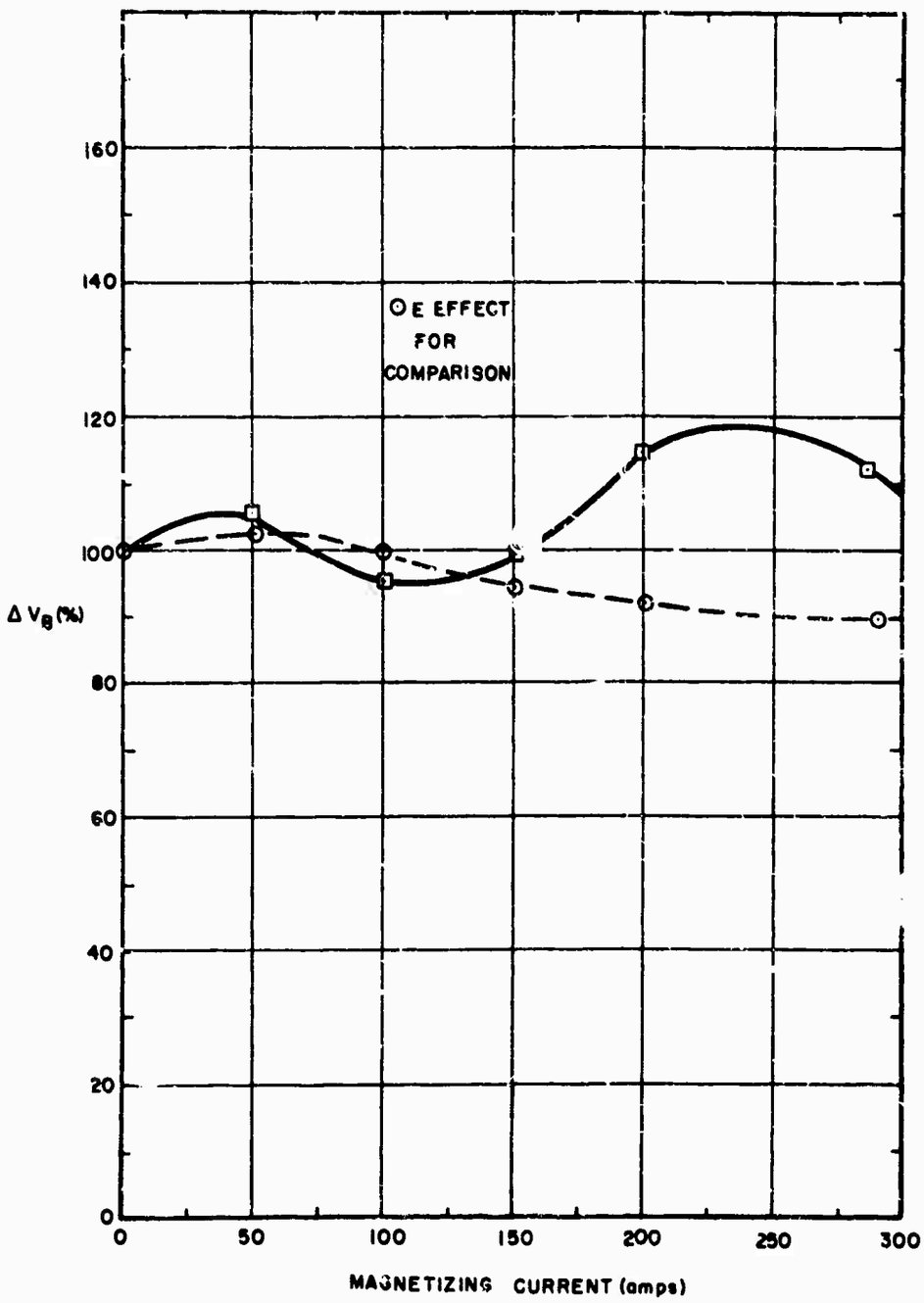

Figure 3-30. The BCE Effect

1-2413

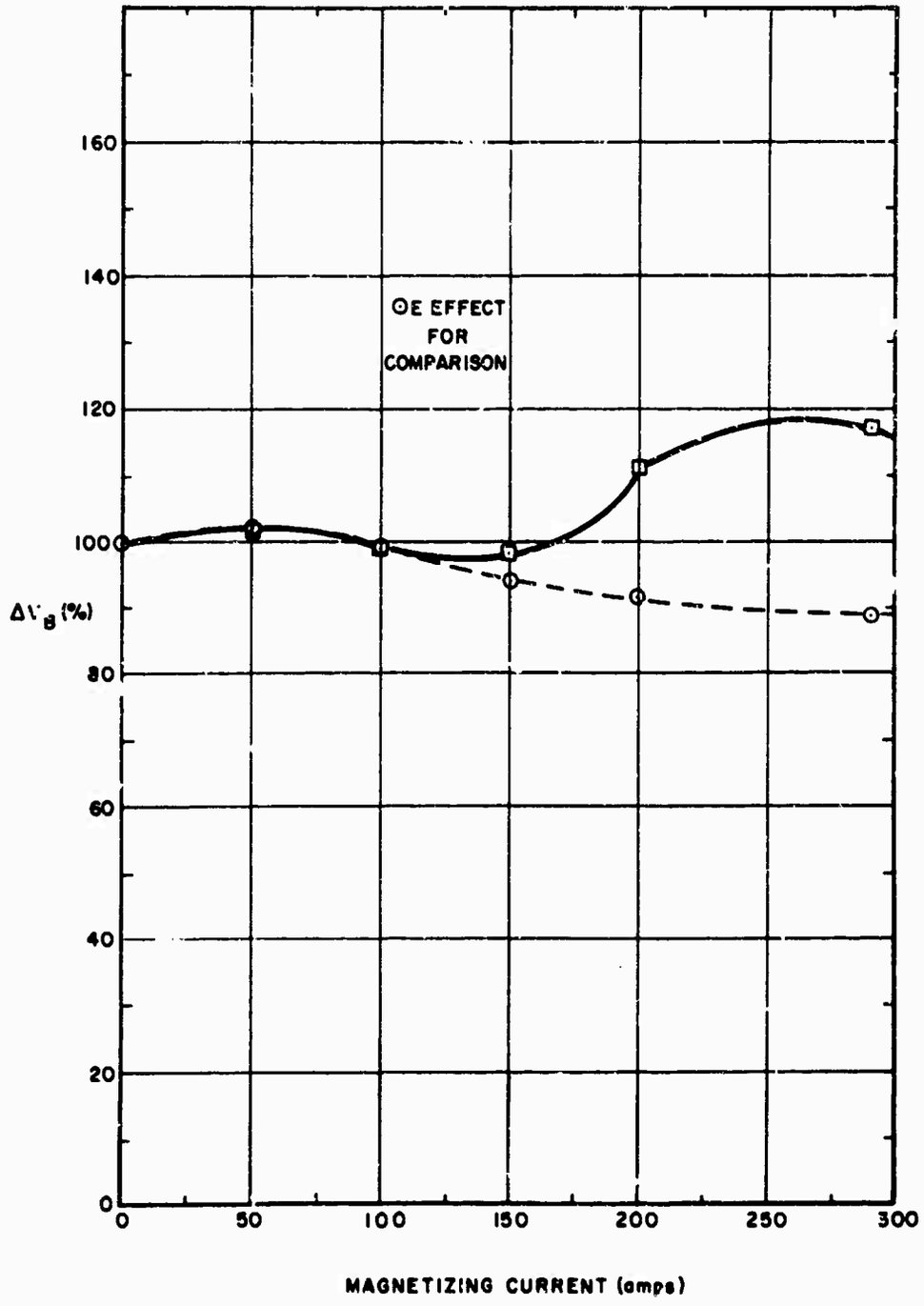

Figure 3-31. The ABCE Effect

1-2414

Table 3-4. Yates Algorithm for log I_{pB} without and with Magnetic Field (Conditioned Data)

	0.5 cm			1.0 cm			1.5 cm			2.0 cm			2.5 cm			3.0 cm		
	No	Yes	No	No	Yes	No	No	Yes	No	No	Yes	No	No	Yes	No	No	Yes	No
(1)	-6.29		-5.33	-7.48		-7.48	-8.55		-7.73	-8.30		-7.36	-8.82		-7.67	-7.19		-5.89
E		-5.53			-9.39			-9.67			-9.04			-8.66			-7.64	
A	-0.75		2.12	0.98		-3.06	-3.46		-2.76	-0.50		2.75	0.69		1.43	2.39		0.49
AE		1.78			-1.37			-4.43			1.91			2.44			1.13	
B	0.62		1.54	-0.48		0.49	0.17		1.32	2.65		0.25	-0.03		2.42	2.75		-1.25
BE		1.67			0.87			+0.93			-0.06			0.86			2.22	
AB	2.89		-1.69	-2.13		-1.29	-2.00		1.02	-2.76		-0.69	-0.22		0.78	-1.63		1.01
ABE		-1.73			-0.02			-1.17			-4.06			-2.68			-5.37	
C	-2.52		-2.06	-2.14		-2.60	-2.52		-3.09	-3.50		-2.75	-1.51		-3.82	-0.53		2.84
CE		-1.93			0.72			-0.47			0.74			1.21			1.63	
AC	-1.99		1.91	-2.09		-1.68	-1.91		-1.91	-2.91		2.31	-4.69		0.72	0.40		-2.90
ACE		1.95			0.13			+0.23			-3.26			2.97			1.22	
BC	1.56		1.75	1.59		2.47	2.17		7.65	1.24		-0.01	1.88		2.43	1.64		-1.16
BCE		1.88			5.07			2.38			1.41			0.33			2.13	
ABC	1.13		-2.30	-3.76		0.03	-0.37		-1.17	-0.65		-0.55	-0.78		1.37	-0.29		1.10
ABCE		-2.04			-1.22			-2.37			-2.59			2.79			1.72	

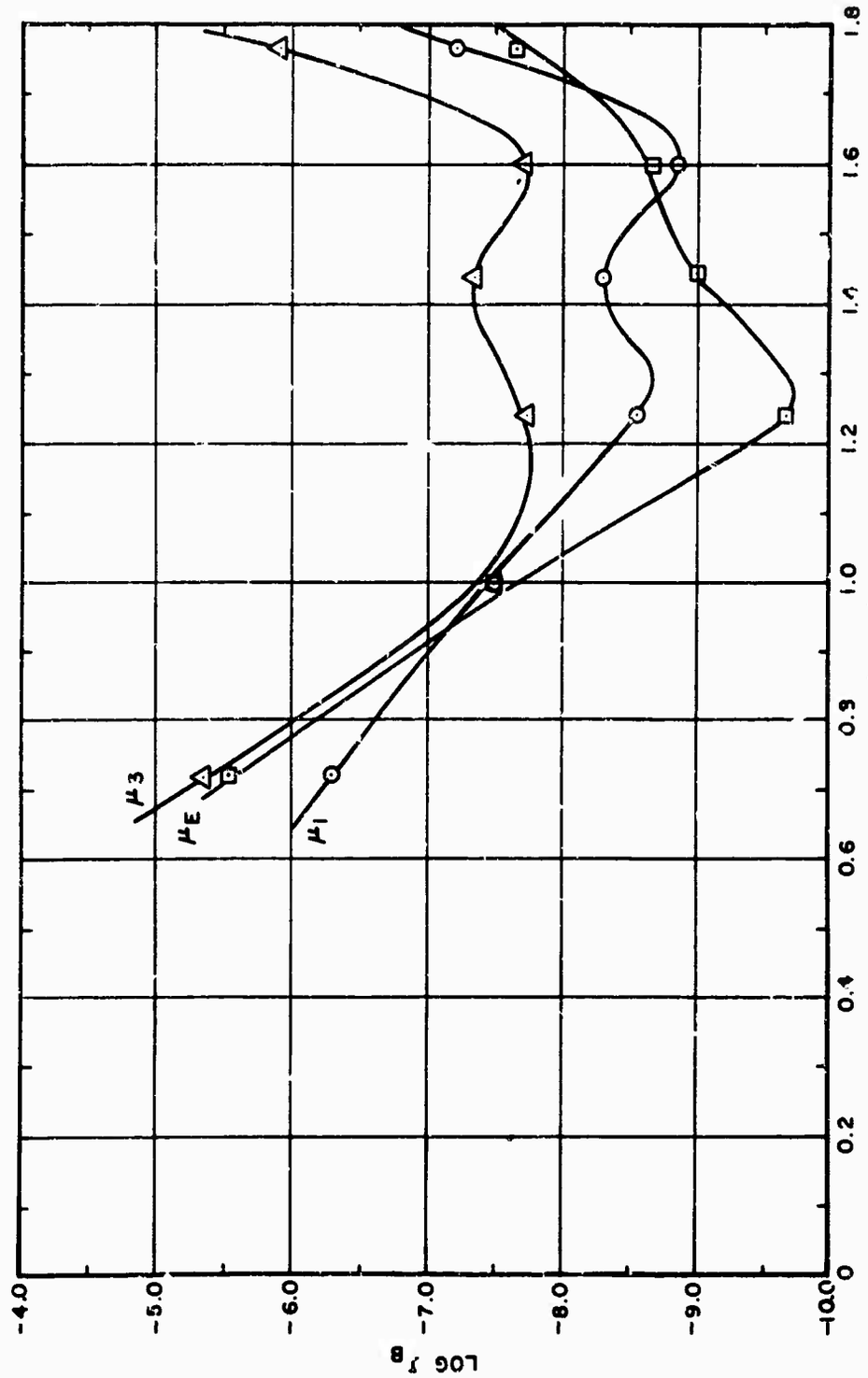

Figure 3-32. The μ Effect on Current

1-2415

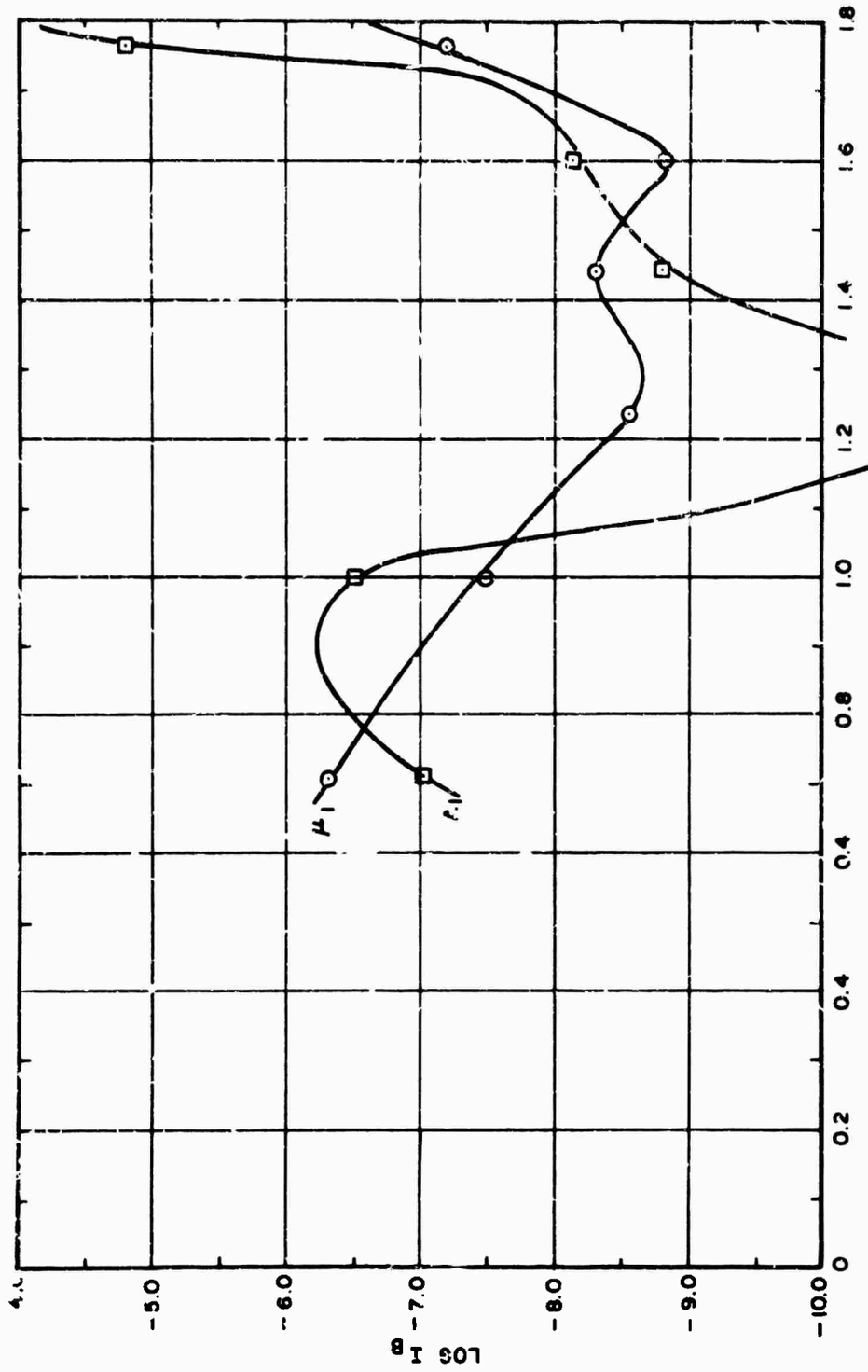

Figure 3-33. The A Effect on Current

1-2416

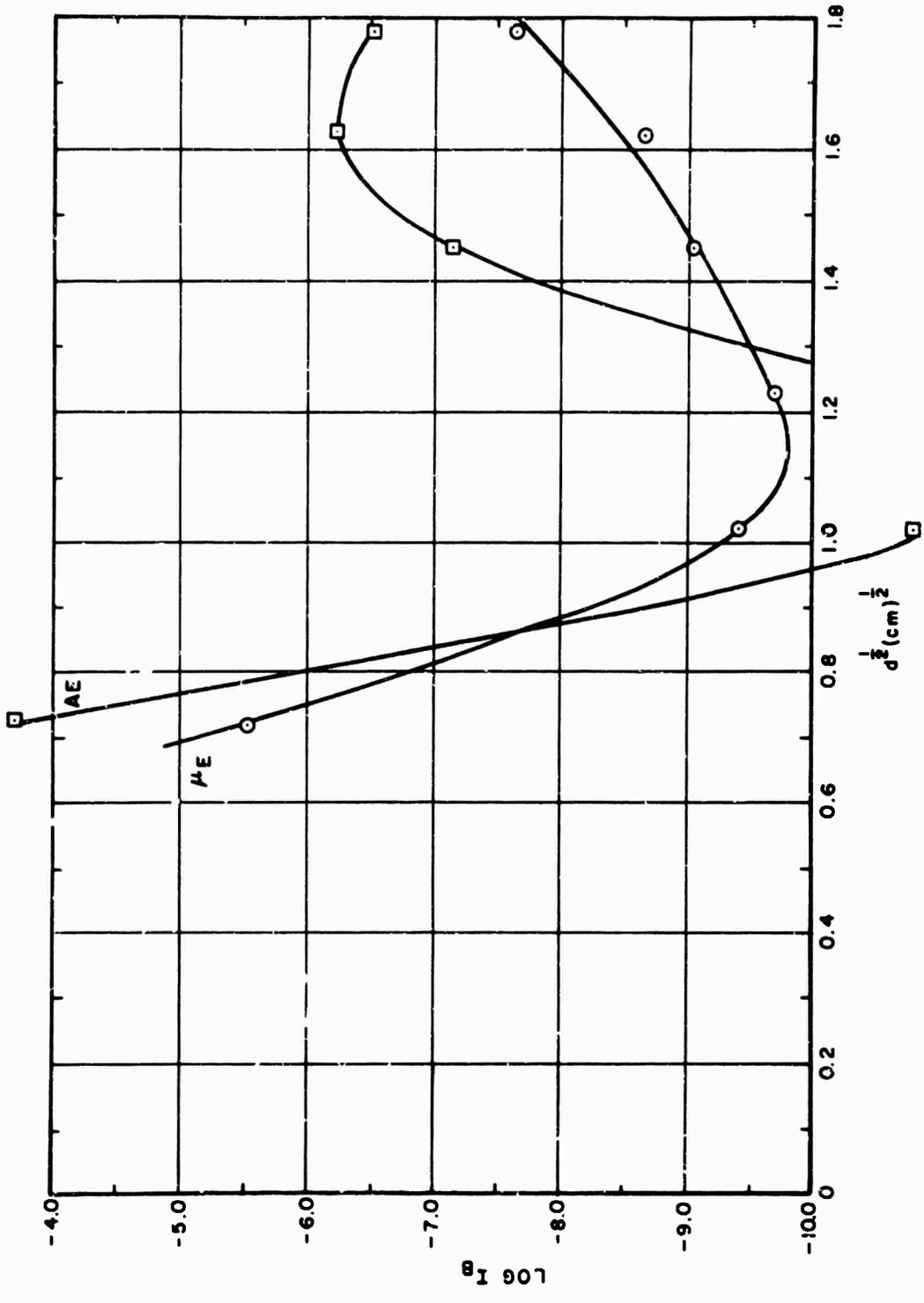

Figure 3-34. The AE Effect on Current

1-2417

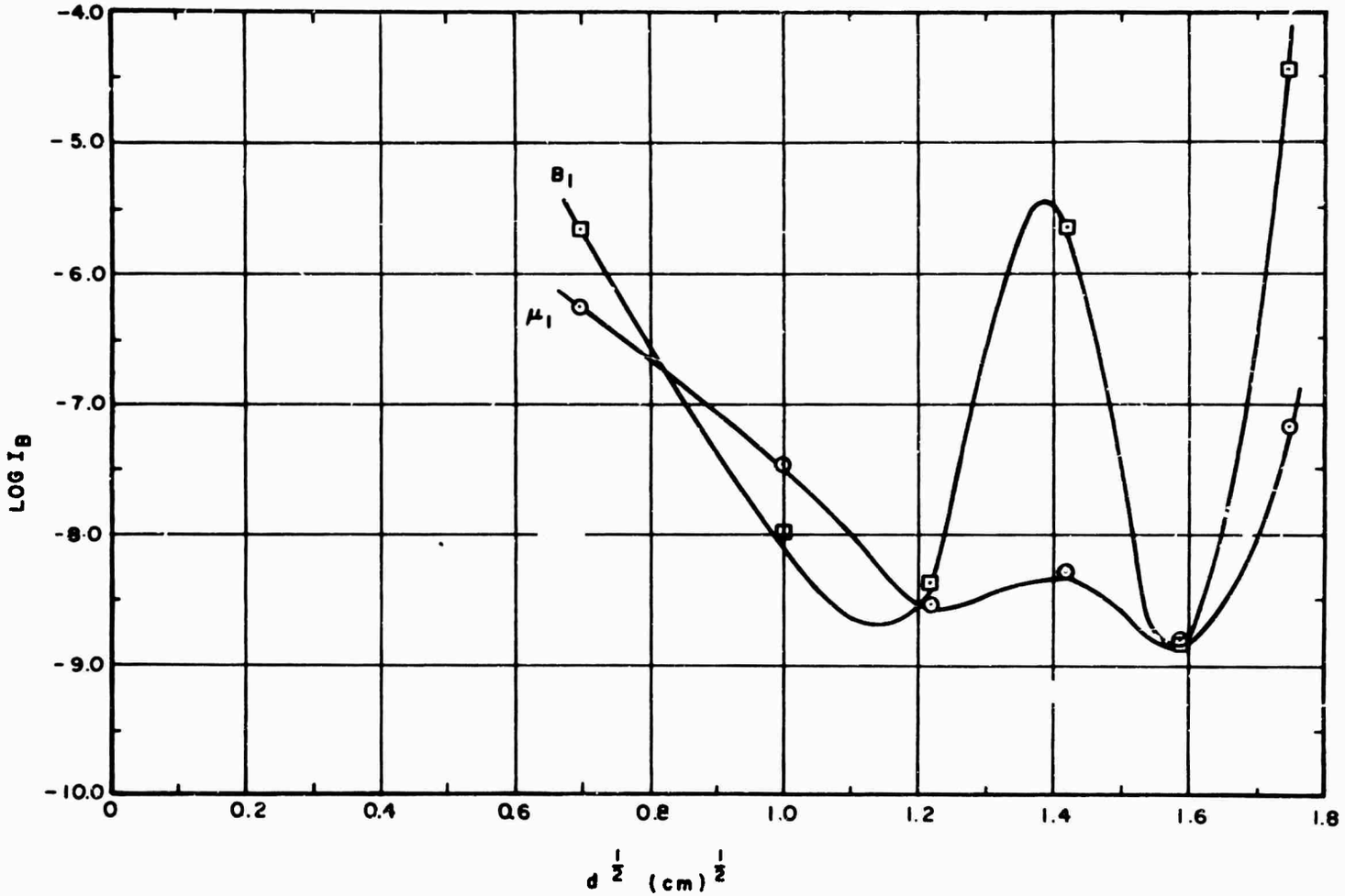

Figure 3-35. The B Effect on Current

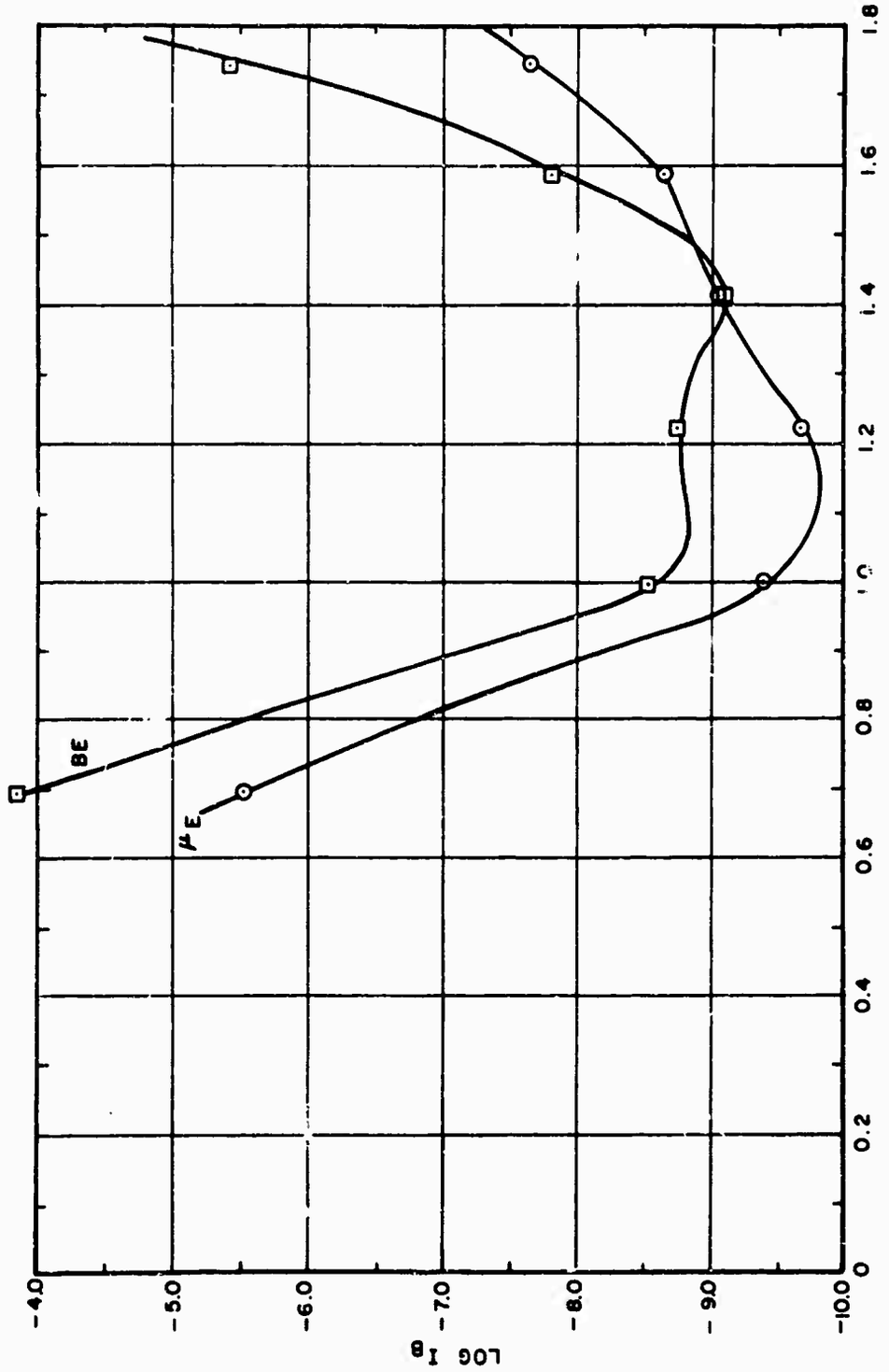

Figure 3-36. The BE Effect on Current

1-2419

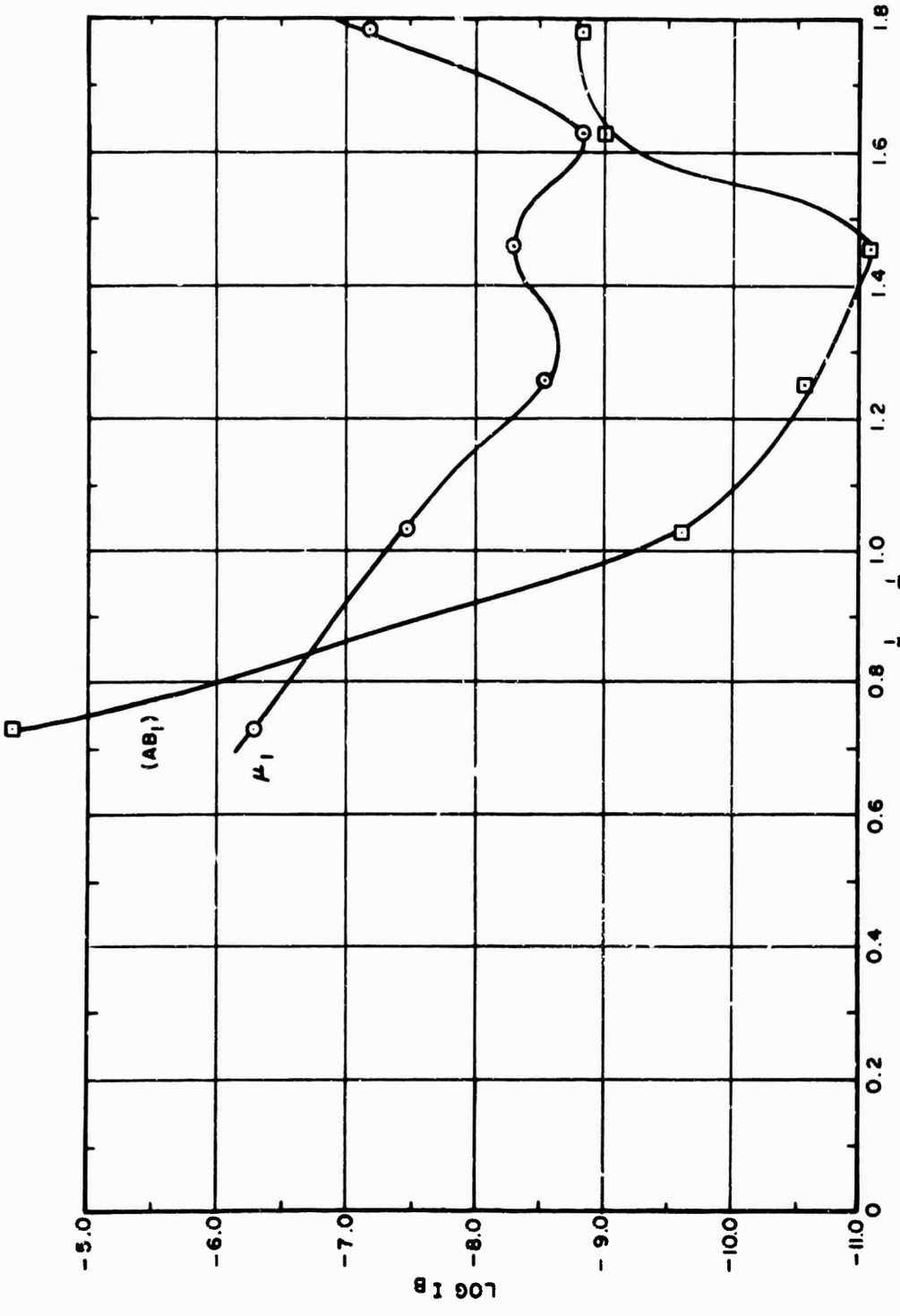

Figure 3-37. The AB Effect on Current

1-2420

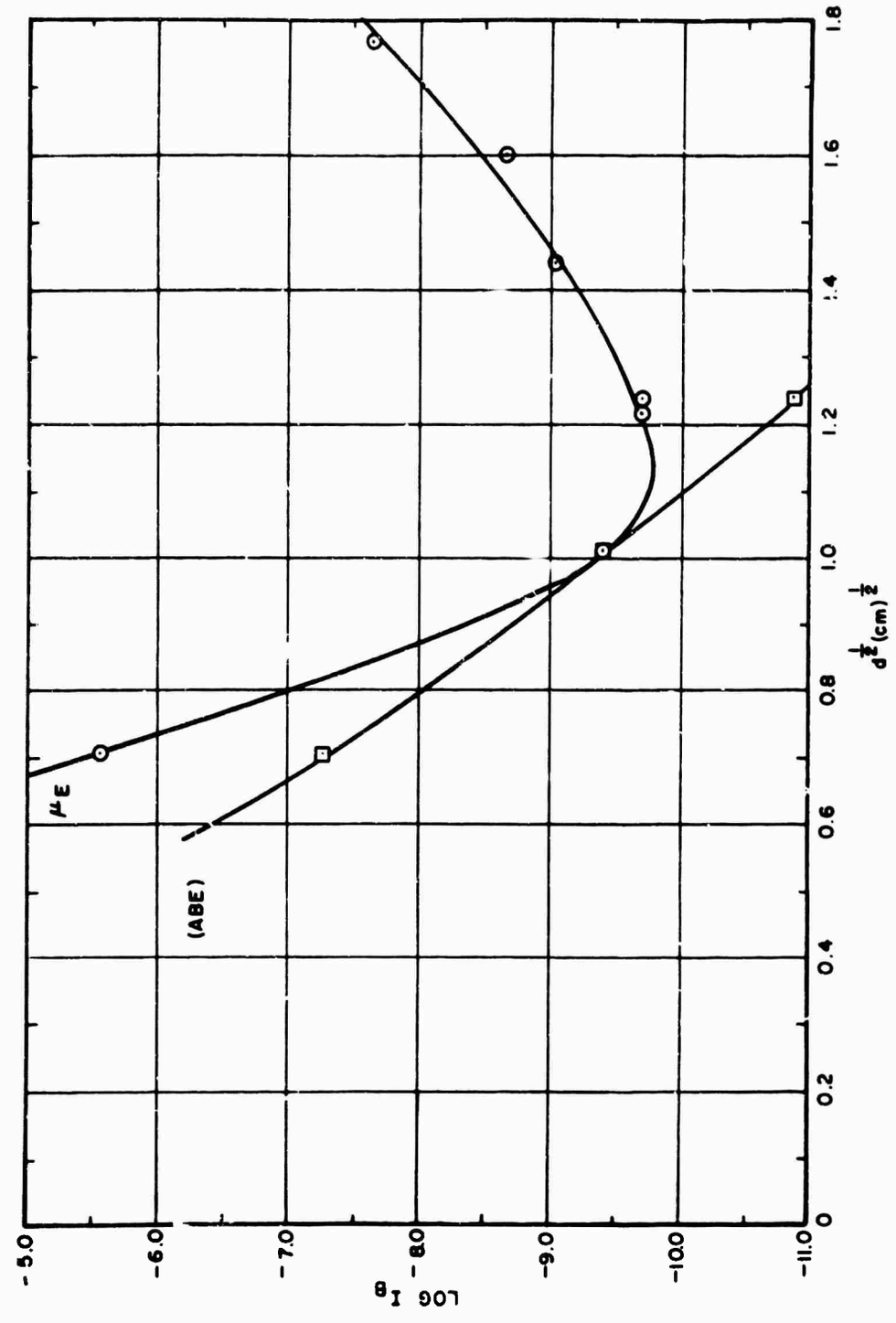

i-2421

Figure 3-38. The ABE Effect on Current

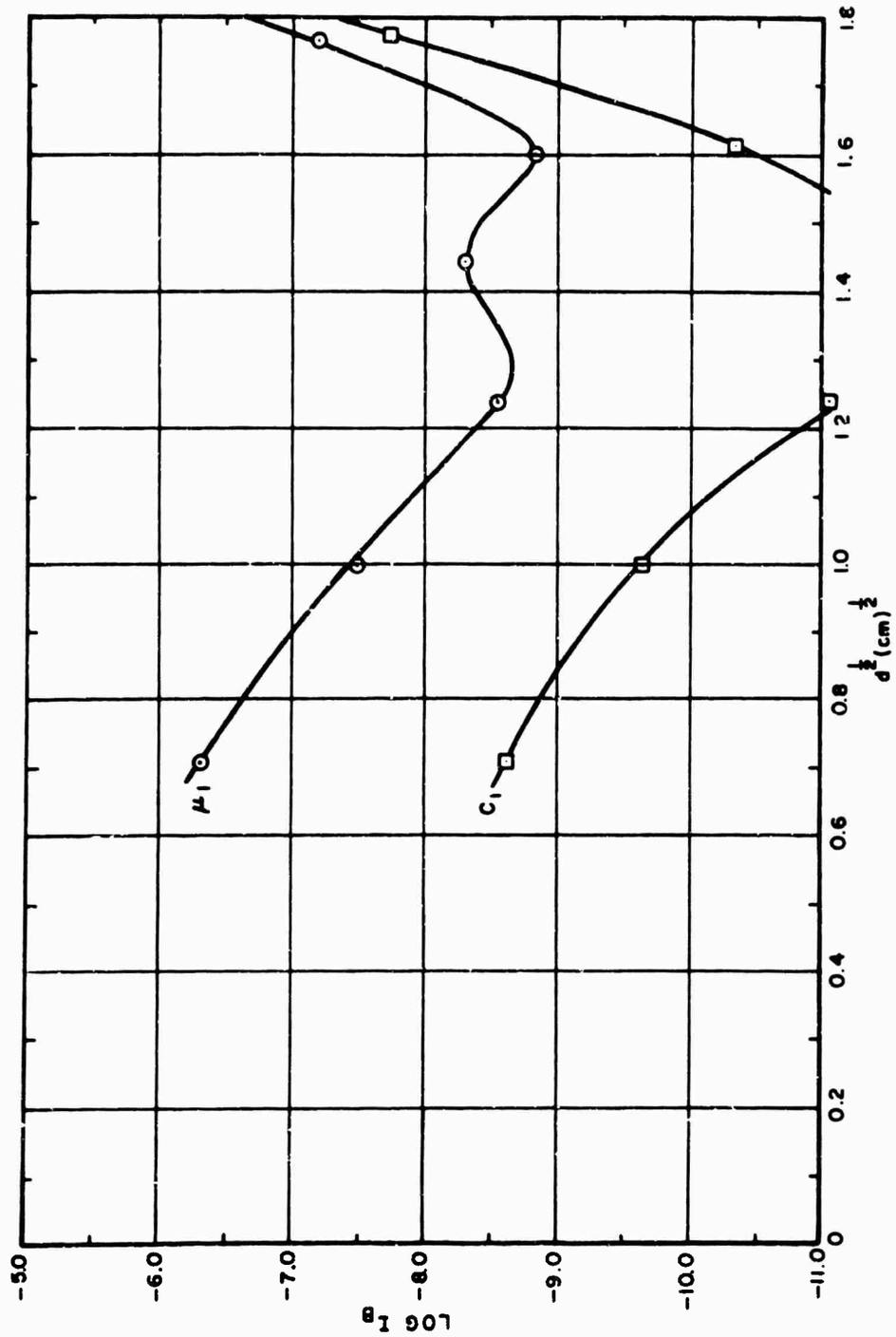

1-2422

Figure 3-39. The C Effect on Current

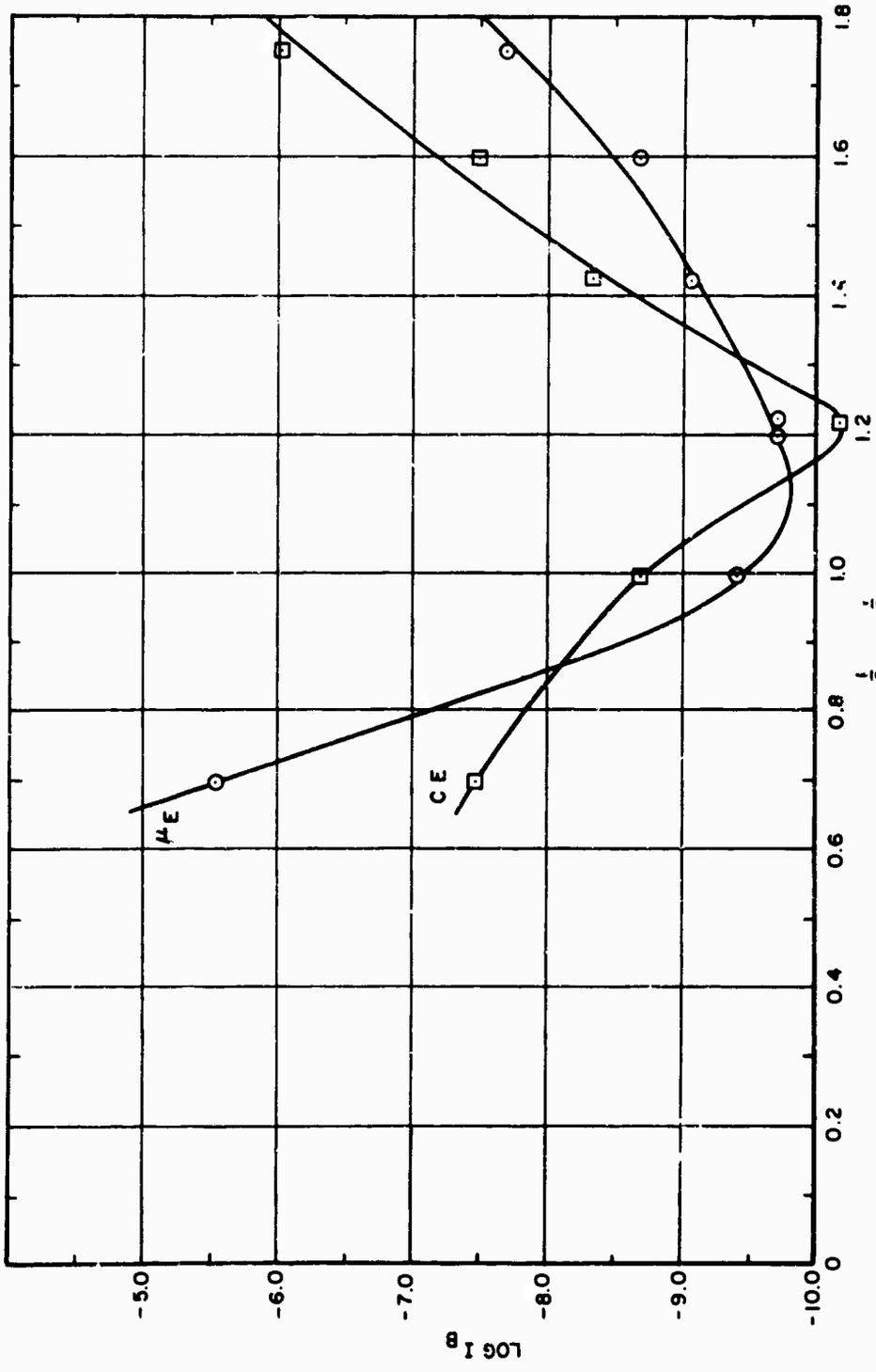

Figure 3-40. The CE Effect on Current

1-2423

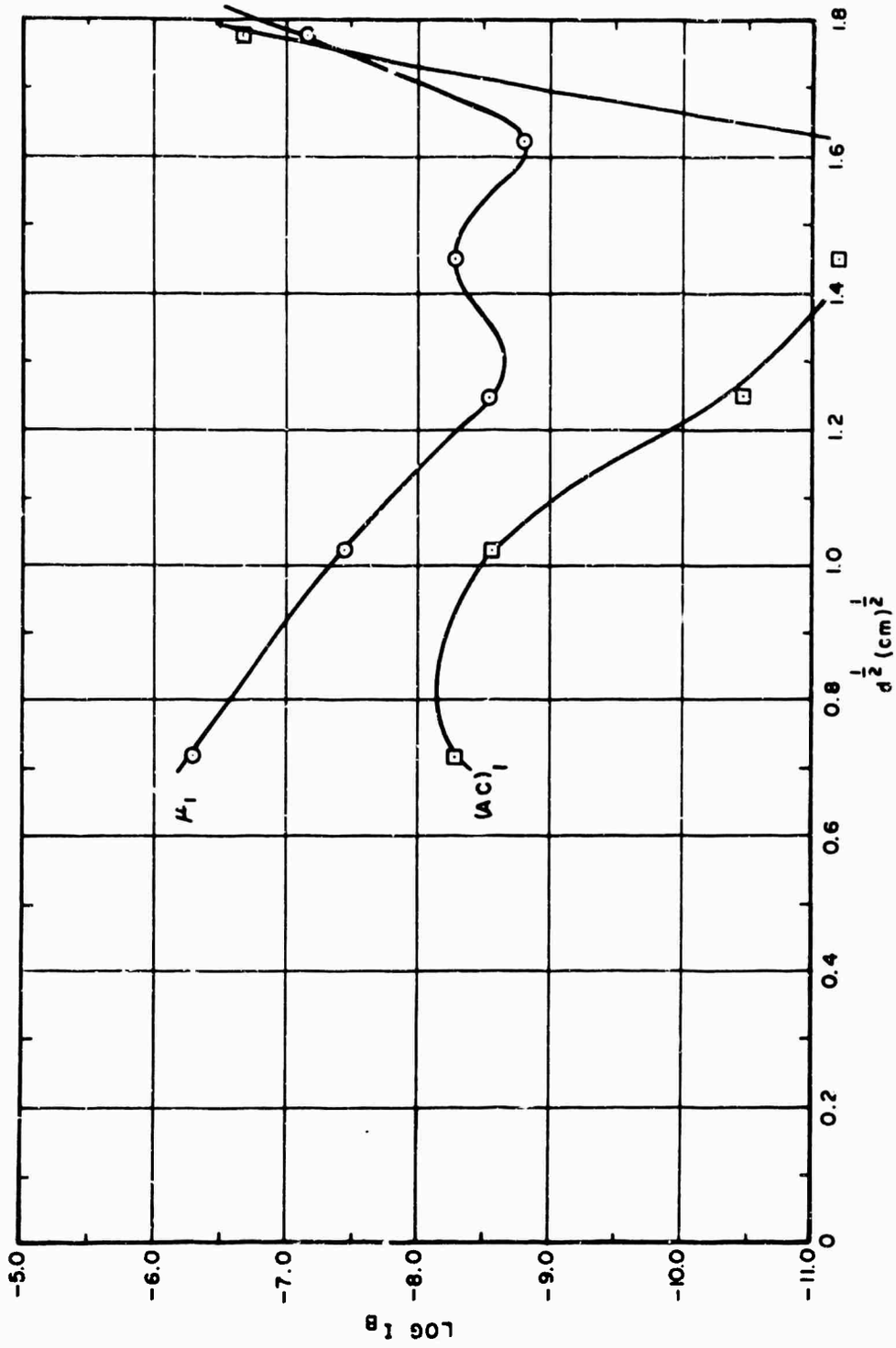

Figure 3-41. The AC Effect on Current

1-2424

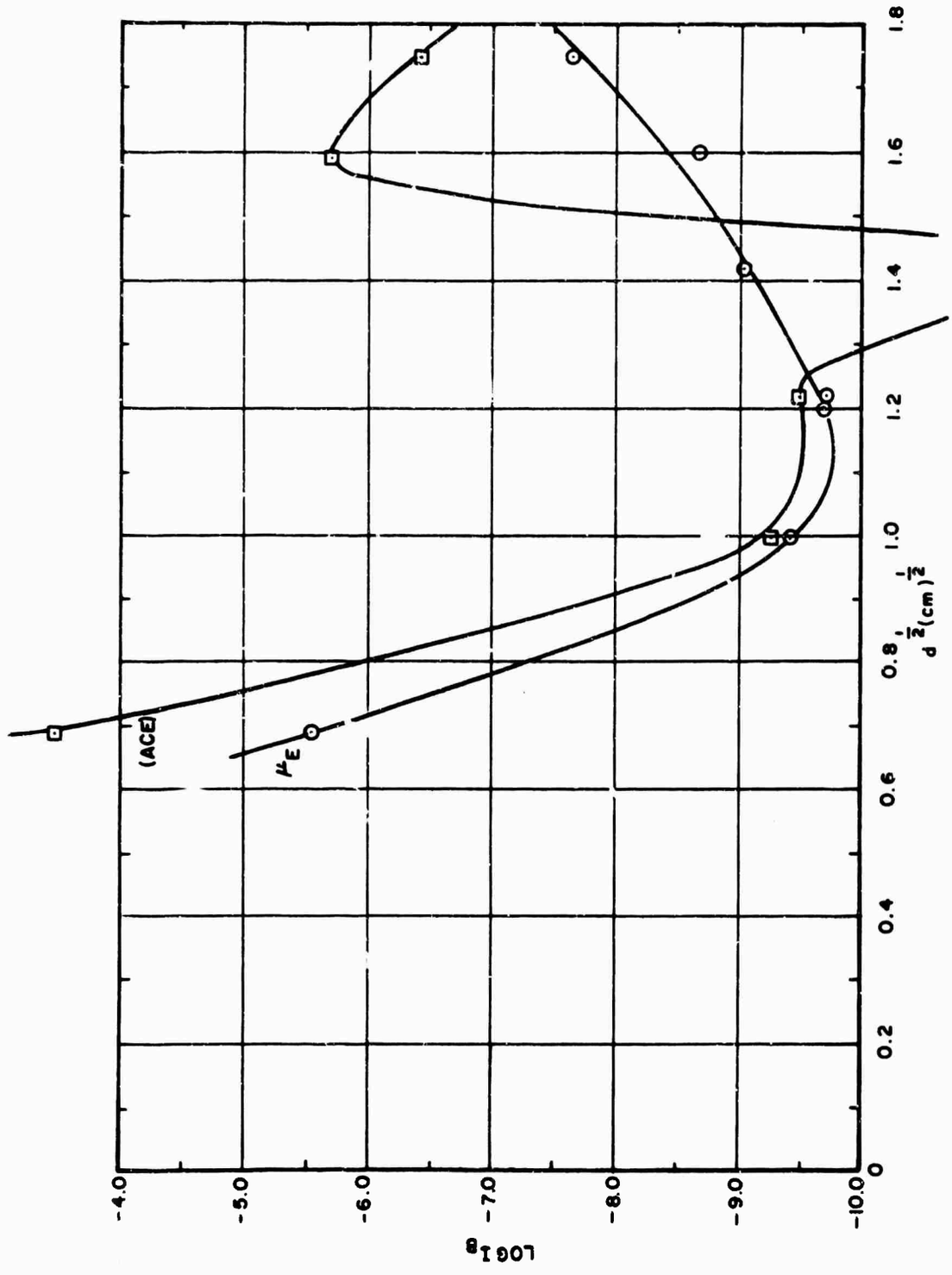

Figure 3-42. The ACE Effect on Current

1-2425

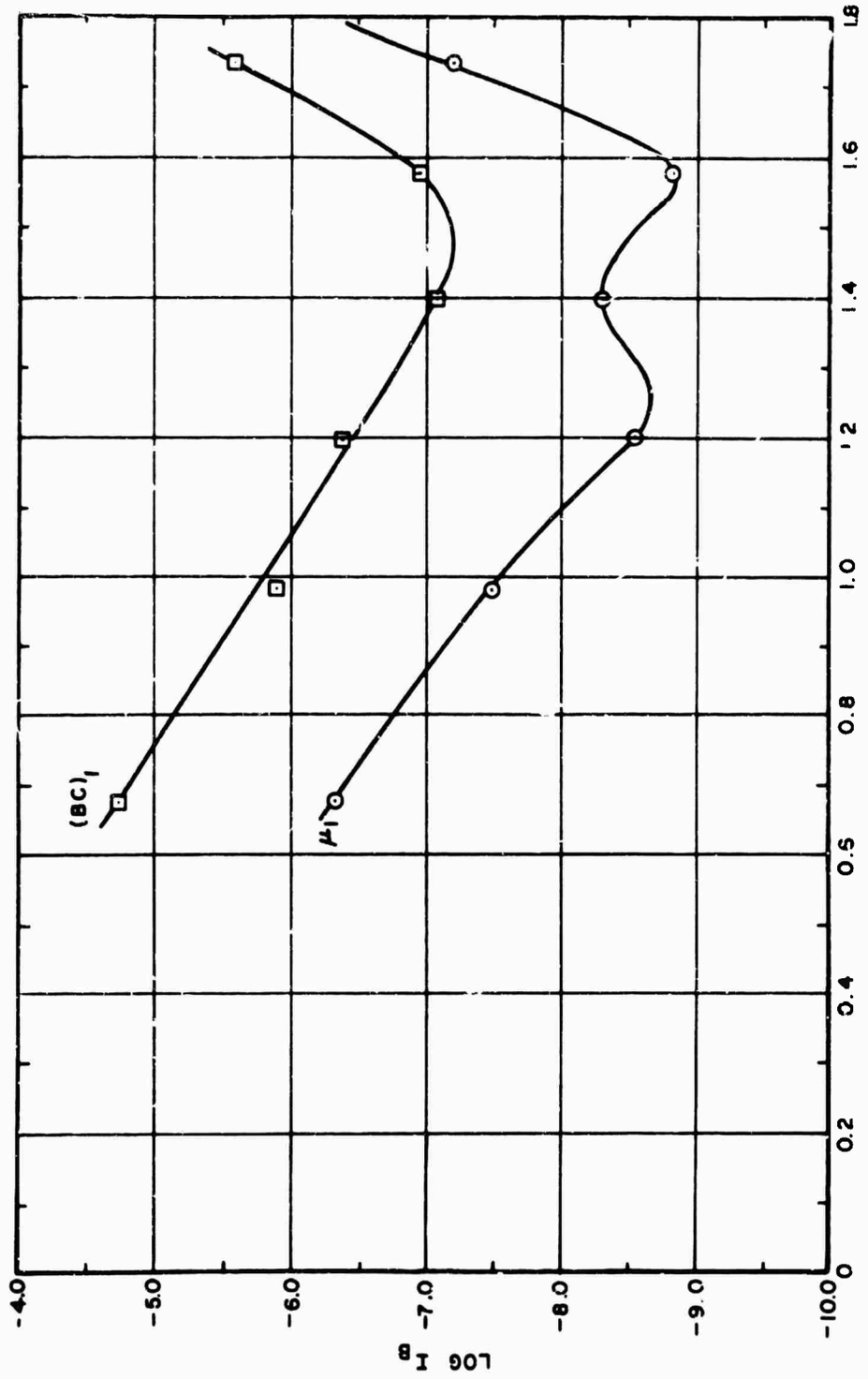

Figure 3-43. The BC Effect on Current

1-2426

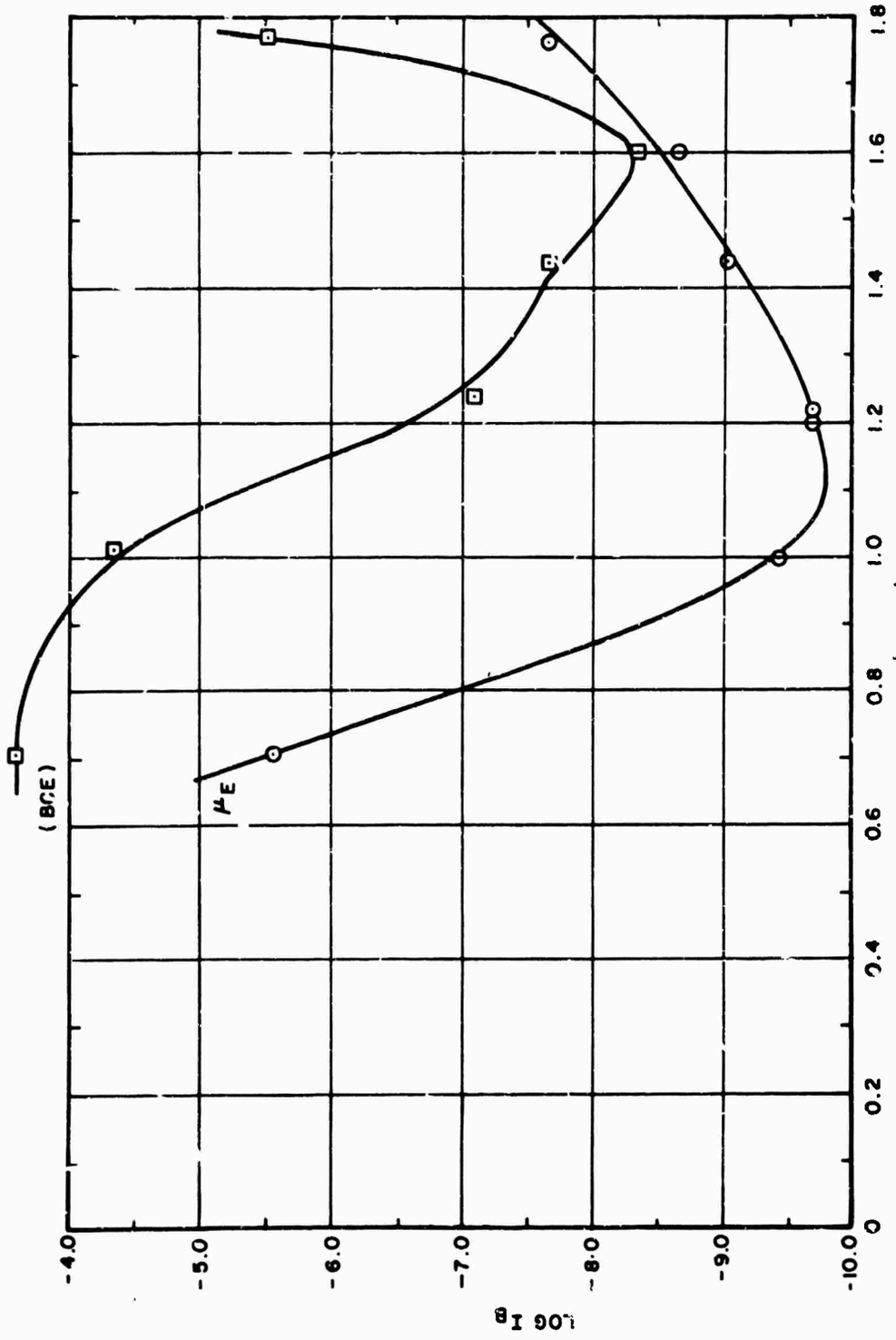

Figure 3-44. The BCE Effect on Current

1-2427

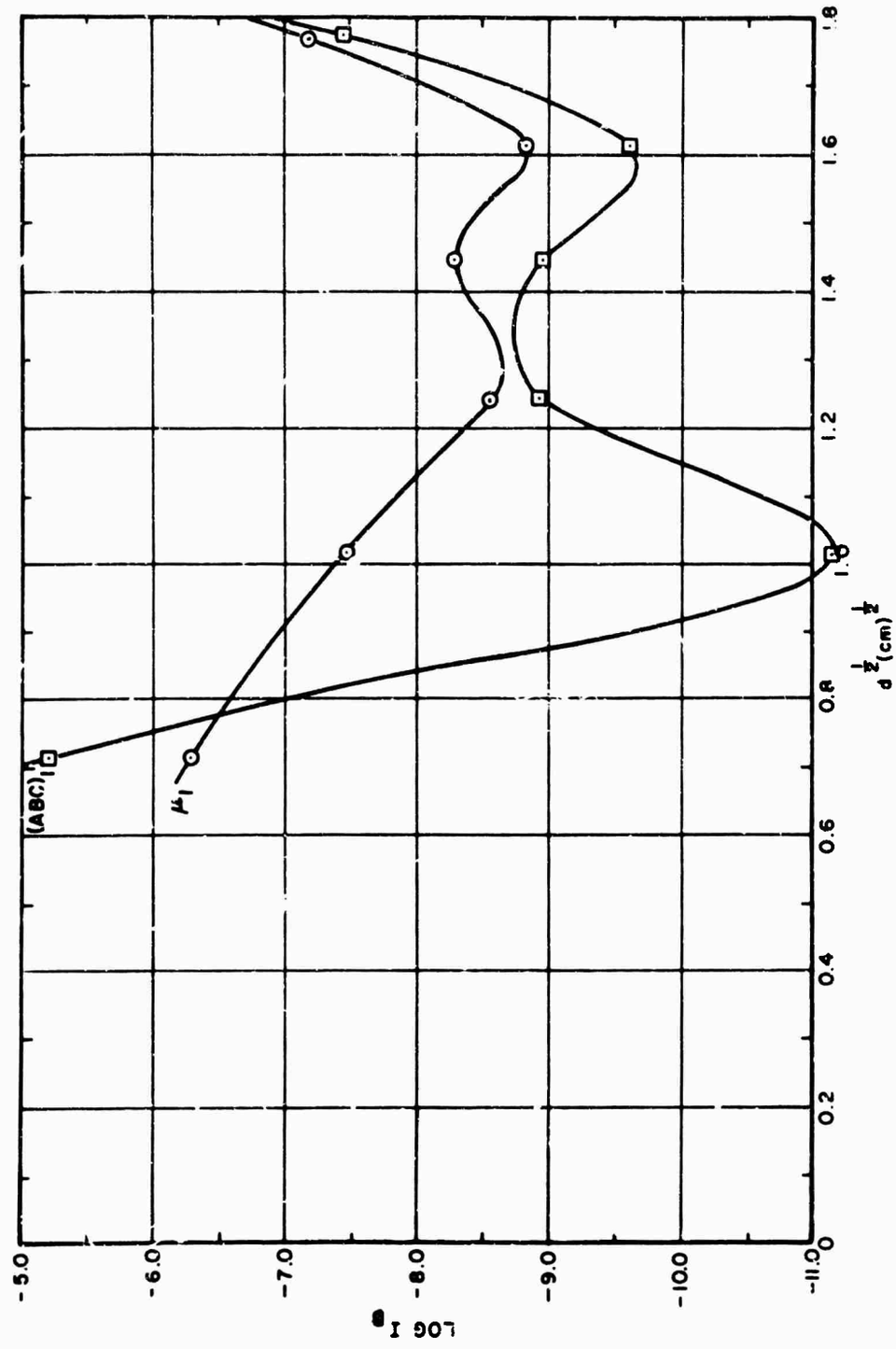

Figure 3-45. The ABC Effect on Current

1-2428

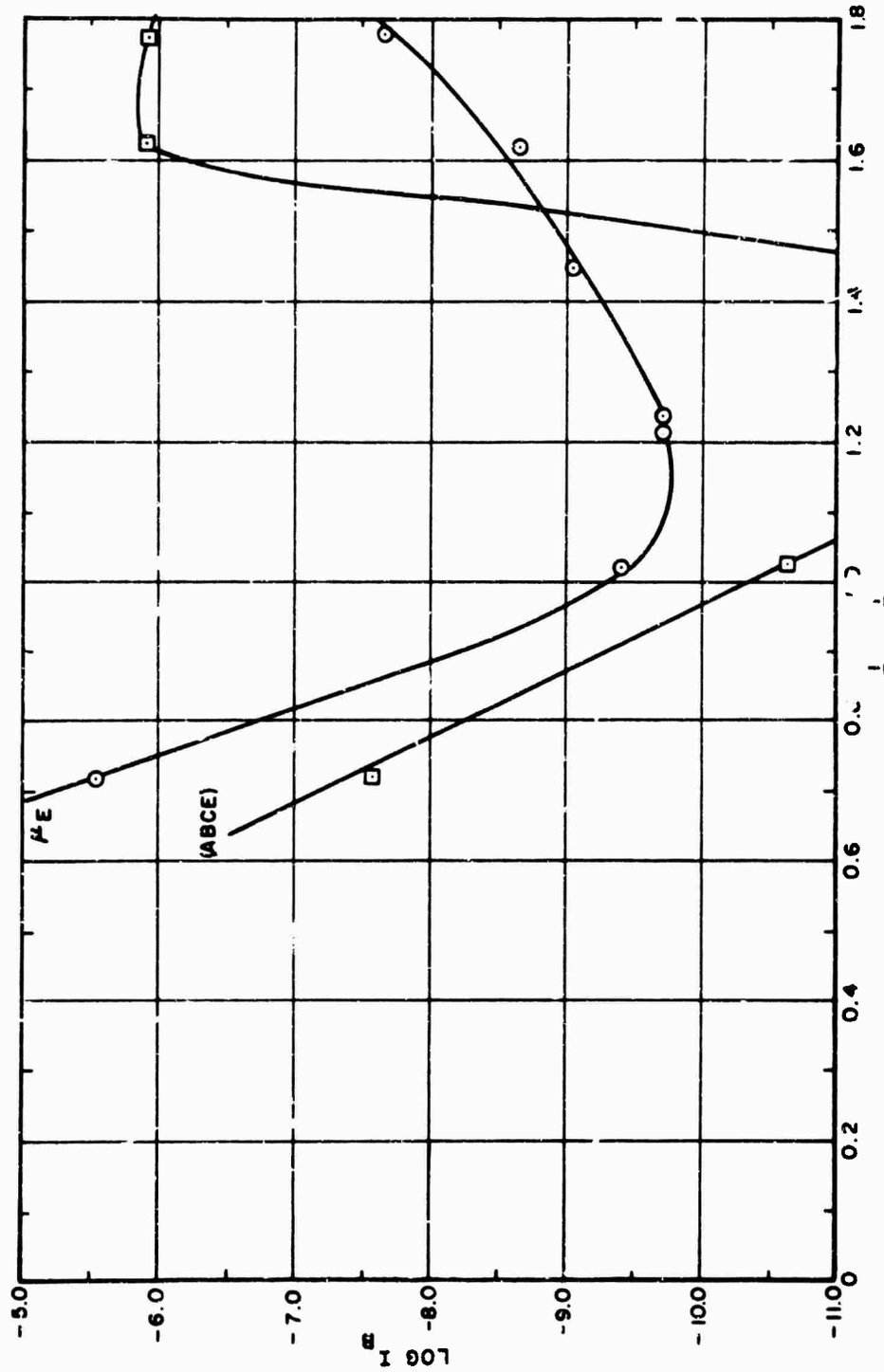

Figure 3-46. The ABCE Effect on Current

1-2429

3.2 Unconditioned and Conditioned Breakdown Voltage

In Figures 3-1 through 3-15 the various effects and interactions have been ploited as a function of gap separation by adding the result of a positive effect to the mean value of breakdown voltage, as was done for the magnetic results reported in the Eleventh Quarterly Report.

The significant results of this analysis are that precisely the same effects and interactions are revealed in the first two cycles as were shown in the third (magnetic test) cycle. In particular the A and B effects which show up very small and hence with rather dubious significance come out much greater but with just the same reproducibility over all gap separation and from test to test. Physically this means that the pretreatment procedure affected both the anode and cathode but after the first test cycle the magnitude of the effects decreased. Again the C and AC effects were the most significant.

3.3 Effect of Conditioning

The magnitude of the increase in breakdown voltage V_B between conditioned and unconditioned has been analysed. There are 12 breakdown events between each measurement and these are equally distributed among gap separations from 0.5 to 3.0 cm.

The principal results are:

(1) The conditioning effect decreases with gap separation. This could also imply a decrease with the total number of sparks.

(2) The C, BC and ABC effects are the most consistently significant, the latter having a steady downward trend, as in the μ-effect.

3.4 Effect of Magnetic Field

After completing the design tasks of the block of eight experiment some exploratory research was done during all treatments to study the effect of magnetic field strength on breakdown voltage. Breakdowns were observed for six values of transverse magnetic field intensity from zero to 290 gauss at either 2 cm or 3 cm gaps. Unfortunately due to the exploratory nature of the work the gap separation was not standardized but the tests were made over all treatments. The change in breakdown voltage ΔV_B over the zero field value was normalized by representing it as a percentage of that value. Various effects and interactions were derived from this set of results by using the Yates Algorithm. There are presented graphically in Figures 3-24 through 3-31.

The average effect of the transverse magnetic field is small and positive up to about 100 amps magnitizing current (~ 80 gauss) and then it goes negative up to about -10% at 250 gauss. This last figure is smaller than the average effect at 3 cm gap taken from the previous stack of the experiment. It is thus important to conduct future experiments over a range of transverse magnetic field strengths. The experiment if conducted for instance at 80 gauss would have yielded a zero effect.

The combined influence of magnetic field and anode baking (AE) becomes steadily more negative with increasing field and the opposite is true for cathode baking (BE). The CE effect (electrode size) is oscillatory and all combinations with this and A are likewise oscillatory.

3.5 The Ultimate Prebreakdown

3.5.1 Current Data

During the third (magnetic test) cycle of data taking the ultimate prebreakdown current was recorded with the breakdown voltage. The logarithm of this current has been used as a parameter with which to study the various possible effects and interactions. The results of the Yates Algorithm are presented in Table 3-4 and in Figures 3-32 through 3-46 in the same manner as V_B has been treated.

The logarithm of the current is strongly indicative of the tunneling probability function for an electron leaving the cathode surface. This in turn depends upon the shape of the cathode surface potential barrier which governs field emission.

The significant results to note are outlined in the following subsections.

3.5.2 The Average Current (μ)

The logarithm of the ultimate prebreakdown current as a function of square root of gap separation shows a deep undulating trough in the gap separation range from 1.5 to 2.5 cm.

The application of a transverse magnetic field reduces this current and after the field is removed there is an increase in the ultimate prebreakdown current. It is the same general function of gap separation in all of these cases.

3.5.3 Principal Effects and Interactions

Without figures of confidence it is difficult to interpret reliable effects. Some phenomena however are worth noting.

Vacuum baking, of the cathode (B effect) strongly influences the undulating shape of the characteristics and the BC effect is consistently positive. Large area electrodes seem to lower the ultimate prebreakdown current below the average and magnetic field influences this.

The factor A (anode treatment) and all of its interactions contribute either positively or negatively to the ultimate prebreakdown current according to the gap separation in similar ways.

SECTION 4

PHYSICAL ANALYSIS OF RESULTS OF THE "BLOCK OF EIGHT" EXPERIMENT

4.1 Prebreakdown Current

Apart from the dramatic effects of the transverse magnetic field strength on breakdown voltage the next most important observation was that the prebreakdown current was reduced progressively as the field strength was increased. Current - voltage characteristics at various magnetic field strengths are presented in Figure 4-1. The undulations in the characteristics are thought to be due to resonant variation of the tunneling probability as proposed by Duke and Afferuff[2].

The field strengths involved were extremely small, the greatest being 250 gauss and the significant current changes are too much to be explained by the minute changes made to the electron vacuum trajectories. It is however possible to explain it in the following manner by studying the surface physics of a field emitter in a transverse magnetic field. This may be termed the Hall effect in field emission.

Consider the physical situation of a strong field emission current density J_x flowing into vacuum across a metal surface. Ordinarily, an ohmic electron field develops inside the metal in the x direction when a transverse H_z field is applied an E_y field develops but is shorted out if there is an internal conduction path. A system of such shorting loops is shown for an emitting tip in Figure 4-2. The reaction of this against the H_z field is such as to reduce the J_x current. Thus J_x and J_y are complimentary to one another and are related by a tensor conductivity. The appropriate conductivity data of course pertain to the surface states of the metal.

If the current strength is governed by a tunneling probability through the barrier this will be a function of θ, the angle of incidence relative to the normal to the barrier. At the same time θ is determined by the tensor conductivity and two expressions will simultaneously fix $J(\theta)$ the current density and direction.

$$J \doteq A E_s^2 \exp \left\{ \frac{B}{E_s \cos \theta} \right\}$$

$$\frac{J_H}{J} = \sin \theta$$

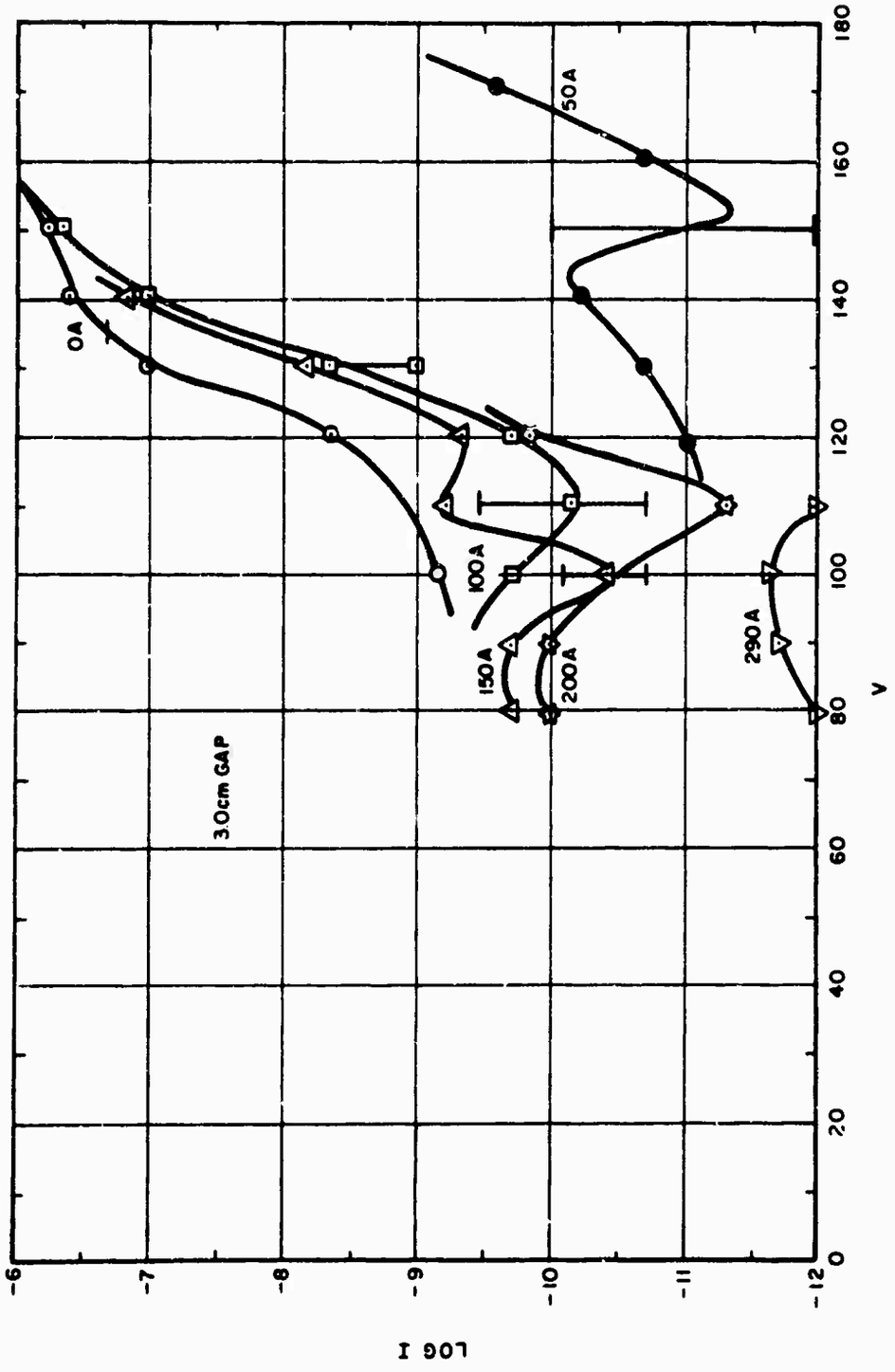

Figure 4-1. V-I Characteristics for Different Magnetic Field Strengths

1-2431

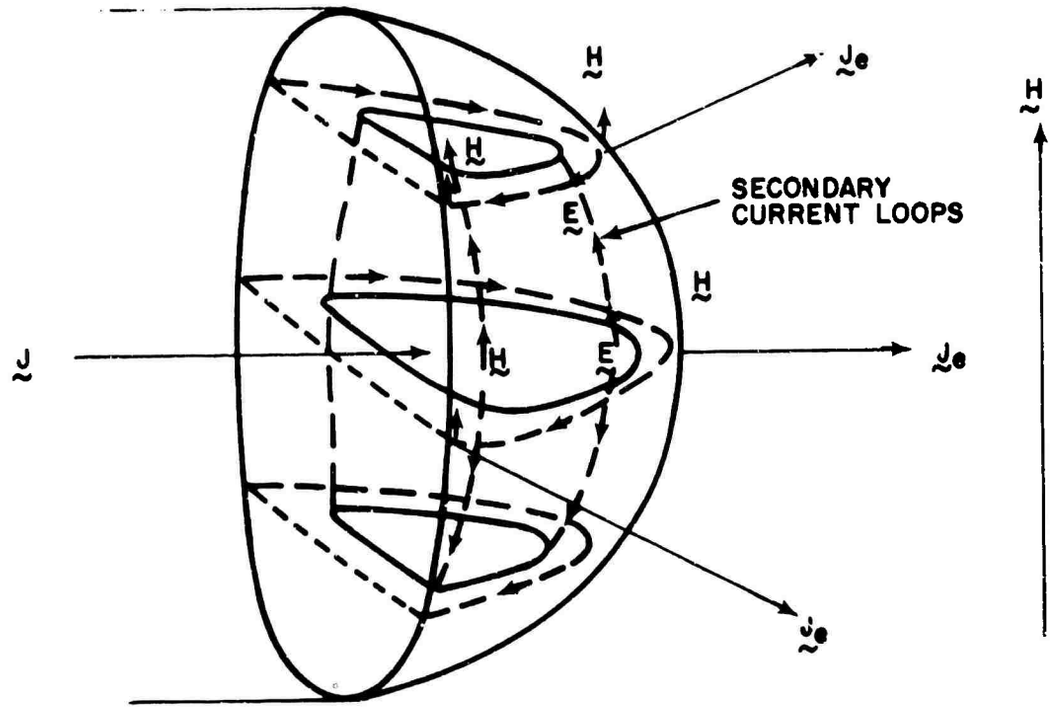

Figure 4-2. Hall Effect in Field Emission

1-2448

The first of these equations arises from analysis of the tunneling probability of an electron approaching a barrier. When the approach is not normal to the surface the electron will see an electric field reduced by the factor cos θ which therefore enters the Fowler-Nordheim exponent linearly. This very simple viewpoint neglects the finer point that electrons cross the barrier at all angles but the average is at an angle θ to the normal. This is however no worse a restriction than is assumed in the usual Fowler-Nordheim theory.

The angle θ can be inferred from the tensor conductivity thus:

$$E_1 = \sigma_{\parallel} J + \sigma_{\perp} J_H$$

$$E_2 = -\sigma_{\parallel} J + \sigma_{\perp} J_H$$

therefore:

$$\frac{J}{J_H} = \frac{E_1 \sigma_{\parallel} - E_2 \sigma_{\perp}}{\sigma_{\parallel}^2 + \sigma_{\perp}^2}$$

and from Figure 4-3:

$$\frac{J_H}{J} = \sin\theta = \frac{E_1}{\sigma_{\parallel}} \left\{ 1 + \left(\frac{\sigma_{\perp}}{\sigma_{\parallel}} \right)^2 \right\}^{-1}$$

if the field E_2 is shorted out and since:

$$\frac{\sigma_{\perp}}{\sigma_{\parallel}} = bH$$

where b = electron mobility on the metal surface. Therefore:

$$\cos\theta = \left[1 - \left(\frac{E_1}{\sigma_{\parallel}} \right)^2 \left\{ 1 + (bH)^2 \right\}^2 \right]^{1/2}$$

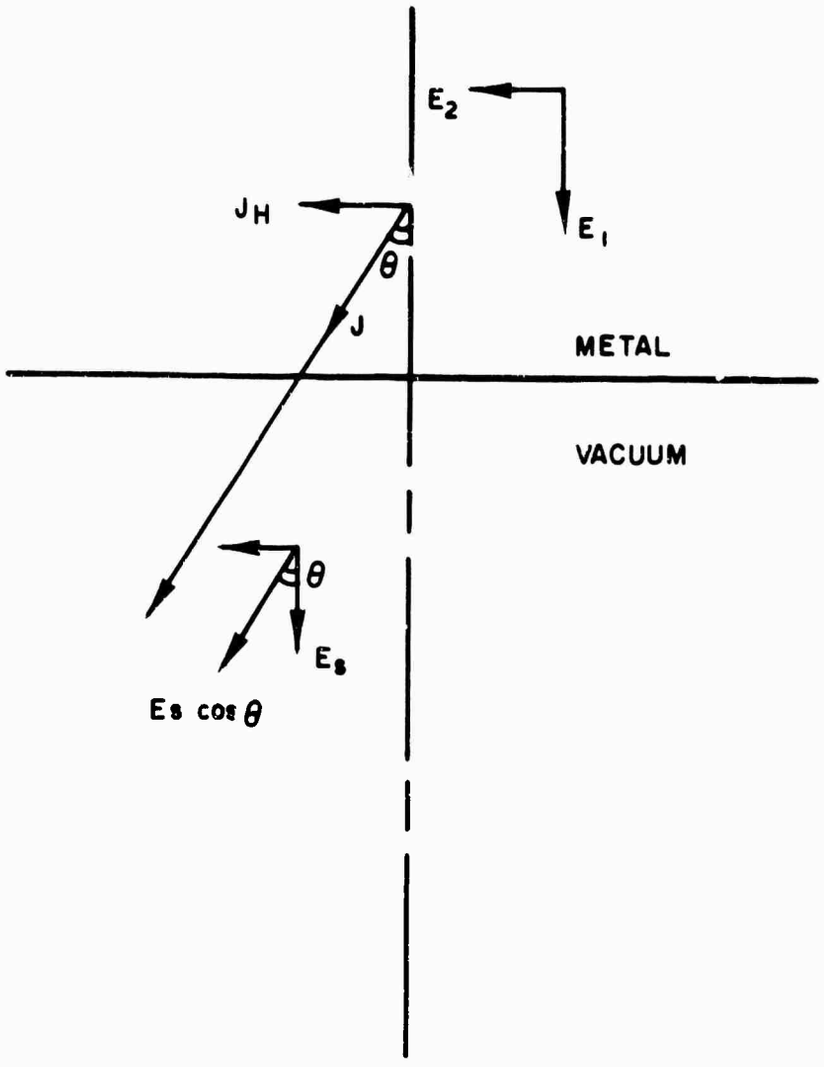

Figure 4-3. Diagram to Illustrate Passage of Electron Current From Metal into Vacuum

1-2432

Hence the Fowler-Nordheim expression is:

$$J = A\,E_s^2 \exp\left\{ -\frac{B}{E_s} \cdot \frac{1}{\left[1 - \left(\frac{E_1}{\sigma_{11}}\right)^2 \left\{1 + (bH)^2\right\}^2\right]^{1/2}} \right\}$$

and since:

$$I = \pi r^2 J$$

$$r = \frac{12\pi\gamma}{E_\varepsilon^2} = \frac{V^2}{12\pi\gamma k^2}$$

then:

$$-\frac{1}{V} \ln\left\{\frac{I}{V^2}\right\} \propto \frac{B}{\left[1 - \left(\frac{E_1}{\sigma_{11}}\right)^2 \left\{1 + (bH)^2\right\}^2\right]^{1/2}}$$

The electric field E_1 is the value pertaining to the narrow region just inside the metal surface. In a perfect conductor $E_1 = 0$ but in real cases it depends upon the electron distribution at the surface and therefore to the properties of the surface states. If E_s were applied to the surface of a perfect conductor in vacuum an appropriate charge sheet would develop to screen it from the interior. In the real case however the charge density falls off more gradually into the metal in accordance with the population density of the surface states. Thus the internal surface field intensity can be represented as a function of depth x from the surface as:

$$E_1 = E_s - \phi_1(x)$$

where:

$$0 < \phi_1(x) < E_s$$

or:

$$E_l = E_s \left\{ 1 - \phi(x) \right\}$$

where:

$$0 < \phi(x) < 1$$

The conductivity σ is also proportional to the electron density at any depth and is therefore proportional to dE_l/dx. Therefore:

$$\frac{E_l}{\sigma_{ll}} \propto \frac{E_s}{\left| \frac{dE_l}{dx} \right|} \left\{ 1 - \phi(x) \right\}$$

Therefore:

$$\frac{E_l}{\sigma_{ll}} \propto \frac{1}{V} \frac{\left\{ 1 - \phi(x) \right\}}{\left| \frac{dE_l}{dx} \right|} = \frac{\psi(x)}{V}$$

since:

$$VE_s = 12 \pi \gamma k$$

Thus:

$$-\frac{1}{V} \ell n \left\{ \frac{I}{V^2} \right\} = \frac{B}{\left[1 - \left(\frac{\psi(x)}{V} \right)^2 \left\{ 1 + (bH)^2 \right\}^2 \right]^{1/2}} + \text{Const}$$

This shows clearly that the expression should increase with H increasing and decrease as V increases. This is shown to be so in Figures 4-4 through 4-9 which were plotted from the results of five consecutive tests in which the ultimate prebreakdown current and breakdown voltage were measured at 2 cm and 3 cm gaps over the range of transverse field strengths from 0 to 250 gauss.

The results show quite clearly that there is a general trend which is critically dependent on the test sequence and is therefore a function of level of conditioning.

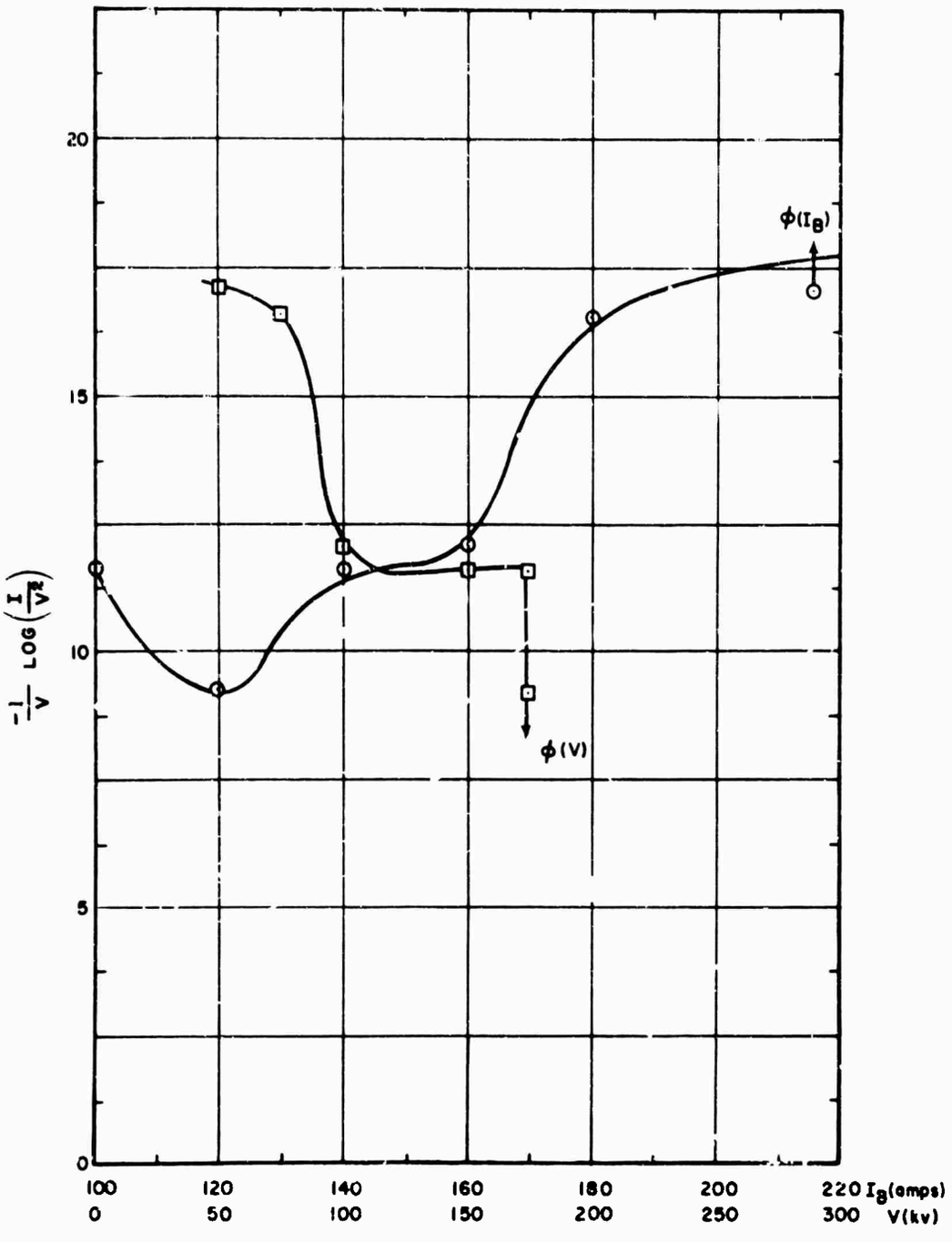

Figure 4-4. I/V Log I/V^2 as a Function of V and Magnetizing Current (3 cm gap - Test No. 1)

1-2433

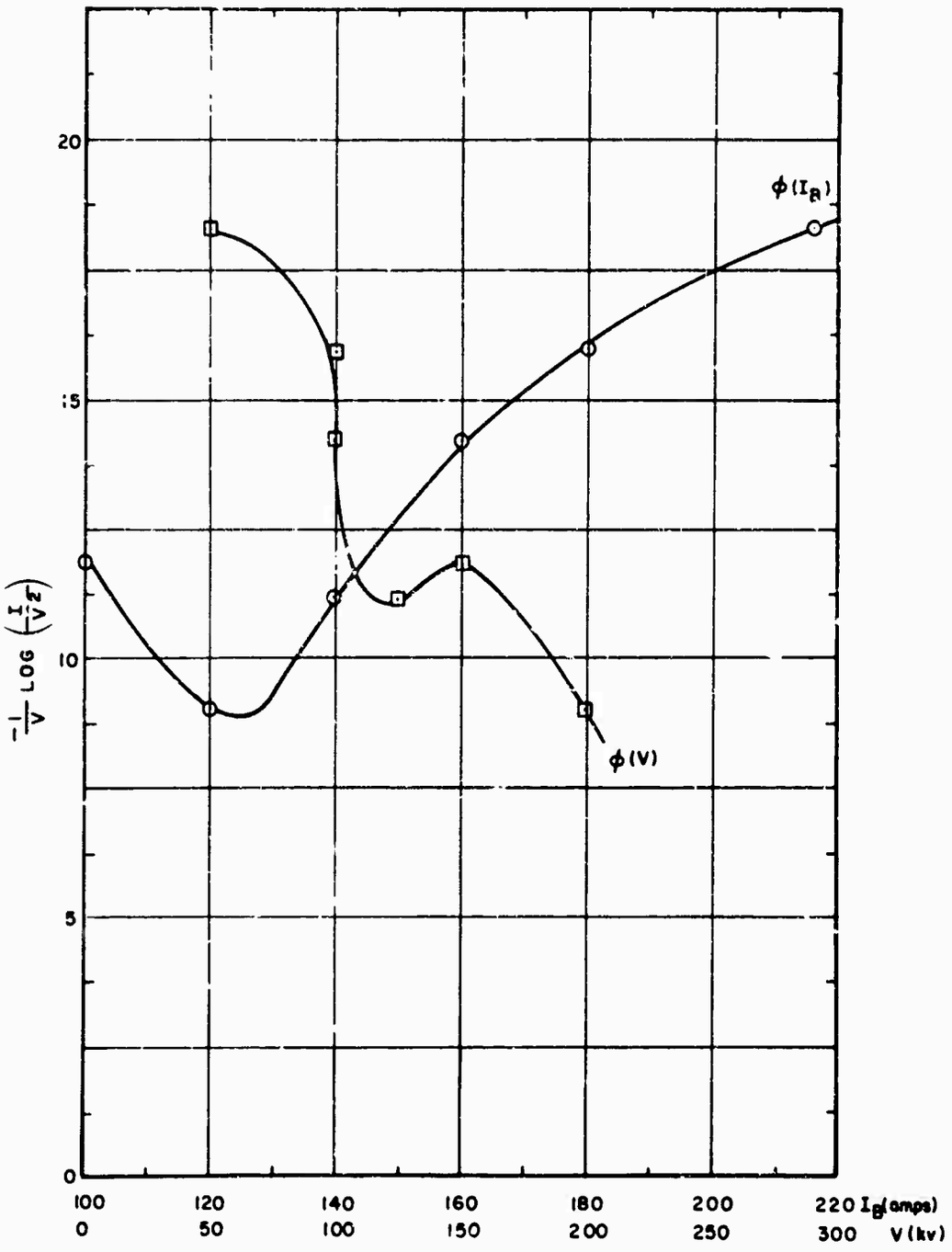

Figure 4-5. I/V Log I/V^2 as a Function of V and Magnetizing Current (.) cm gap - Test No. 2)

1-2434

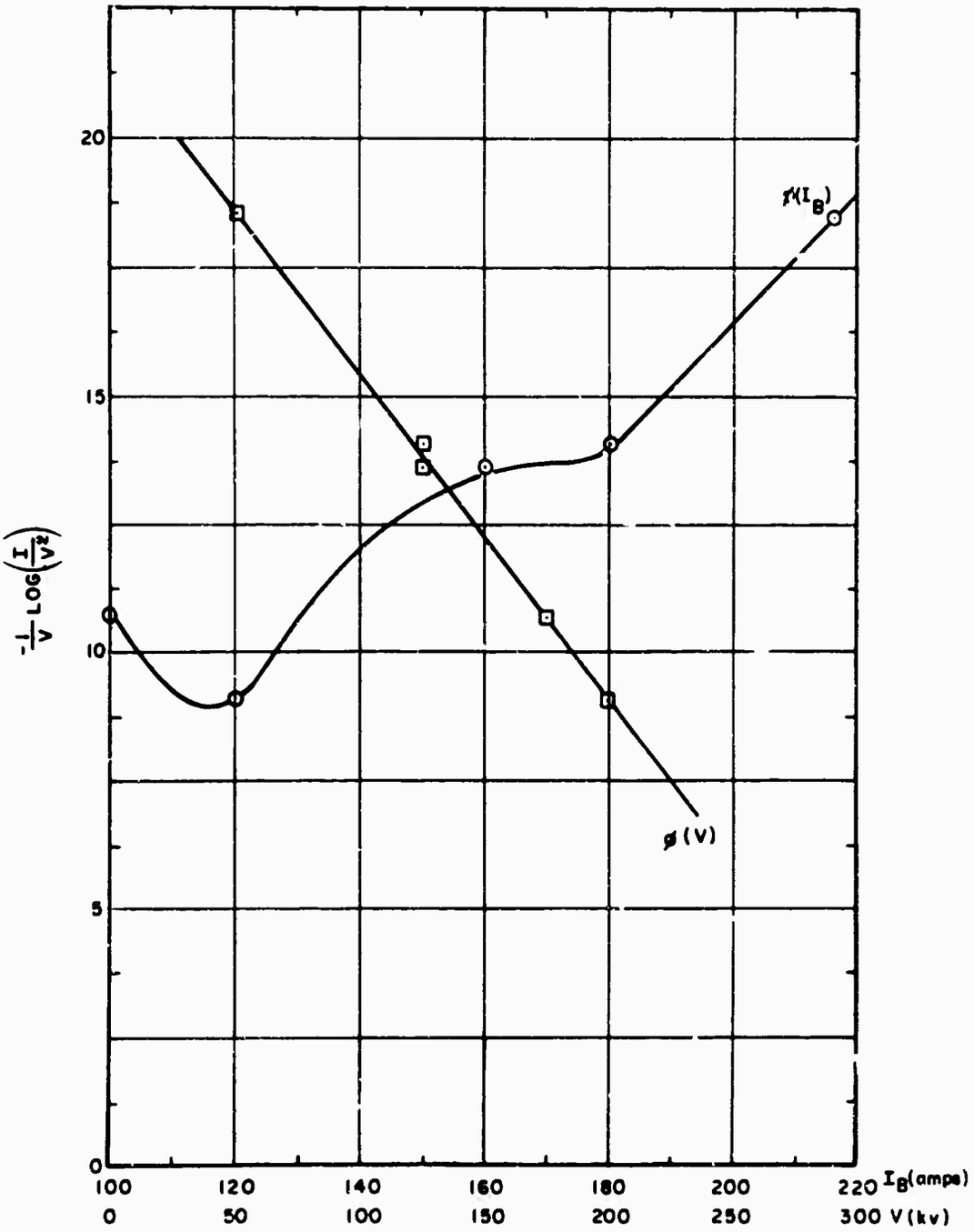

Figure 4-6. I/V Log I/V^2 as a Function of V and Magnetizing Current (2 cm gap - Test No. 3)

1-2435

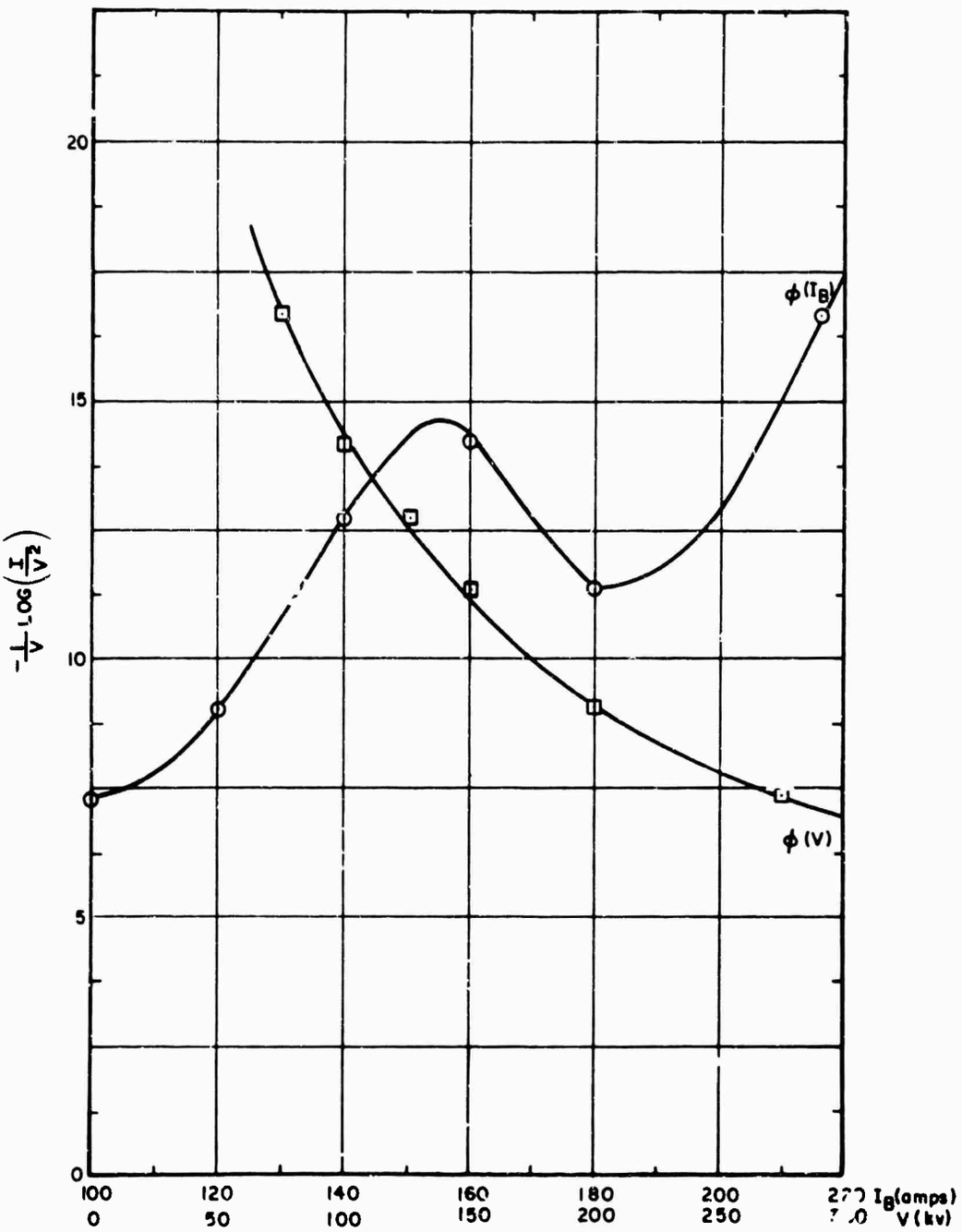

Figure 4-7. I/V Log I/V^2 as a Function of V and Magnetizing Current (3 cm gap - Test No. 4)

1-2436

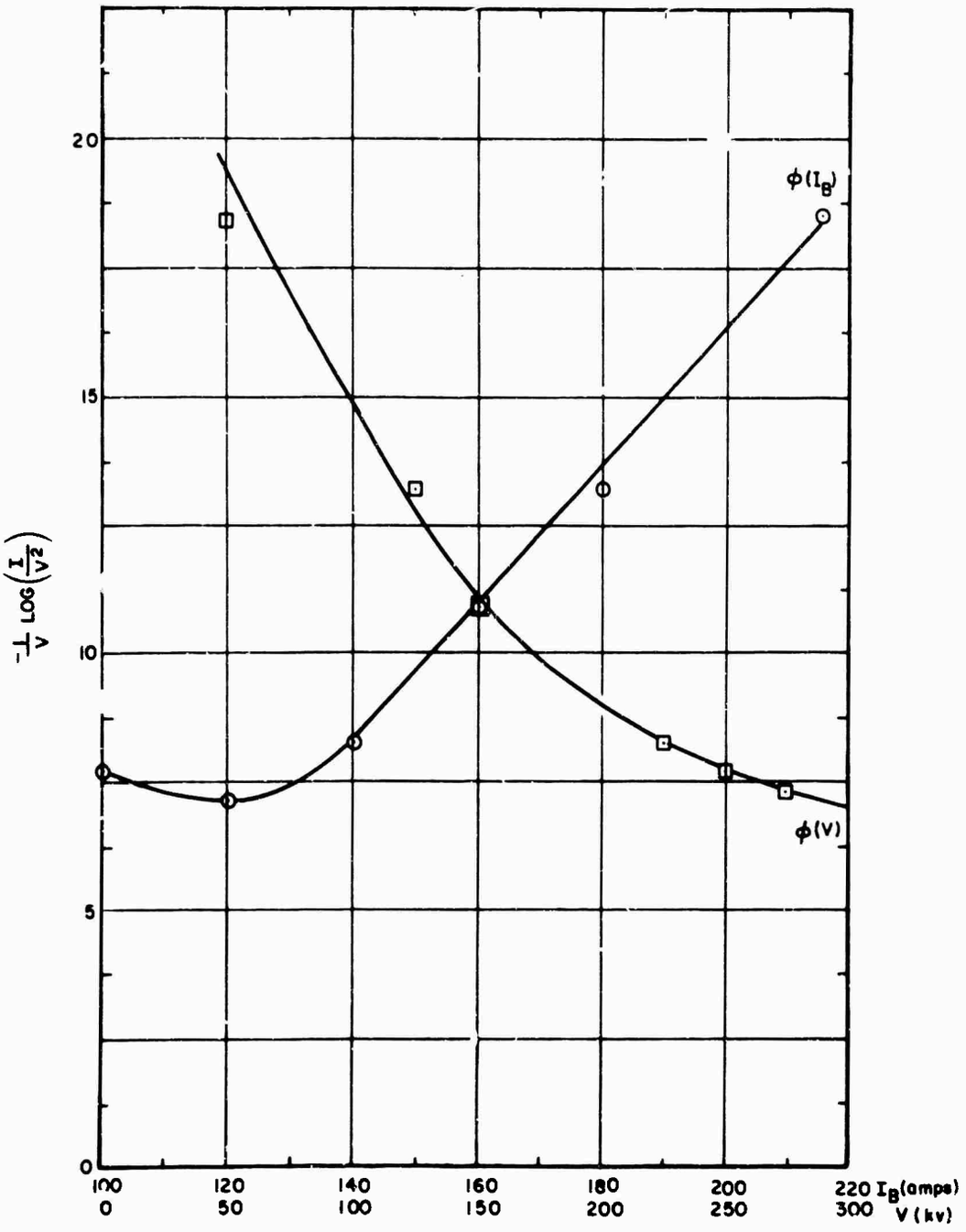

Figure 4-8. I/V Log I/V^2 as a Function of V and Magnetizing Current (3 cm gap - Test No. 5)

1-2437

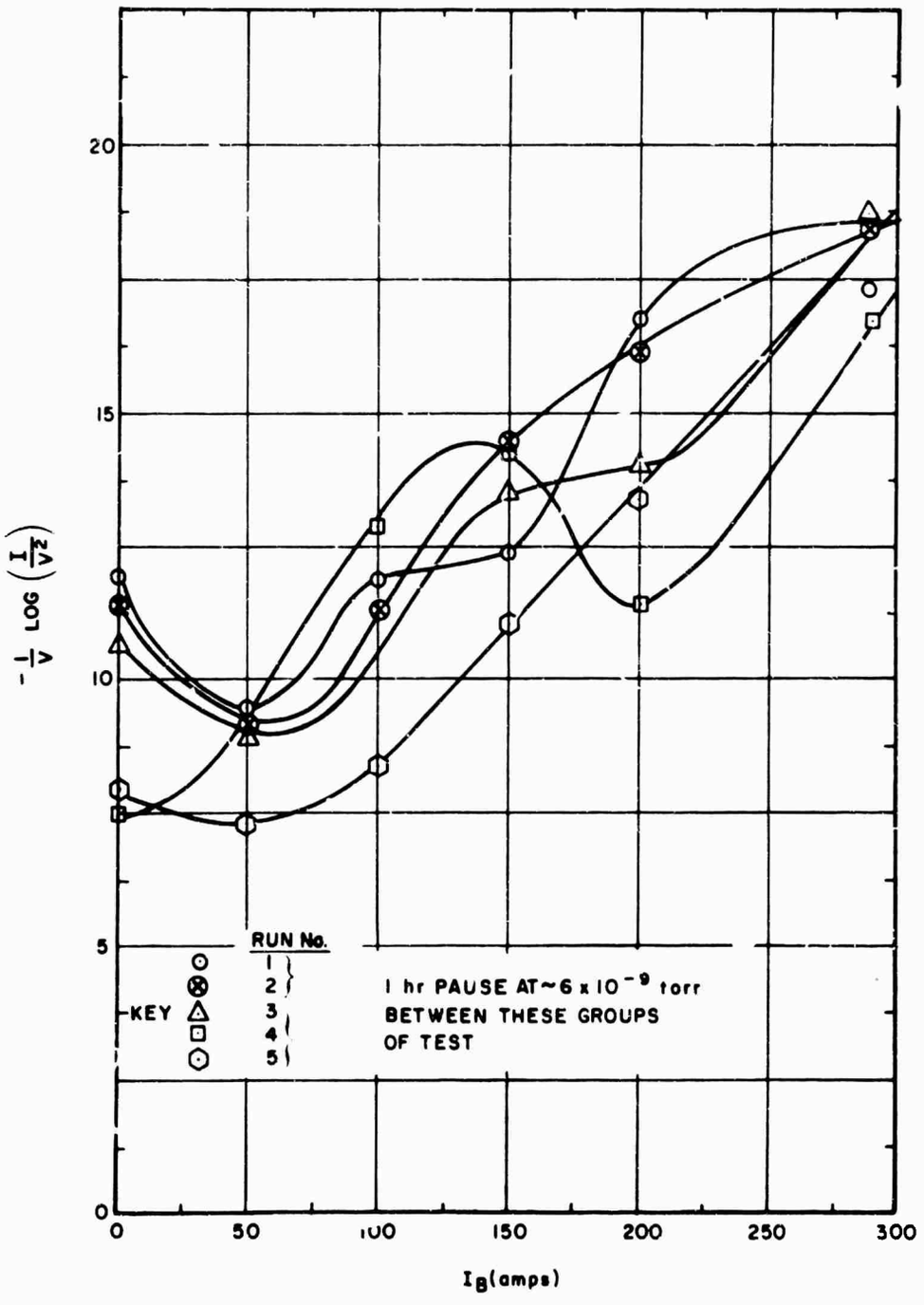

Figure 4-9. I/V Log I/V^2 as a Function of Magnetizing Current in Five Consecutive Tests

1-2438

The theoretical interpretation of this data indicates that the details of the phenomena will . explained by some knowledge of the surface physics of the cathode.

4.2 Collapse of Gap Voltage

For five of the block of eight experiments, waveforms showing collapse of gap voltage were taken during the early part of the test (up to 25 breakdowns). The time to collapse is defined as the time interval between the scope triggering and collapse of gap voltage to almost zero, the probe requiring a rapid gap voltage fluctuation of several kilovolts to cause it to trigger the oscilloscope (Figure 4-10).

The results are shown in Figures 4-11 through 4-15 and all data collected together in Figure 4-16 with the overall mean time shown for each gap. It is seen that up to 1.5 cm gap the mean collapse time increases almost linearly with spacing (150×10^{-9} sec/cm) while for 2 to 3 cm gaps is approximately 550 nsec.

In the majority of waveforms, the gap voltage tended to collapse partially (20 to 30%) and then recover before proceeding to total collapse. During the total collapse some oscillation on the decaying voltage was usually observed. In the few cases where corresponding current waveforms were recorded, the voltage waveforms oscillations coincided with current oscillations. At a given gap, the waveforms were seldom reproducible suggesting variations of gap impedance as being the main cause of oscillations rather than the external circuit (Figure 4-17).

The frequency of the main oscillation of the breakdown current (taken from relatively few results) depends on gap separation in the manner shown in Figure 4-17. The peak current is normally several hundred amperes (200 to 1500 amp) i.e. in reasonable agreement with the value calculated from the voltage and source impedance (160 ohms). It is lower than the calculated value due to the peak current occuring when there is still much of the voltage across the gap, that is, in the high impedance phase (~ 100 ohms). The reason for current reversal of 10 to 20 per cent is not clear (Figure 4-18).

Heard[3] when applying pulses superimposed on a steady voltage observed a time delay between the application of the pulse and current build-up and suggested a transit time effect. He observed a slowly rising current prior to rapid current build-up. Steps or the current build-up waveform were suggested as being caused by an ion-electron process (ions arriving at the cathode). Smith and Mason[4] when applying a 4/5000 microsecond impulse wave to large stainless steel electrode (2 cm gap) noted two distinct types of gap voltage collapse. Some 16 to 28 microseconds after applying the impulse the gap voltage either (a) collapsed rapidly in less than one microsecond or (b) fell slowly over

Gap (cm)	V_{BD} (kv)
1.0	100
1.25	130
1.5	147
1.75	130
2.0	130
2.5	160
2.75	180
3.0	150

Figure 4-10. Voltage Collapse Waveforms (Treatment ac)

2-750

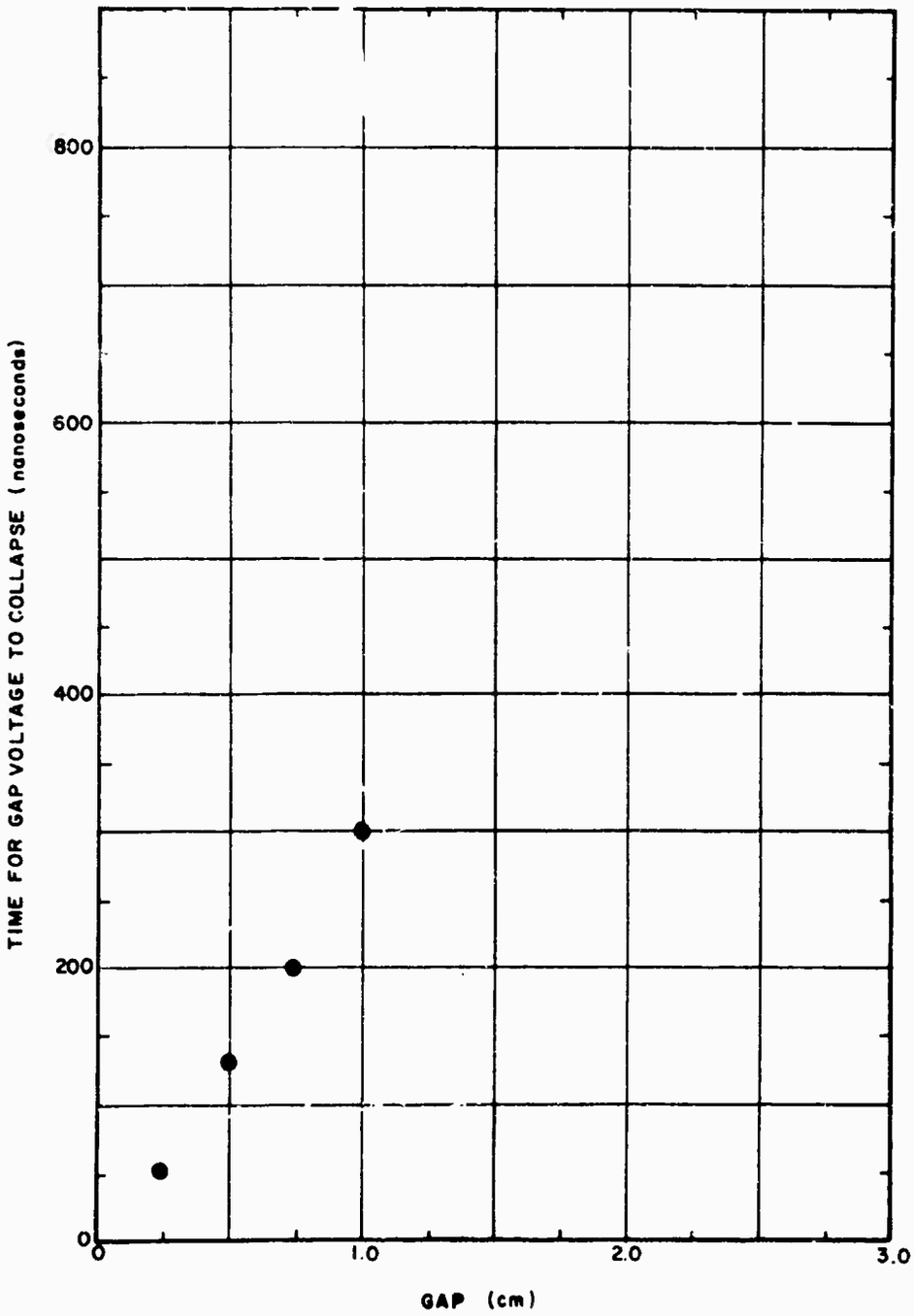

Figure 4-11. Collapse of Gap Voltage (Treatment b)

1-2439

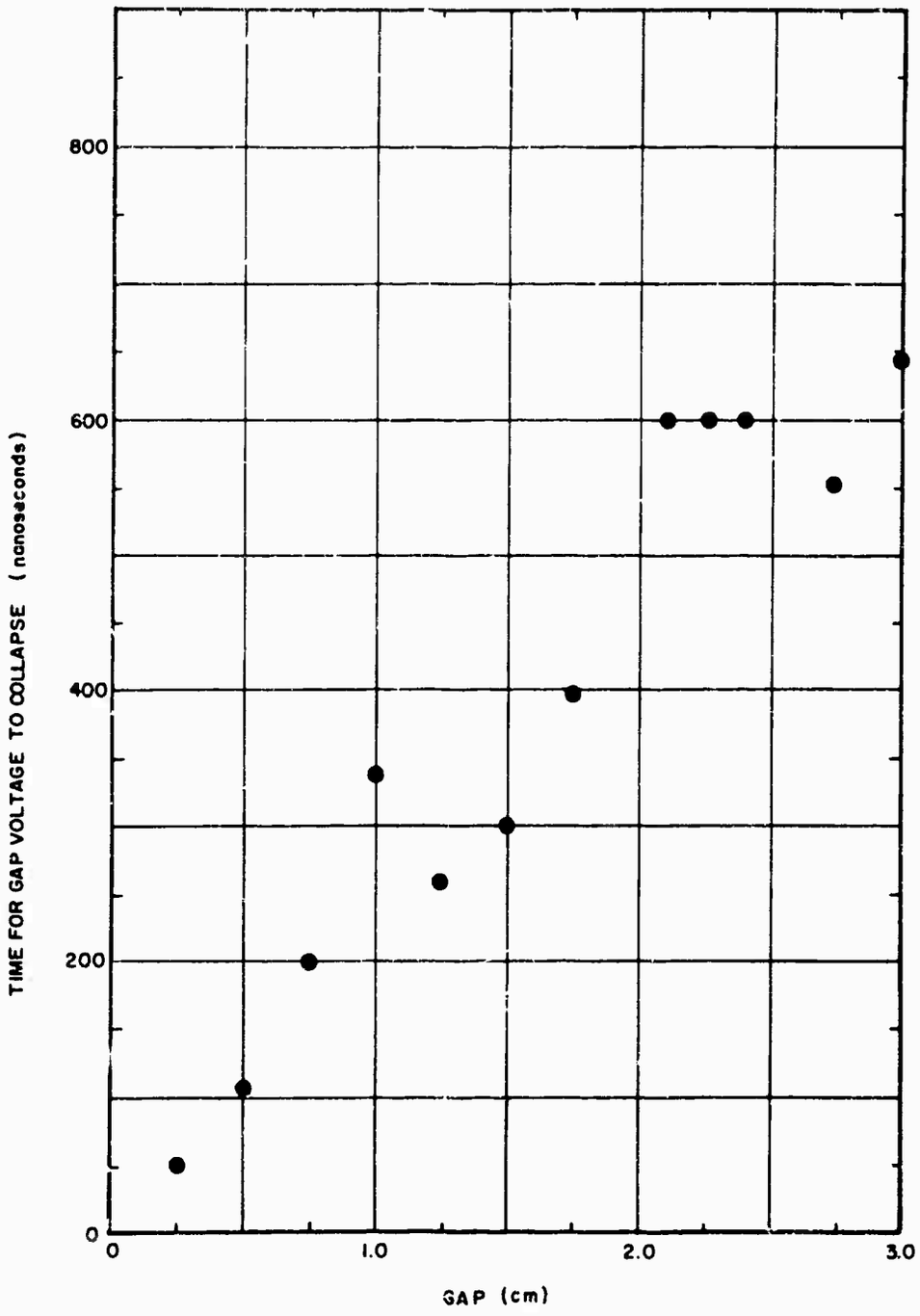

Figure 4-12. Collapse of Gap Voltage (Treatment a)

1-2440

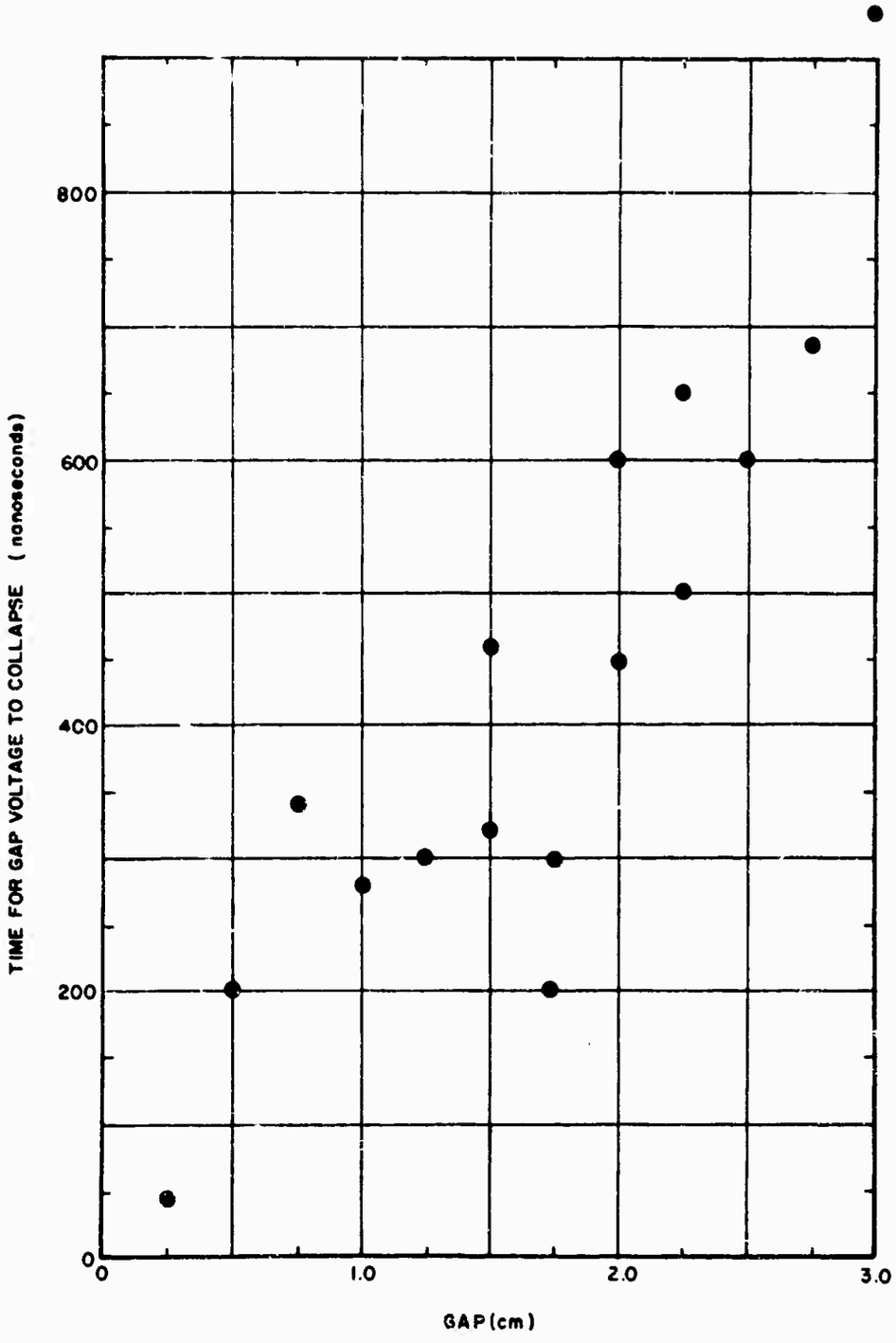

Figure 4-13. Collapse of Gap Voltage (Treatment abc)

1-2441

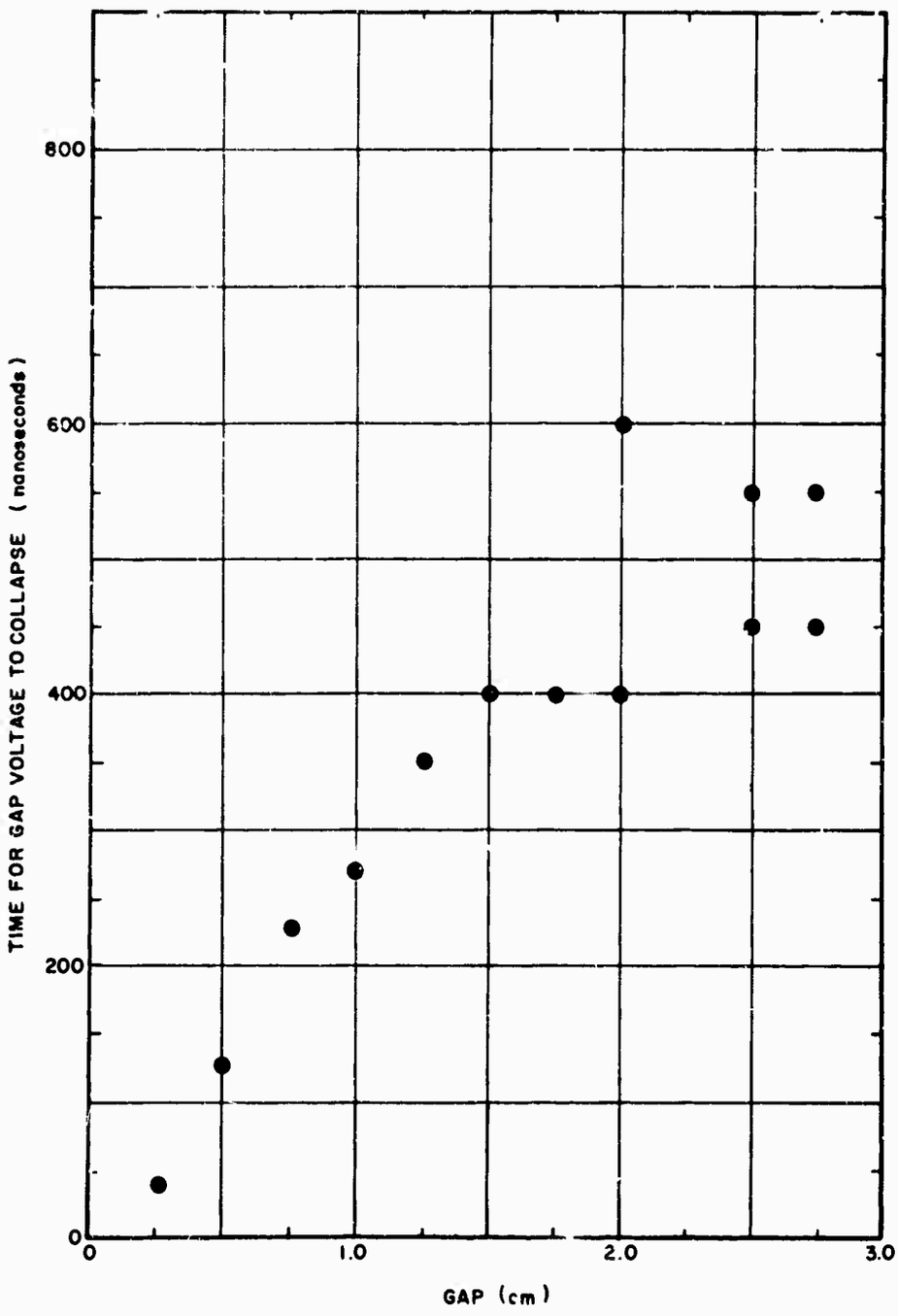

Figure 4-14. Collapse of Gap Voltage (Treatment ac)

1-2442

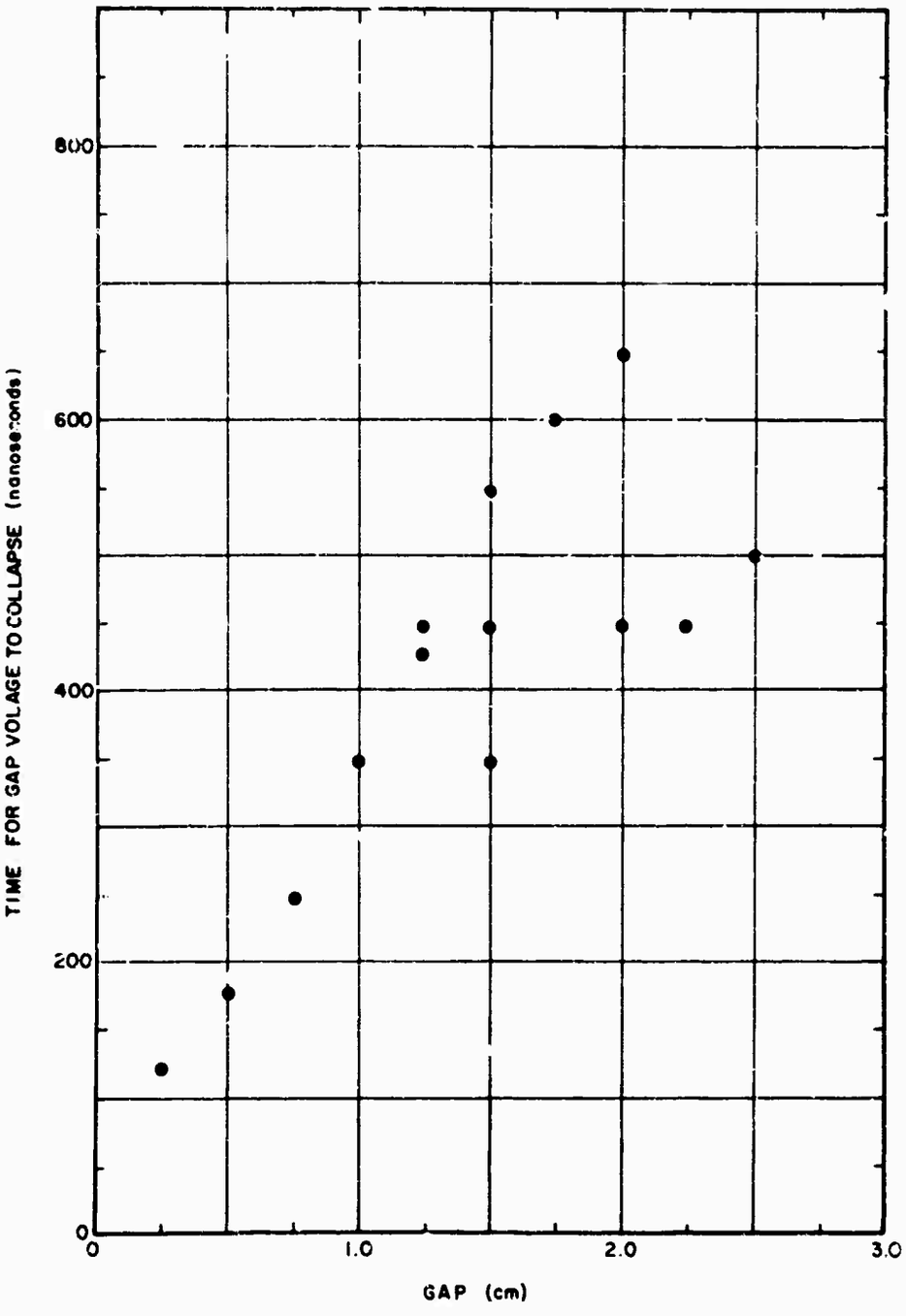

Figure 4-15. Collapse of Gap Voltage (Treatment b2)

1-2443

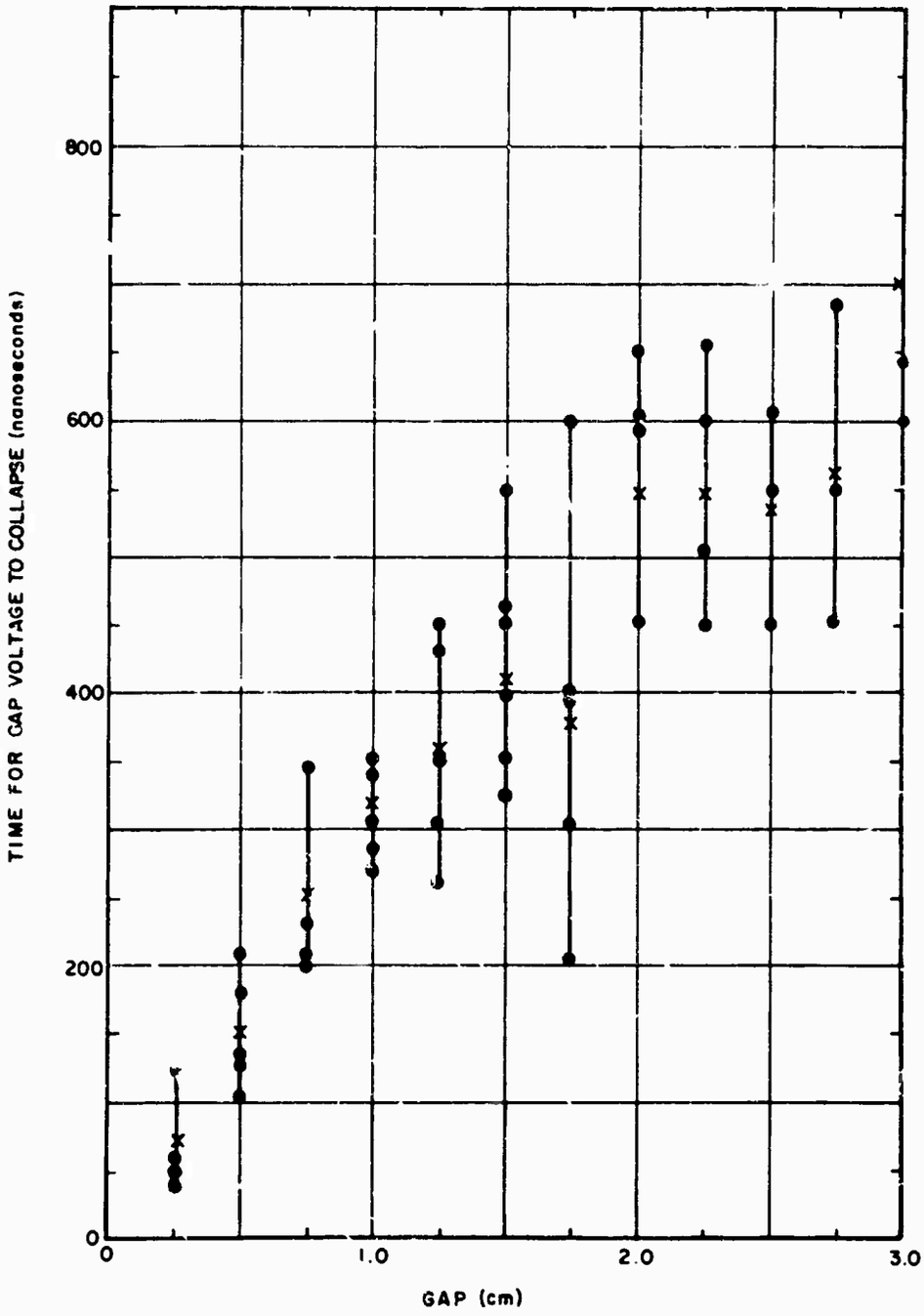

Figure 4-16. Collapse of Gap Voltage

1-2444

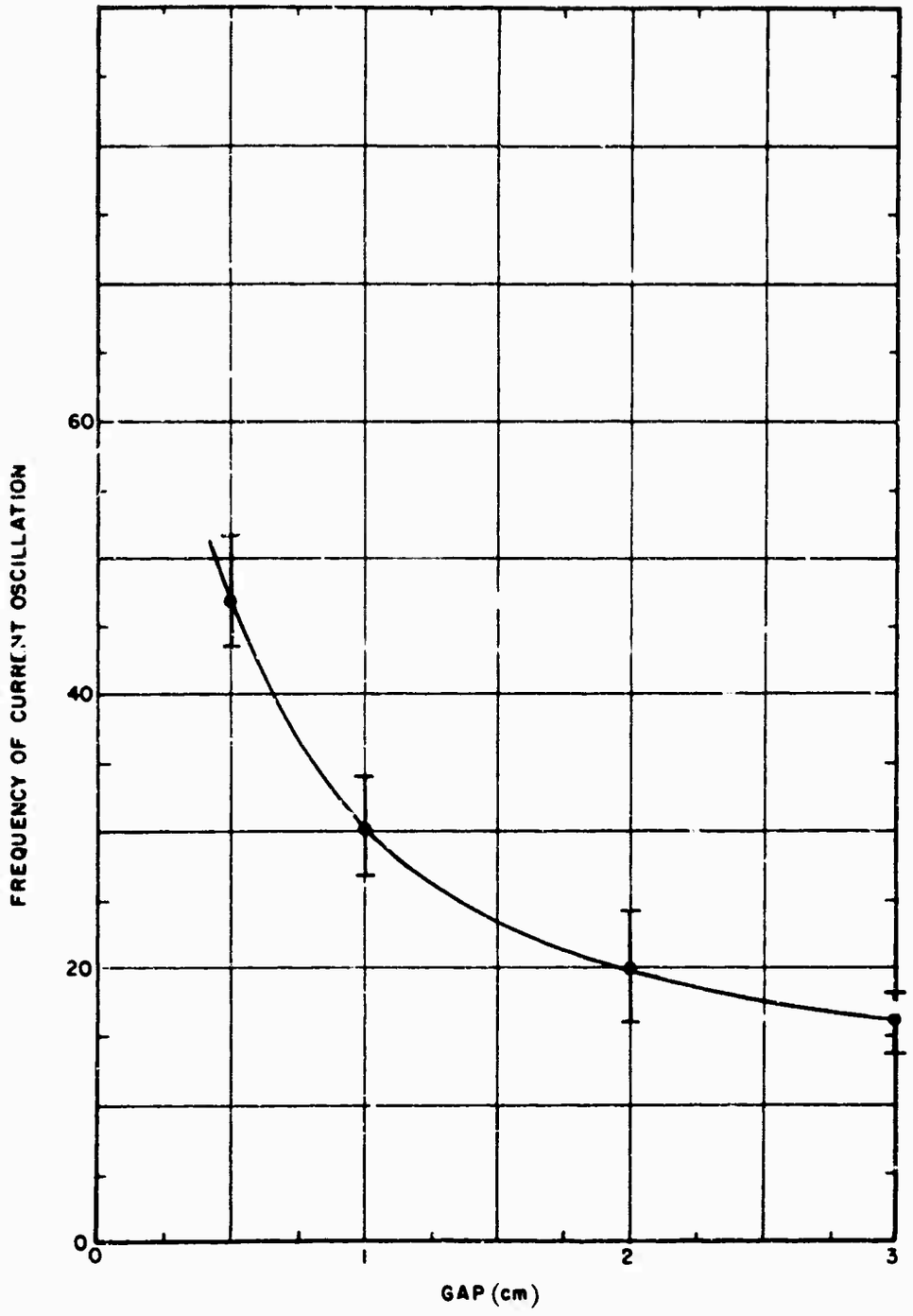

Figure 4-17. Frequency of Current Oscillations as a Function of Gap Spacing

1-2445

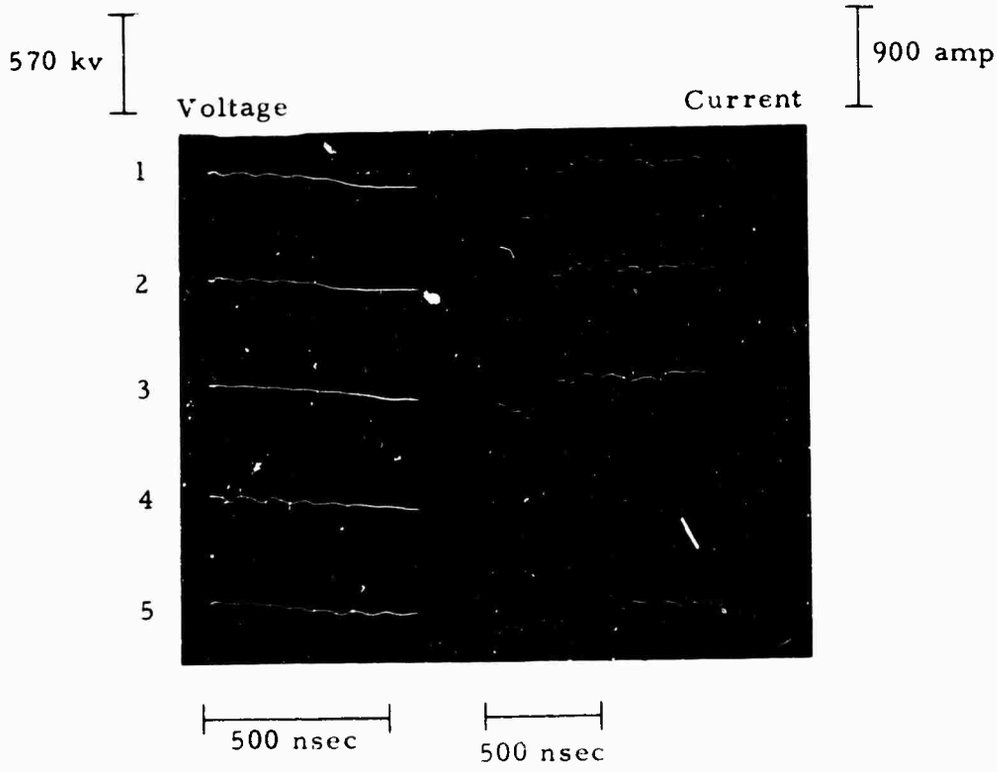

1 = 135 kv
2 = 105 kv
3 = 133 kv
4 = 146 kv
5 = 155 kv

Figure 4-18. Gap Voltage and Current Waveforms for 3.0 cm Gap

2-749

several microseconds. In the latter case the gap current was estimated at 20 amperes. Visually type (a) was a violet filamentary breakdown and type (b) a pale diffuse glow filling most of the gap space. They suggest that the most probable mechanism is vaporization of cathode or anode by electron current, the vapor filling the gap at 10^5 cm/second and gas breakdown occuring in the gap.

Since our experiments were conducted with sensibly steady potentials it is not apparent as to what the breakdown initiating event is and how current builds up from the 10^{-12} to 10^{-5} ampere range to the hundred ampere range. Breakdowns have occurred with prebreakdown currents ranging from 10^{-12} to 10^{-5} amperes suggesting that the value is not too important. Several breakdowns occurred which failed to trigger the oscilloscopes monitoring voltage and current. The low frequency cut-off of the probes would make them insensitive to slow changes of V and I such as those observed by Smith and Mason and could account for the failure to trigger. This effect was more noticeable with magnetic field present.

SECTION 5
EXPERIMENTAL DESIGN

5.1 General

The factors selected for the next experiment are given in Table 5-1 and are seen to consist of five inflexible factors and four flexible factors. They are as follows:

(1) Inflexible: Anode material, cathode material, electrode treatment, anode size and anode shape. These are all constructional and cannot be varied without opening up the vacuum test chamber.

(2) Flexible: Magnetic field, gas exposure and energy storage. Electrode spacing may also be considered a flexible factor. These can be varied continuously without disturbing the test set up.

All factors will be investigated at two levels which are designated high and low and are represented by the lower case letter and numeral one respectively

It has been decided to perform a complete 2^5 factorial experiment for the inflexible factors since third order interactions may have possible significance and it was therefore judged imprudent at this stage in the program to neglect them by confounding with main factors in a partial factorial experiment. Once the magnitude and significance of such interactions is evaluated they can be confounded with confidence in any future experiments introducing further factors.

The full experiment will consist of 32 individual experiments or treatments. These will be divided into two blocks typically as shown in Table 5-2. The selection of the treatments will be made as follows. Each block will consist of a full factorial for factors A, B, C and D with factor E held constant at the low level for the first block and at the high level for the second. The order in each block will be randomized. As a result of this "blocking" a statistical analysis at the half way stage will yield both main effects and higher order interactions for the 4 factors varied, with factor E at high level. Upon completion of the 32 treatments the experience will then be equivalent to a full factorial 2^5 block, if there is no history effect, and will be analysed accordingly.

To incorporate the flexible factors the technique of stacking will be employed. This has been used for the previous 2^3 block experiment and is described in the Eleventh Quarterly Progress Report. However, since additional factors are presently involved and since this marks the beginning of a

Table 5-1. Factors for Second Stacked Block Experiment

Inflexible		Flexible	
Anode Material	A		
Cathode Material	B	Magnetic Field	F
Electrode Treatment	C	Gas Exposure	G
Anode Size	D	Energy Storage	H
Anode Shape	E	Gap	I

Table 5-2. Arrangement of Treatments in Blocks for Stacked Experiments

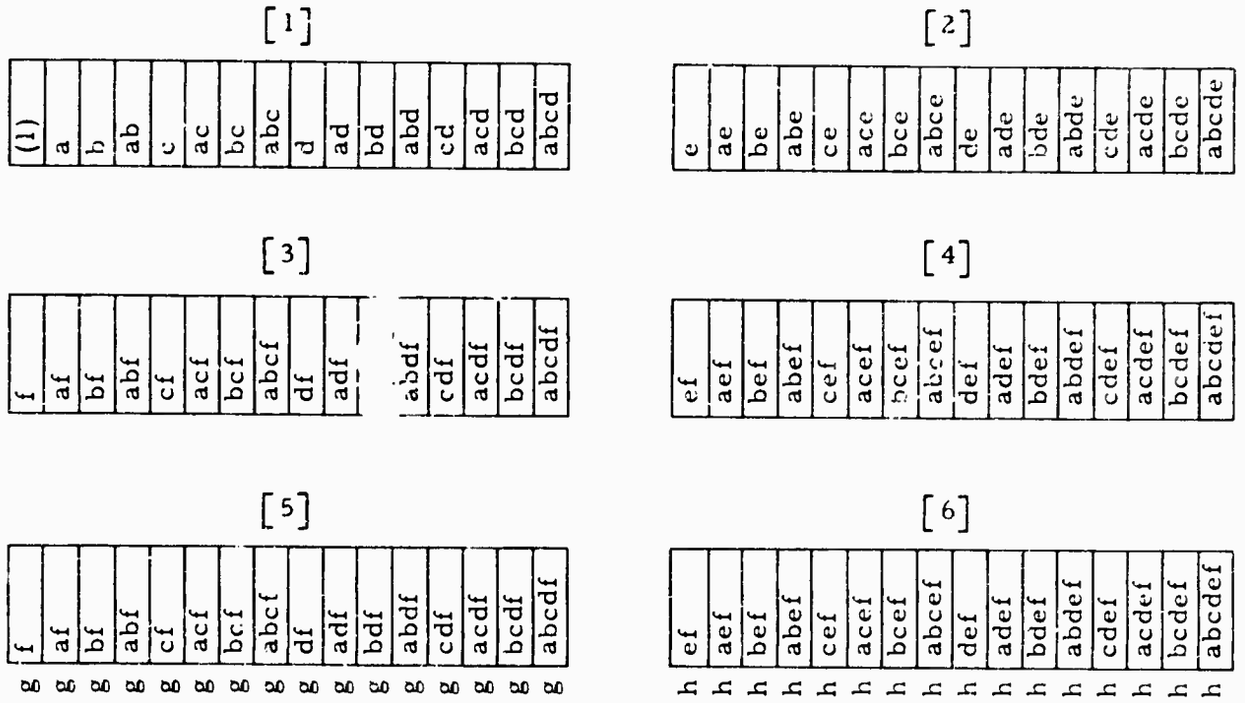

major experiment, the parameters to be used in the analyses, the factor levels, and the complete procedures for both main and stacked experiments are now presented.

5.2 Electrode Shape and Variables to be Investigated

In addition to the breakdown voltage V_B, the following variables will also be used in the analysis:

$V_{\Delta P}$ the threshold voltage for the appearance of pressure surges.

I_{PB} the logarithm of the ultimate prebreakdown current.

T the formative time lag for the collapse of voltage across the gap.

V_B and I_{PB} will be measured for all treatments and $V_{\Delta P}$ is expected should be measureable in most. The formative time lag T should be measured as widely as possible over the parameters already shown to affect it, namely gap separation and magnetic field strength as well as with the other parameters. It should be measured at two widely different gaps (e.g., 1.0 and 4.0 cm, and at 0 and 400 gauss), since these values will be used in all the treatments involving magnetic field.

The relative pumping conductance and field distributions, it is hoped, can be calculated for each configuration. It may then be possible by techniques of regression analysis to relate area and shape effects at different gap separations with either of these two physically meaningful parameters.

The following sizes and geometries were chosen for the electrodes:

(1) Anode: 1-1/4 inch and 4 inch diameter spherical and Bruce profile electrodes.

(2) Cathode: 2 inch diameter spherical electrodes.

5.3 The Choice of Materials

A review will now be given of the possible selections of material and the reasons for the final choice.

(i) Copper. This material has been investigated in previous experiments. A process of learning about its various interactions with other materials is taking place and besides being readily obtainable, it is used extensively in

devices limited by vacuum breakdown. It has moreover very well investigated physical properties which make data analysis and theoretical calculations much more meaningful.

(2) Titanium. Although this material has been investigated and has highly desirable properties, it can not be baked in hydrogen because of the formation of a hydride powder. The electrodes would simply turn into dust and the interactions with processing could not be investigated.

(3) Tungsten, Molybdenum and Tantalum. These materials at the moment have long delivery times inconsistent with the program.

(4) Nickel. This material is readily available and widely used in vacuum equipment but it magnetizes with an associated hysteresis which it is felt would be undesirable.

(5) Stainless Steel. This material is widely used in high voltage vacuum equipment, dissolves hydrogen much more than copper, and could be pretreated in the same manner as copper. The correct choice of type is moreover non-magnetic.

(6) Aluminum. This material is readily available but sorbs much less hydrogen than copper and at a much lower rate (see Tabel 5-3 and Figure 5-1). The material melts at a much lower temperature and will require a different pretreatment.

It does however have desirable more widely different physical characteristics from those of copper when seen from the point of view of an anode heating model. Zinn[1] et al, have found strong correlation between experimental data and the empirical formula:

$$V_B = k\, C_s^{\,a}\, T_v^{\,b}\, d^n$$

where:

C_s = specific heat of anode material

T_v = temperature at which a vapor pressure of 10^{-5} torr is obtained

d = gap separation

Table 5-3. Constants for Rates of Diffusion of Gases through Metals and Values of t°C for $Q_{\mu l}$ = micron · liters (0°C) per cm^2 per min per mm Thickness at 1 atm Pressure (From Dushman and Lafferty, "Scientific Foundations of Vacuum Technique", Wiley, 1965)

System	Ref.	C	B	t° C for $Q_{\mu l}$ =			
				0.1	1.0	10	100
H_2-Ni	1	4.4611	3371	344	483	701	1097
	2	4.0288	3031	330	479	727	1221
	3	4.1206	2929	299	438	666	1108
	4	4.2455	3017	302	438	657	1071
	5	4.2578	2898	278	408	616	1010
H_2-Pt	6	4.2486	4285	544	736	1016	1732
	3	4.1713	3936	488	671	968	1539
	7	5.010	4220	429	571	779	1130
H_2-Pd	9, 1	5.783	2318	69	128	212	340
	8	4.5765	2296	139	229	369	618
H_2-Cu	5	3.4611	3629	541	775	1041 (5)	
	10	3.2755	4307	734	1042		
H_2-Fe	5	3.3116	2100	214	361	735	1029 (50)
	4	3.3035	2055	204	349	619	1303
	11	3.480	2405	264	418	697	1352
H_2-Al	5	5.723	6735	$Q_{\mu l} = 1.03 \cdot 10^{-3}$ for 500° C $= 1.02 \cdot 10^{-2}$ for 600° C			
H_2-Mo	5	4.0679	4417	598	813	1167	1862
N_2-Mo	5	5.0185	9837	1362	1687	2174	2444 (25)
N_2-Fe	11	3.7526	5204	822	1114	1431 (5)	
CO-Fe	11	3.2133	4066	692	993	1344 (5)	
O_2-Ag	12	4.413	4941	640	846		
	13	4.673	4941	598	784	940 (4)	
	13	5.121	4941	534	692	926 (4)	

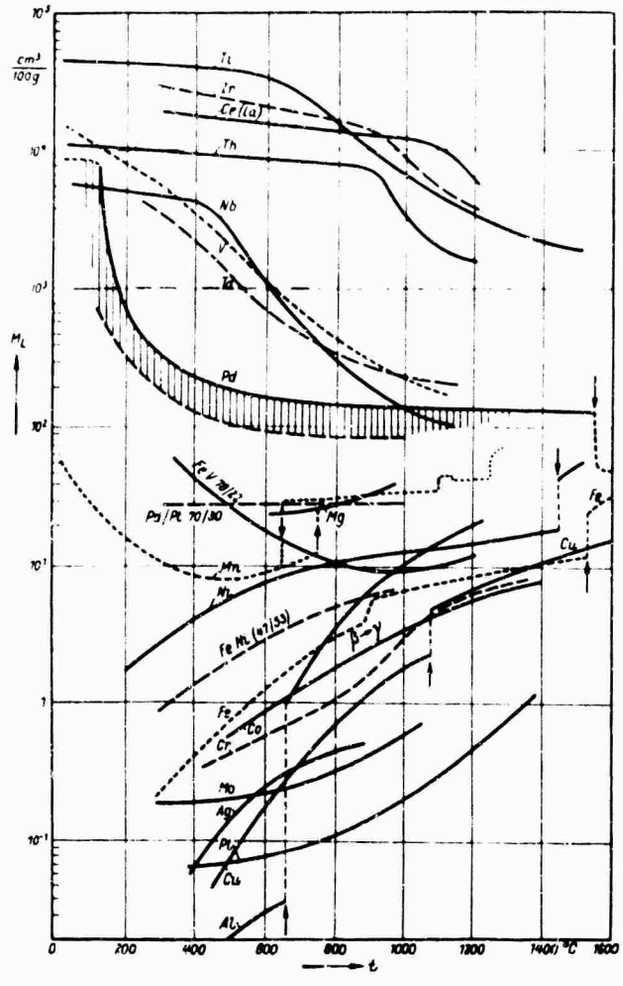

Figure 5-1. Solubility of Hydrogen in Various Metals as a Function Temperature (After Waldschmidt) (Metall-Verlag GMBH, Berlin)

(Kohl, Walter H., "Materials and Techniques for Electron Tubes", General Telephone and Electronics Technical Series, 1960)

1-2446

Aluminum has a widely different value of k from that of copper so that a large variation of V_B would be expected. The choice of materials is thus copper and aluminum.

5.4 Electrode and System Preparation

(1) Vacuum or hydrogen firing of electrodes for 6 hours at 900°C for copper and 600°C for aluminum, because of the lower melting point of the latter. Test samples will be prepared and analysed for gas content so that differences in gas content will be known. Due to the very different sorption properties of Cu and Al to H_2 it is expected that a strong interaction of anode material with treatment should show up in the results.

(2) When cooled to ambient temperature, electrode transfer in a dry nitrogen atmosphere to the test chamber.

(3) Overnight pumping to less then 10^{-7} torr.

(4) Chamber bake at 375°C for 6 hours with concurrent electrode bake at 400°C for 8 hours.

(5) Chamber and electrodes are allowed to cool to ambient temperature.

5.5 Main Experiment

The main experiment will cover blocks [1] and [2] of Table 5-2, viz the full factorial of the 5 inflexible factors. It will be split as indicated in Section 5.1 into two separate 4 factor full factorial experiments thus permitting separate analyses after 16 treatments and upon completion of all 32 treatments. At the latter stage the fifth factor, anode shape, may also be incorporated for analysis on the basis of a full factorial 2^5 experiment. This may necessitate making allowance for an experimental history effect if one is present.

A range of gaps from 0.5 to 4.0 cm will be examined as follows to provide information both for unconditioned and conditioned electrodes.

(1) 3 breakdowns at 1.0 cm gap

(2) 1 breakdown at each higher gap setting up to 4.0 cm

(3) 1 breakdown at 0.5 cm gap

(4) repeat cycle for "conditioned" breakdown voltage with again a 1 breakdown at each gap setting.

This will occupy the first day of the test program.

5.6 First Stacked Experiment - Magnetic Field

Upon completion of this main experiment for each treatment of blocks [1] and [2] a second or stacked treatment will be carried out to investigate the effect of the magnetic field. This is shown on Table 5-1 by blocks [3] ≡ f [1] and [4] ≡ f [2] where f represents the addition of magnetic field factor. This will be carried out over a range of gap separations and transverse magnetic field strengths in the following manner.

First, a zero field measurement is made and will be repeated at 100, 200, 300 and 400 gauss. This procedure will be performed firstly at 1.0 cm gap, then at 1.5, 2.0, 2.5, 3.0, 3.5, 4.0, 0.5 and finally 1.0 cm again. The start is made at 1.0 cm as before because prebreakdown current increases below this gap and it is feared that it may do some unwanted conditioning. This will take up the second day of test and on the third day the appropriate treatment of experiments [5] or [6] will be performed.

5.7 Second Stacked Experiment - Gas Exposure and Energy Storage

These blocks [5] and [6] represent respectively the effects of gaseous exposure and energy storage respectively. By this it is meant that for the 16 treatments of block [5] the vacuum system will be exposed to oxygen at 10^{-5} torr for a measured period and then pumped back to its base pressure before testing. This will be done for the first 16 treatments both with and without magnetic field applied. During the next 16 treatments, instead of exposing the system as described, some energy storage will be added and the tests will again be repeated as before, with and without the magnetic field. The maximum field strength of 400 gauss is recommended for [5] and [6].

$$[5] \equiv g\,[1]$$
$$\text{and also} \equiv g\,[3]$$

$$[6] \equiv h\,[2]$$
$$\text{and also} \equiv h\,[4]$$

where g and h represent the addition of the gas exposure and energy storage respectively.

In all these experiments, the only effect which will be confounded will be those involving the interactions gas exposure x anode shape and energy storage x anode shape. These have been judged to be least likely to be of importance.

SECTION 6

FUTURE EFFORT

During the next quarter the following will be pursued:

- Continue analysis of the results of the pilot experiment.
- Continue analysis of the results of the block of eight experiment.
- Decide on experimental order and initiate second block experiment.
- Redesign, fabrication and checkout of new electrode heating system.
- Conditioning and commissioning of second bakeable column.
- Checkout of energy storage and crowbar systems.
- Analysis of results of second block experiment.
- Complete overhaul of 300 kv system and maintain it in an operational state.
- Prepare, process and examine electrodes.

SECTION 7

IDENTIFICATION OF PERSONNEL

The following personnel were active in the program during the period under review:

S. V. Nablo	- Vice President Director, Particle Physics Division
M. J. Mulcahy	- Project Manager
A. C. Stewart	- Engineering Manager
W. R. Bell	- Senior Electrical Engineer
M. M. Thayer	- Senior Metallurgist
A. Watson	- Senior Scientist
R. M. Parsons	- Engineering Aide
R. Benoit	- Design Engineer
C. Boudreau	- Engineering Aide
L. Indingaro	- Metallurgical Technician
D. J. Maynard	- Senior Mechanical Engineer
S. K. Wiley	- Group Leader/Mechanical Engineering
Prof. H. Freeman	- Consultant Massachusetts Institute of Technology Department of Economics and Social Science
Prof. A. Argon	- Consultant Massachusetts Institute of Technology Department of Mechanical Engineering
Dr. N. E. Woldman	- Consultant Metallurgy

SECTION 8

REFERENCES

(1) Zinn, M.H., Taylor, G W. and Chrepta, M M., "Influence of Electrode Material on High Voltage Vacuum Breakdown", IEEE International Electron Devices Meeting, Washington, D C. (1967)

(2) Duke, C. and Alferieff, M., J.Chem.Phys. 46, 923 (1967).

(3) Heard, H.G., University of California Radiation Laboratory Report.

(4) Smith, W.A. and Mason, T.R , "Preliminary Measurements of Time Lags to Breakdown of Large Gaps", presented at the Proc. Second International Symposium on Insulation of High Voltages in Vacuum (1966).

APPENDIX A

ELECTRODE DAMAGE FROM TRANSIENT HEAVY CURRENT SPARKS

ELECTRODE DAMAGE FROM TRANSIENT HEAVY CURRENT SPARKS

Introduction

A model is presented to describe electrode damage due to heavy currents flowing in spark channels for time durations of tens of nanoseconds. Characteristically, the observed damage comprises a ring of frozen metal projecting from the surface with regularly spaced spikes superimposed azimuthally upon it.

Vacuum spark damage also exhibits similar features except that many frozen rings appear with ripples superimposed. The damage is thought to occur by the same mechanism but a different kind of current rise as a function of time changes the form somewhat.

The following analysis is aimed at clarifying the mechanism.

Statement of Problem

At the center of each ring, observation shows that there is a small crater where metal immediately below the spark channel was vaporized. No account will be taken here of spark channel expansion and it will be formalized simply as a fixed conducting cylinder produced instantaneously between two high voltage electrodes. Current however cannot be established until magnetic flux has diffused into the conductors. The channel conductivity is much less than that of the electrode metal and diffusion into it is rapid enough to be considered instantaneous by comparison.

Flux diffusion into the electrode surface will cause melting because of the accompanying resistive power dissipation. Electromagnetic forces also act normally into the electrode surface but decrease in strength radially. Since the surface becomes fluid with a radial electromagnetic pressure gradient, a steady flow will occur in such a manner as to cancel it.

The problem can now be formulated as that of determining the hydromagnetic flow pattern of a fluid with a free surface flowing radially outwards across an azimuthal magnetic field.

The Hydromagnetic Flow Equations

Hydromagnetic flow will be considered radially across an azimuthal magnetic field distribution for a disc of conducting fluid initially of uniform depth but with a free surface. There is no indication from the conditions of the problem that melting occurs to a uniform depth but this will be assumed as a first approximation to demonstrate the essential principles of the mechanism. Azimuthal symmetry will be assumed so as to reduce the problem to two dimensions.

Two fundamental equations must be satisfied by the flow. The first, to be referred to as the flux transport equation (FTE) embodies Ohm's Law and Faraday's Law in a moving reference frame to describe the flux distribution:[1]

$$\frac{\partial \vec{B}}{\partial t} = \eta \nabla^2 \vec{B} + \text{curl} (\vec{u} \wedge \vec{B}) \qquad \text{(A-1)}$$

where:

$$\eta \equiv \frac{1}{\mu_o \sigma}$$

The second equation describes the fluid mechanics with a distributed electromagnetic force distribution and is cast in a form similar to the Bernoulli Equation. It will, therefore, be referred to as the magnetic Bernoulli Equation (MBE):

$$p + \frac{1}{2} \rho u^2 + \frac{B^2}{2\mu_o} = \text{Constant} \qquad \text{(A-2)}$$

where:

$$u^2 = v^2 + w^2$$

and:

p = hydrostatic pressure

A radial velocity component, $v(r)$, and an axial component, $w(r)$, constitute the total velocity, u. The equation of mass flow is:

$$\frac{m}{2\pi\rho r} = v\,h(r) + \frac{1}{r}\int_{o}^{r} w(r)\, r\, dr \qquad (A-3)$$

and the equation of streamline flow gives:

$$w(r) = v(r)\frac{dh}{dr} \qquad (A-4)$$

The value of m must be independent of r and inspection of the above equations shows that v(r) must be of the form:

$$v(r) = \frac{f}{r} \qquad (A-5)$$

where:

$$f = \text{Constant}$$

Hence:

$$w(r) = -\frac{f}{r}\frac{dh}{dr} \qquad (A-6)$$

The Electrode Surface Flow

In cylindrical coordinates the FTE becomes:

$$\eta\left[\frac{\partial^2 B}{\partial r^2} + \frac{1}{r}\frac{\partial B}{\partial r} + \frac{\partial^2 B}{\partial z^2}\right] + (v - w)\frac{\partial B}{\partial r} + B\frac{\partial}{\partial r}(v - w) = \frac{\partial B}{\partial t} \qquad (A-7)$$

Substituting Equations (A-5) and (A-6), and rearranging, this becomes:

$$\frac{\partial^2 B}{\partial r^2} + \left\{ \frac{1 + \left(\frac{f}{\eta}\right)(1 - h')}{r} \right\} \frac{\partial B}{\partial r}$$

$$+ \left[\frac{\partial}{\partial r} \left\{ \frac{\left(\frac{f}{\eta}\right)}{r} (1 - h') \right\} \right] B \qquad \text{(A-8)}$$

$$= \frac{1}{\eta} \frac{\partial B}{\partial t} - \frac{\partial^2 B}{\partial z^2}$$

Now f/η has the dimensions of a magnetic Reynolds number and will be represented by R_m:

$$\frac{\partial^2 B}{\partial r^2} + \left\{ 1 + R_m (1 - h') \right\} \frac{1}{r} \frac{\partial B}{\partial r} + \frac{R_m (1 - h')}{r^2} B$$

$$- \frac{R_m}{r} h'' B = \frac{1}{\eta} \frac{\partial B}{\partial t} - \frac{\partial^2 B}{\partial z^2} \qquad \text{(A-9)}$$

Solving this by separation of variables, we have:

$$B \equiv \beta(r)\, \zeta(z)\, \tau(t) \qquad \text{(A-10)}$$

and the equations in each variable reduce to:

$$\frac{d^2 \beta}{d r^2} + \left\{ 1 + R_m (1 - h') \frac{1}{r} \frac{d\beta}{dr} \right\}$$

$$- \left\{ \alpha^2 + \frac{R_m (1 - h')}{r^2} + \frac{R_m h''}{r} \right\} \beta = 0 \qquad \text{(A-11)}$$

$$\frac{d^2\zeta}{dz^2} - \gamma^2\zeta = 0 \qquad \text{(A-12)}$$

$$\frac{d\tau}{dt} - \eta(\alpha^2 + \gamma^2)\tau = 0 \qquad \text{(A-13)}$$

Thus the solution is of the form:

$$B = \text{Constant } \beta(r) \exp\left[-\left\{\gamma_z + \eta(\alpha^2 + \gamma^2)t\right\}\right] \qquad \text{(A-14)}$$

The solution $\beta(r)$ must satisfy Equation (A-9) derived from the FTE and at the same time must satisfy the MBE.

Equation (A-2) can be written for u = 0 with the corresponding solution B_o. Thus:

$$p + \frac{B_o^2}{2\mu_o} = \text{Constant} \qquad \text{(A-15)}$$

Subtracting from Equation (A-2), we have:

$$\rho u^2 + \frac{B^2 - B_o^2}{2\mu_o} = 0 \qquad \text{(A-16)}$$

The form of $B_o(r)$ is obtained by solving Equation (A-11) with $R_m = 0$ for which modified Bessel solutions are obtained:

$$B_o = \mu_o I U_o(\alpha r) \qquad \text{(A-17)}$$

where $U_o(\alpha r)$ is an appropriate solution. When α is small, $U_o(\alpha r) \rightarrow 1/\pi r$. Hence:

$$R_m^2 (1 + h'^2) + K_1 (B r)^2 - K_2 I^2 = 0 \qquad \text{(A-18)}$$

where K_1 and K_2 are constant.

Therefore:

$$B = \left\{ \frac{K_2 I^2 - R_m^2 (1 + h'^2)}{K_1} \right\}^{1/2} \frac{1}{r} \qquad \text{(A-19)}$$

If $dh/dr \equiv h' = \text{Constant}$, then $B(r) \propto 1/r$. This must be consistent with the solution of Equation (A-11) which, for the same assumption ($h' = \text{Constant}$), can be reduced to the form:

$$\beta'' + \left\{ 1 + R_m (1 - h') \right\} \frac{\beta'}{r} - \left\{ \alpha^2 + \frac{R_m (1 - h')}{r^2} \right\} \beta = 0 \qquad \text{(A-20)}$$

The solution of Equation (A-20) will be of the general form:[2]

$$\beta = r^{-\lambda} \left\{ A_1 I_p (\alpha r) + A_2 K_p (\alpha r) \right\} \qquad \text{(A-21)}$$

where:

$$p^2 = \lambda^2 - 4\lambda$$

and:

$$\lambda = R_m (1 - h')$$

which may be either positive or negative.

The appropriate solution for a stationary fluid may be obtained by allowing R_m to tend to zero. Thus:

$$\beta = A_1 I_o (\alpha r) + A_2 K_o (\alpha r) \qquad \text{(A-22)}$$

Comparison of Equations (A-21) and (A-22) shows that the multiplier, $r^{-\lambda}$, and the change in order of the modified Bessel functions are produced by the action of the flow. There is, of course, no MBE to be satisfied in this case because a pressure gradient will be sustained by the stationary conducting fluid or solid.

The problem in the hydromagnetic flow case is in finding a flow solution to the FTE which will at the same time have no pressure gradient. This necessitates a particular form for the depth h(r) of the channel as a function of radius.

Pressure Balance

The condition that there should be no gradient of electromagnetic force is:

$$\nabla (\vec{J} \wedge \vec{B}) = 0 \tag{A-23}$$

where:

$$\vec{J} = \sigma (\vec{E} + \vec{u} \wedge \vec{B})$$

Hence:

$$\vec{J} \wedge \vec{B} = \sigma (\vec{E} \wedge \vec{B} + \vec{u} \wedge \vec{B} \wedge \vec{B}) \tag{A-24}$$

The second term is $- B^2 \vec{u}$. Hence:

$$\nabla (\vec{J} \wedge \vec{B}) = - B^2 \nabla \vec{u} \tag{A-25}$$

and:

$$u^2 = v^2 + w^2 = \frac{f}{r} \left\{ 1 + h'^2 \right\} \tag{A-26}$$

The condition that there is no pressure gradient in the flow is thus that:

$$\nabla \vec{u} = 0 \tag{A-27}$$

Considering the flow in two dimensions as a radial outward movement, the equation of continuity:

$$\nabla \vec{u} = 0$$

requires:

$$u = \frac{\text{Constant}}{r} \tag{A-28}$$

Hence:

$$f(1 + h'^2) = \text{Constant} \tag{A-29}$$

and since:

$$f = \frac{m}{2\pi\rho}\left\{h + \int_o^r h'\,dr\right\}^{-1} = \frac{\dot{m}}{4\pi\rho\, h(r)} \tag{A-30}$$

then for a pressure balanced flow:

$$(R_{mo}\, h_o)\left(\frac{1 + h'^2}{h^2}\right) = \text{Constant} \tag{A-31}$$

where:

$$R_m = \frac{i}{\eta} = \frac{(R_{mo}\, h_o)}{h} \tag{A-32}$$

and R_{mo}, h_o are the initial values of R_m and h at the beginning of the flow at r = a.

We can write:

$$\frac{1 + h'^2}{h^2} = k_1\left(k_1 + \frac{2h'}{h}\right) + 2\left(\frac{h'}{h}\right)^2 \tag{A-33}$$

with:

$$k_1 \equiv \frac{1 - h'}{h} = \frac{\lambda}{R_{mo}\, h_o} \tag{A-34}$$

Thus, if k_1 = Constant, then the solution for h is:

$$h(r) = \frac{1}{k_1} + k_2 \exp(-k_1 r) \tag{A-35}$$

where:

$$k_2 = \left(h_o - \frac{1}{k_1} \right) \exp (k_1 a)$$

and k_1 may be either positive or negative according to whether the flow depth increases or decreases with radius. The latter case seems appropriate to the present problem. Hence:

$$\frac{h'}{h} = \frac{- k_1 k_2 \exp (-k_1 r)}{- \frac{1}{k_1} + k_2 \exp (-k_1 r)} \qquad \text{(A-36)}$$

Thus, h'/h, which from Equations (A-5) and (A-6) is seen to be the slope of the flow direction at any radius, will have a pole at $h = 0$; i. e. :

$$k_1 k_2 \exp (- k_1 r) = 1 \qquad \text{(A-37)}$$

Now the choice of k_1 = Constant will permit modified Bessel solutions of the FTE which will approximately match the values of B given by the MBE; but if:

$$(R_{mo} h_o) \left(\frac{1 + h'^2}{h^2} \right) = \text{Constant} \qquad \text{(A-38)}$$

then $(1 - h')/h$ will switch between two values as h'/h goes through infinity. This means that the modified Bessel solutions will be appropriate on each side of a critical radius at which $h'/h = \infty$, but with different parameters.

From Equation (A-37), we have:

$$\begin{aligned} r_c &= \frac{1}{k_1} \ln k_1 k_2 \\ &= a + \frac{1}{k_1} \ln (k_1 h_o + 1) \\ &= a + \frac{R_{mo} h_o}{\lambda} \ln \left\{ \frac{\lambda}{R_{mo}} + 1 \right\} \end{aligned} \qquad \text{(A-39)}$$

The approximate form of the MBE shows that the value of r_c will increase almost linearly with I.

Conclusions

It appears that the reason for the characteristic form of electrode damage is that hydromagnetic flow outwards on a disc of decreasing depth cannot take place at zero pressure gradient without a discontinuity at a particular radius. This radius increases with the current but otherwise no more serious damage will occur unless the pulse duration increases.

Examples of damage are given for a wide range of current in Figures A-1, A-2 and A-3.

A schematic diagram illustrating the analytical findings is presented in Figure A-4. Analysis of the sparking conditions and the dimensions of the corresponding photographs provided data for Figure A-5, showing damage size as a function of estimated current. The approximately linear dependence of r_c on I is consistent with the theory.

There is no fundamental difference in the damage mechanism in vacuum except that the spark is more often oscillatory or slowly rising (~ 300 nanoseconds). Either of these features will transform the damage appearance somewhat but it is nevertheless believed to be inducative of the current growth history of the spark channel.

Acknowledgement

This work was supported in part by the Defence Atomic Support Agency under Contract DA-01-67C-001.

References

(1) Ferraro, V. C. A. and Plumpton, "An Introduction to Magneto-Fluid Mechanics", Oxford University Press (1961).

(2) Murphy, G. M., "Ordinary Differential Equations and Their Solutions", Van Nostrand (1960).

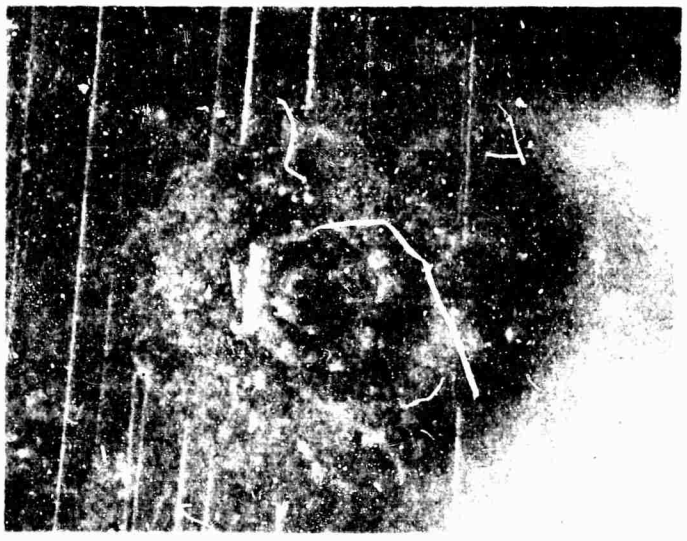

Breakdown Voltage = 1.4 Mv
Output Impedance = 50 Ω
Estimated Current = 7 ka
Discharge Duration = 20 nsec
Magnification = 60X

Figure A-1. Spark Damage From FX-15 Machine

2-725

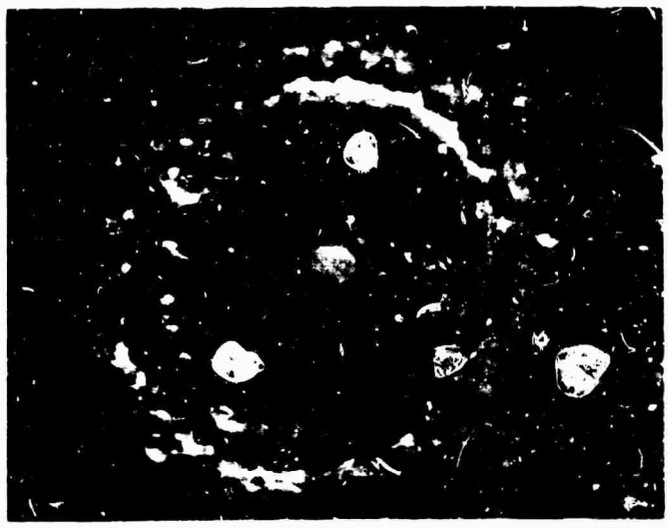

Breakdown Voltage = 5.5 Mv
Output Impedance = 57 Ω
Estimated Current = 100 ka
Discharge Duration = 25 nsec
Magnification = 30X

Figure A-2. Spark Damage From FX-45 Machine

2-726

Breakdown Voltage = 10 Mv
Output Impedance = 42 Ω
Estimated Current = 250 ka
Discharge Duration = 70 nsec
Magnification = 9X

Figure A-3. Spark Damage From FX-100 Machine

2-727

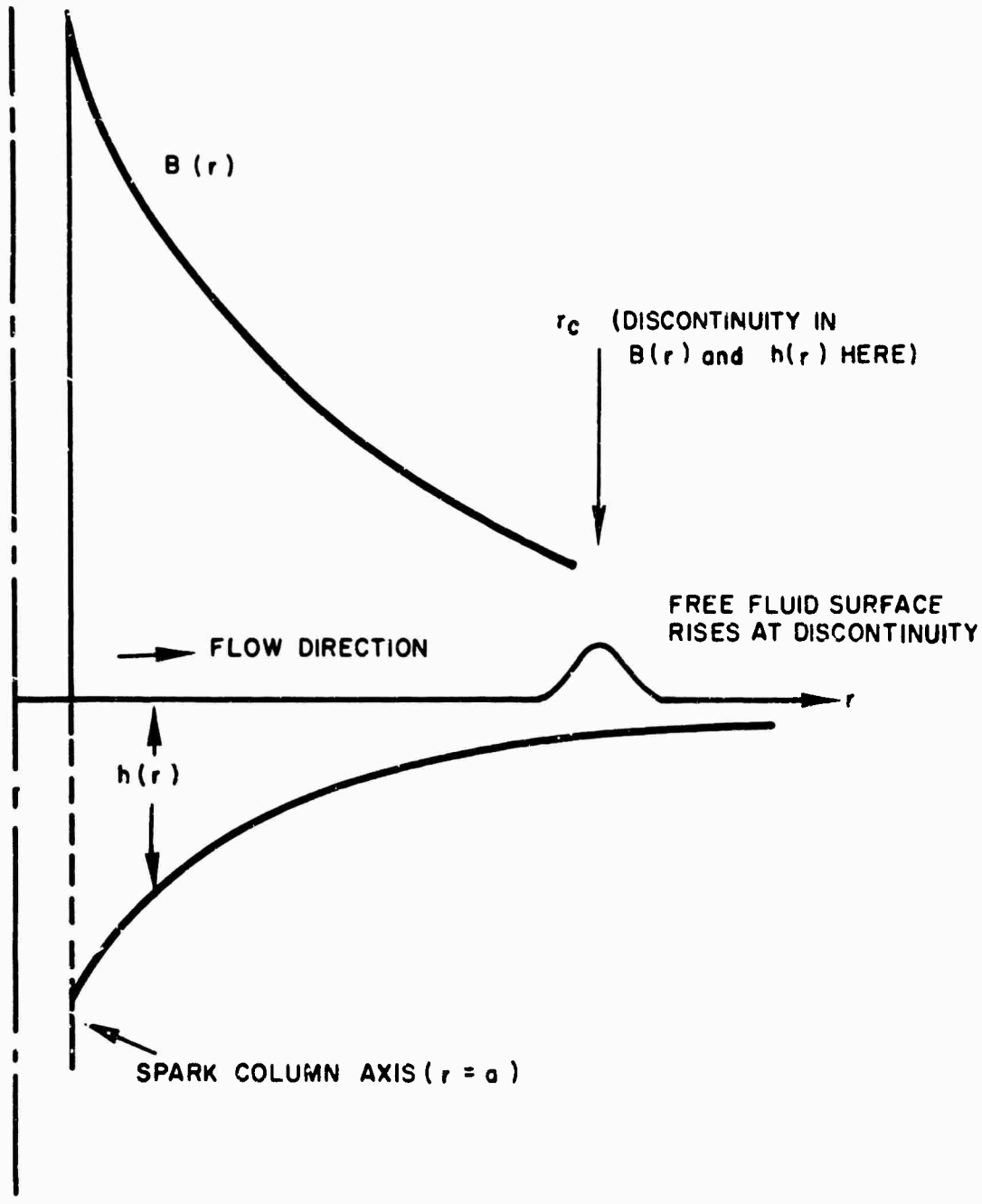

Figure A-4 Diagram to Illustrate the Hydromagnetic Flow Solution

1-2352

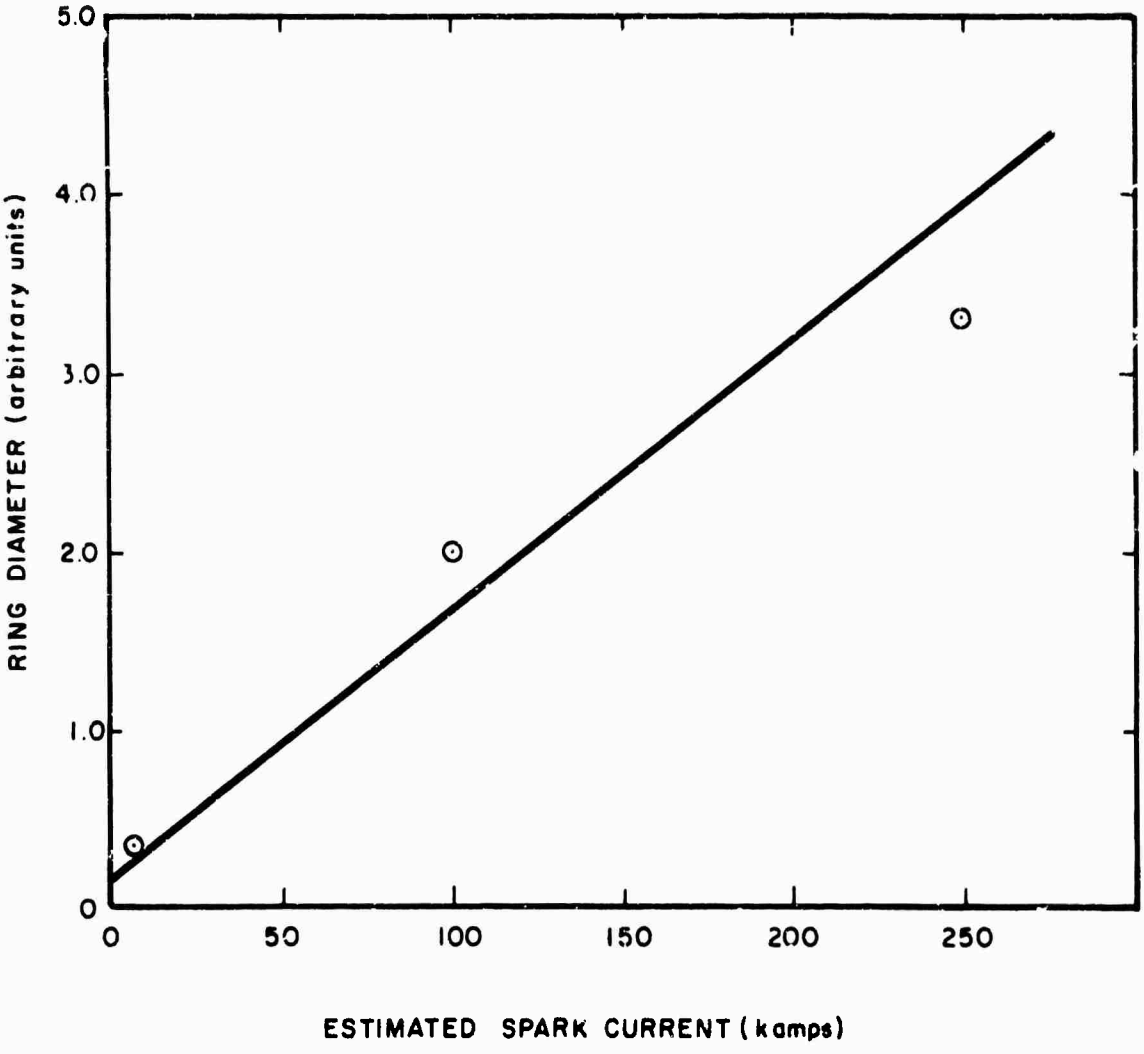

Figure A-5 Scale of Damage as a Function of Current

1-2353

Security Classification

DOCUMENT CONTROL DATA - R&D

(Security classification of title, body of abstract and indexing annotation must be entered when the overall report is classified)

1. ORIGINATING ACTIVITY (Corporate author)	2a. REPORT SECURITY CLASSIFICATION
Ion Physics Corporation S. Bedford Street Burlington, Massachusetts 01803	Unclassified 2b. GROUP

3. REPORT TITLE

High Voltage Breakdown Study

4. DESCRIPTIVE NOTES (Type of report and inclusive dates)

Twelfth Quarterly Progress Report 16 August - 15 November 1967

5. AUTHOR(S) (Last name, first name, initial)

W. R. Bell, M. J. Mulcahy and A. Watson

6. REPORT DATE	7a. TOTAL NO. OF PAGES	7b. NO. OF REFS
March 1968	132	

8a. CONTRACT OR GRANT NO.	9a. ORIGINATOR'S REPORT NUMBER(S)
DA28-043 AMC-00394(E) b. PROJECT NO. 7900.21.243.40.00 c. TASK d.	9b. OTHER REPORT NO(S) (Any other numbers that may be assigned this report) ECOM-00394-12

10. AVAILABILITY/LIMITATION NOTICES

This document has been approved for public release and sale; its distribution is unlimited.

11. SUPPLEMENTARY NOTES	12. SPONSORING MILITARY ACTIVITY
Advanced Research Projects Agency ARPA Order No. 517	U.S. Army Electronics Command Fort Monmouth, New Jersey 07703 ATTN: AMSEL-KL-TS

13. ABSTRACT

Statistical and physical analyses of the block of eight experiments were carried out for unconditioned gaps and for conditioned gaps with and without perpendicular magnetic field. The other factors examined were anode and cathode treatment (vacuum or hydrogen firing) and electrode size. Prebreakdown current and breakdown voltage values were examined in the statistical analysis. Second order and higher order interactions were found to be important in addition to main factor effects. The magnetic field significantly affected the breakdown voltage and also interacted with other factors. The theoretical model of the breakdown mechanism developed was consistent with the results and trends of the statistical analysis. The 300 kv apparatus was disassembled for complete overhaul, cleaning and remachining. This included electropolishing of the vacuum chamber and polishing of all gold O-ring surfaces. The box heating oven was replaced with a form fitting as heater blanket unit and the controls for both and the electrode heaters were made completely automatic. The latter have now been removed from the vacuum envelope and the complete system has been reassembled, baked and made vacuum tight.

DD FORM 1 JAN 64 1473

Security Classification

14. KEY WORDS	LINK A		LINK B		LINK C	
	ROLE	WT	ROLE	WT	ROLE	WT
Electrical Breakdown in Vacuum Conditioning Procedures Optical and X-Radiation Partial Pressure and Gap Current Etching						

INSTRUCTIONS

1. ORIGINATING ACTIVITY: Enter the name and address of the contractor, subcontractor, grantee, Department of Defense activity or other organization *(corporate author)* issuing the report.

2a. REPORT SECURITY CLASSIFICATION: Enter the overall security classification of the report. Indicate whether "Restricted Data" is included. Marking is to be in accordance with appropriate security regulations.

2b. GROUP: Automatic downgrading is specified in DoD Directive 5200.10 and Armed Forces Industrial Manual. Enter the group number. Also, when applicable, show that optional markings have been used for Group 3 and Group 4 as authorized.

3. REPORT TITLE: Enter the complete report title in all capital letters. Titles in all cases should be unclassified. If a meaningful title cannot be selected without classification, show title classification in all capitals in parenthesis immediately following the title.

4. DESCRIPTIVE NOTES: If appropriate, enter the type of report, e.g., interim, progress, summary, annual, or final. Give the inclusive dates when a specific reporting period is covered.

5. AUTHOR(S): Enter the name(s) of author(s) as shown on or in the report. Enter last name, first name, middle initial. If military, show rank and branch of service. The name of the principal author is an absolute minimum requirement.

6. REPORT DATE: Enter the date of the report as day, month, year, or month, year. If more than one date appears on the report, use date of publication.

7a. TOTAL NUMBER OF PAGES: The total page count should follow normal pagination procedures, i.e., enter the number of pages containing information.

7b. NUMBER OF REFERENCES: Enter the total number of references cited in the report.

8a. CONTRACT OR GRANT NUMBER: If appropriate, enter the applicable number of the contract or grant under which the report was written.

8b, 8c, & 8d. PROJECT NUMBER: Enter the appropriate military department identification, such as project number, subproject number, system numbers, task number, etc.

9a. ORIGINATOR'S REPORT NUMBER(S): Enter the official report number by which the document will be identified and controlled by the originating activity. This number must be unique to this report.

9b. OTHER REPORT NUMBER(S): If the report has been assigned any other report numbers *(either by the originator or by the sponsor)*, also enter this number(s).

10. AVAILABILITY/LIMITATION NOTICES: Enter any limitations on further dissemination of the report, other than those imposed by security classification, using standard statements such as:

(1) "Qualified requesters may obtain copies of this report from DDC."

(2) "Foreign announcement and dissemination of this report by DDC is not authorized."

(3) "U. S. Government agencies may obtain copies of this report directly from DDC. Other qualified DDC users shall request through

_____."

(4) "U. S. military agencies may obtain copies of this report directly from DDC. Other qualified users shall request through

_____."

(5) "All distribution of this report is controlled. Qualified DDC users shall request through

_____."

If the report has been furnished to the Office of Technical Services, Department of Commerce, for sale to the public, indicate this fact and enter the price, if known.

11. SUPPLEMENTARY NOTES: Use for additional explanatory notes.

12. SPONSORING MILITARY ACTIVITY: Enter the name of the departmental project office or laboratory sponsoring *(paying for)* the research and development. Include address.

13. ABSTRACT: Enter an abstract giving a brief and factual summary of the document indicative of the report, even though it may also appear elsewhere in the body of the technical report. If additional space is required, a continuation sheet shall be attached.

It is highly desirable that the abstract of classified reports be unclassified. Each paragraph of the abstract shall end with an indication of the military security classification of the information in the paragraph, represented as *(TS)*, *(S)*, *(C)*, or *(U)*.

There is no limitation on the length of the abstract. However, the suggested length is from 150 to 225 words.

14. KEY WORDS: Key words are technically meaningful terms or short phrases that characterize a report and may be used as index entries for cataloging the report. Key words must be selected so that no security classification is required. Identifiers, such as equipment model designation, trade name, military project code name, geographic location, may be used as key words but will be followed by an indication of technical context. The assignment of links, rules, and weights is optional.